REFLECTION AND TRANSMISSION FUNCTIONS IN REACTOR PHYSICS

Thesis by

Wayne Wallace Pfeiffer

In Partial Fulfillment of the Requirements

For the Degree of

Doctor of Philosophy

California Institute of Technology

Pasadena, California

1969

(Submitted May 14, 1969)

ACKNOWLEDGMENTS

I am deeply thankful to my advisor, Dr. Jerome Shapiro, for the guidance he provided throughout my thesis research. In particular, he greatly simplified my task by clearly defining the problem from the very outset and consistently recalling that definition as research progressed. The consequent, frequent discussions, coupled with a warm personal relationship, were a source of continual encouragement and satisfaction. Thanks are also due to Dr. Harold Lurie for suggesting that I pursue my graduate research in nuclear engineering and to Dr. Noel Corngold for bringing related research to my attention.

Dr. D. R. Mathews supplied both the input and output of his shielding calculations, which allowed comparison calculations to be made. Dr. E. L. Slaggie discussed the multiple scattering correction problem with me and D. Huffman provided the computer code FLANGE and the input scattering kernel. Dr. R. E. Kalaba stimulated much of this research through discussions with both my advisor and myself.

Finally I am grateful to the National Science Foundation for providing financial support for my entire stay, except for the summers of 1965 and 1967 which were funded by Caltech and the Ford Foundation, respectively.

ABSTRACT

The utility of reflection and transmission function (or collectively, response function) concepts in reactor physics is extensively investigated. Previously obtained differential (invariant imbedding) and functional (adding) equations for the response functions are rederived in a unified manner. In addition a numerical halving technique is developed from the adding relations.

Existing response function calculations are summarized and extended by combining the invariant imbedding and functional equations. For deep-penetration shielding problems in slab geometry, this combined response function approach is shown to be more efficient than conventional Monte Carlo or discrete ordinates techniques. The response function approach is also shown to be efficient for a criticality search in slab geometry. As a step toward a more general treatment, invariant imbedding equations are derived, but not solved, in finite cylindrical geometry.

Finally the feasibility of performing response function experiments to obtain cross-section and criticality information is examined. The envisioned experimental set-up is described and calculations are carried out to verify the analytical procedures, with particular emphasis on the propagation of errors. Cross-sections can be determined using the halving scheme, which provides a theoretically sound technique for multiple scattering correction. Thus experiments may be done on moderately thick slabs. Criticality parameters can be obtained from measured response functions using the criticality

search procedure. Because response function experiments are expected to be relatively quick and cheap compared to present cross-section and critical experiments, it is concluded that response function experiments should be carried out as soon as possible to determine whether they are as useful as our analysis indicates.

TABLE OF CONTENTS

I. INTRODUCTION

A. Purpose of Thesis

In this thesis we will present a unified treatment of reflection and transmission functions (or collectively, response functions) as applicable to reactor physics. The original interest in response functions (particularly the reflection function) arose in the study of light. The possibility of applying response function techniques to reactor physics has only been recently considered. Consequently few realistic reactor calculations have been carried out, while the experimental possibilities of measuring response functions have received no attention at all. We will summarize and extend existing calculations as well as investigate the previously ignored experimental aspects. Throughout our emphasis will be on techniques for solving practical reactor problems. Primarily we will be concerned with fast reactors.

B. Response Function Approach - - Differential Equations and Functional Equations

Transport theory problems may be approached in several ways. At present the Monte Carlo and Boltzmann approaches are most commonly used. In the Monte Carlo approach, the motion of individual particles is simulated and their average behavior is predicted by tracing many individual histories. The Boltzmann approach is developed in terms of an average particle angular flux and results in a first order, linear, integro-differential equation. In this thesis we will use the response function approach in which the dependent variables are

the average reflected and transmitted angular fluxes. Two different kinds of equations arise from this approach. The so-called invariant imbedding equations are second order, non-linear, integro-differential equations. The response functions also satisfy functional equations ("adding relations") which relate the response functions of a composite piece of material to the response functions of its constituent parts. Although the invariant imbedding equations and the adding relations can be shown to be mathematically equivalent (and both are equivalent to the Boltzmann equation), they have significantly different physical interpretations. The invariant imbedding equations contain the material cross-sections and so, require microscopic information for their solution. The adding relations, on the other hand, are macroscopic as they contain no cross-sections, requiring instead knowledge of the response functions for some material thickness as their input information. It is this macroscopic property that makes the functional equations especially attractive from an experimental point of view and which provided much of the motivation for this thesis.

C. Review of Previous Work

Both the functional and differential equations originated with Stokes[1] in 1862 in his study of the reflection and transmission of light through a stack of glass plates. Stokes derived the adding relations and from them obtained the differential equation (invariant imbedding equation) for the reflection function. In 1907, more than fifty years later, Schmidt[2] carried out a similar treatment for the

reflection and transmission of electrons through slabs of material. By restricting the electron motion to be normal to the slabs, he obtained the same equations as Stokes plus the differential equation for the transmission function.

No further work was done until the 1940's when response functions were used in radiative transfer by Ambarzumian[3,4] and Chandrasekhar[5,6], in microwave transmission by members of the M.I.T. Radiation Laboratory[7,8], and in neutron and gamma ray penetration by Bobrowsky[9]. The microwave and neutron work was similar to that of Stokes and Schmidt in that only "right" and "left" motion was considered.

Ambarzumian's work in radiative transfer using "principles of invariance" was an innovation, however, in that angular dependence was incorporated in the equations. These invariance principles were generalized and used extensively by Chandrasekhar. In 1956 Bellman and Kalaba[10] coined the name "invariant imbedding" and suggested its appliability to neutron transport. In the succeeding years Bellman and co-workers have written many papers on invariant bedding. Good reviews of this work are Bellman, Kalaba, Bailey, and Wing[11-14]. This work provided a sound theoretical basis for the invariant imbedding technique, but produced no realistic neutron calculations as energy dependence was not considered. The first numerical treatments of multi-energetic invariant imbedding were done by Beissner[15,16] and Mathews et al[17] for neutron shielding and by Shimizu and Mizuta[18-20] for gamma ray penetration. The time-

dependent work of Bellman et al[21,22] was extended by Mockel[23,24] to include energy dependence. Finally, Mingle[25] has done some criticality calculations using invariant imbedding, but only for one-energy transport.

In essentially all of this development it was the differential equations that were used. The functional equations were only occasionally mentioned as a curiosity. The one exception was the work by Shimizu and Mizuta. They utilized a functional equation in conjunction with the differential equations to obtain an efficient numerical scheme for deep-penetration calculations.

Simultaneous with this development of differential equation techniques, there were a number of independent studies using the functional equations. Peebles and Plesset[26] and Aronson and Yarmush[34] considered angular - and energy-dependent gamma ray penetration, while Ribarič[27], Selengut[28], Shimizu et al[29-31], Vértes[32], and Nuding[33] considered neutron transport or diffusion.

In the meantime work was continuing in the field of microwave transmission. In fact the scattering matrices introduced in the 1940's had become standard tools in transmission-line and network analysis[35] and similar techniques were being used for mechanical vibration problems[36-38]. Because there was no angular dependence, the relationship between the differential equations and the functional equations was clearer. This motivated Redheffer[39] to develop a general theory of scattering processes encompassing microwave, light, and neutron problems alike. It is this theory that shows that the differential

equations and the functional equations are mathematically equivalent[40,41] as stated previously. The work of Bailey and Wing[42,14] and Devooght[43] has shown the equivalence between the invariant imbedding equations and the Boltzmann equation for neutron transport. We thus have available several mathematically equivalent approaches for transport problems.

As for numerical implementation, however, the different approaches are not at all equivalent. Response function approaches are very efficient for slab geometry, but can be extended to other geometries only with great difficulty. The invariant imbedding equations have been derived in spherical and infinite cylindrical geometry[44-46] but numerical calculations have been done only for spherical shells[47] and two-dimensional blocks[31].

Finally note that all of the previous work has been theoretical. Response functions are easily measured and thus particularly well suited for experimental work. The feasibility of using experimentally measured response functions to determine significant reactor physics parameters will be the subject of Chapter IV.

D. Outline of Thesis

The outline of the thesis is as follows. Following the introduction, Chapter II is devoted to the basic theory of response functions. The response functions are defined in slab geometry and the functional equations and differential equations are derived for both transport and diffusion theory. The major new result in this chapter is the

development of a halving scheme. Most of Chapter IV will be based on this scheme.

In Chapter III we will discuss the purely calculational aspects of working with response functions. It will be shown that for slab geometry shielding problems, response function techniques are more efficient than conventional Monte Carlo or Boltzmann techniques. Next the utilization of response functions in criticality calculations is discussed. In higher dimensions the use of response functions appears to be severely restricted because of their Green's function nature. The chapter is concluded with a discussion of the invariant imbedding equations in finite cylindrical geometry, which are derived, but not solved, in Appendices A and B.

Chapter IV is devoted to possible experimental applications of response function techniques. The most promising application appears to be in cross-section determination. The halving scheme developed in Chapter II provides a theoretically sound technique for multiple scattering correction. Experiments can thus be done on moderately thick slabs of material. The use of response function experiments for direct determination of criticality is also discussed. Propagation of errors through the ensuing calculations is considered for both the cross-section and criticality determinations.

The last chapter summarizes the thesis and points the way toward further research.

II. THEORY OF RESPONSE FUNCTIONS

A. Transport Theory

1. Definitions

First let us define the response functions and derive the equations governing them for time-independent processes in slab geometry. Throughout we will speak of neutrons rather than photons, although the same equations govern the transport of both.

Consider a slab of material of thickness x with an azimuthally symmetric angular flux $\delta(\mu-\mu_o)\delta(E-E_o)$ incident uniformly on the left face of the slab (see Fig. 1). Then the resulting reflected and transmitted angular fluxes, $r^+(x,\mu,E,\mu_o,E_o)$ and $t^+(x,\mu,E,\mu_o,E_o)$, are called the reflection and transmission functions (or response functions). Physically

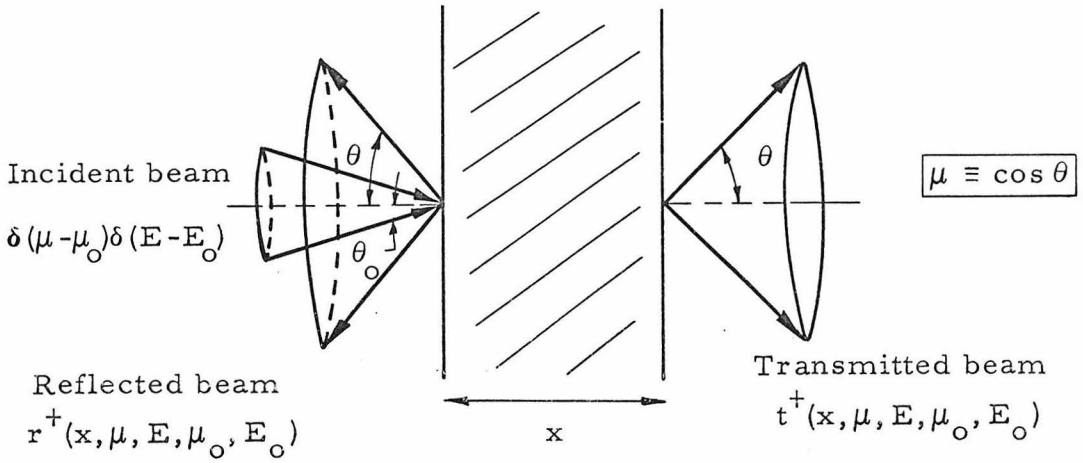

Fig. 1

$r^+(x,\mu,E,\mu_o,E_o)d\mu\,dE$

= the number of neutrons per unit time per unit area reflected from a slab of thickness x into $d\mu$ about $-\mu$ and dE about E due to an incident beam of one neutron per unit time per unit area in direction μ_o with energy E_o. (The incident and exit areas are measured normal to the neutron motion. Also μ and μ_o will always be positive.) (2-1)

and

$t^+(x,\mu,E,\mu_o,E_o)d\mu\,dE$

= the number of neutrons per unit time per unit area transmitted through a slab of thickness x into $d\mu$ about μ and dE about E due to an incident beam of one neutron per unit time per unit area in direction μ_o with energy E_o. (2-2)

Thus r^+ and t^+ are the Green's functions for reflected and transmitted angular fluxes due to an incident angular flux from the left. Consequently we can write the reflected and transmitted angular fluxes for an arbitrary incident angular flux, $\phi^+(0,\mu',E')$, as

$$\phi^-(0,-\mu,E) = \int_o^\infty dE' \int_o^1 d\mu' r^+(x,\mu,E,\mu',E')\phi^+(0,\mu',E') \qquad (2\text{-}3)$$

$$\phi^+(x,\mu,E) = \int_o^\infty dE' \int_o^1 d\mu' t^+(x,\mu,E,\mu',E')\phi^+(0,\mu',E') \quad . \qquad (2\text{-}4)$$

Since all our work will be numerical, we discretize the r^+ and t^+ functions in both energy and angle. Suppose we have n energy groups with mean energies $E_1, \ldots, E_n$ and widths $\Delta E_1, \ldots, \Delta E_n$ and m directions $\mu_1, \ldots, \mu_m$ with widths $\Delta\mu_1, \ldots, \Delta\mu_m$. Each combination of energy group and direction

will correspond to a state of the neutron motion to which we will assign a new index. Thus $\mu = .2, E = 10$ MeV might correspond to state 1; $\mu = .2$, $E = 3$ MeV to state 2; etc. It is the state index which will appear in all of the equations below. For n energy groups and m directions, we have $N = n \times m$ states. This assumes, of course, that we use the same energy mesh for each direction and vice versa. This is not necessary, though. As Peebles and Plesset[26] pointed out, the meshes can be chosen non-uniformly and so tailored to a particular problem. For all our calculations, however, we will use uniform meshes.

Let

$$\begin{aligned} \phi_i^+(x) &\equiv \phi^+(x, \mu_i, E_i) \\ \phi_i^-(x) &\equiv \phi^-(x, -\mu_i, E_i) \\ r_{ij}^+(x) &\equiv r^+(x, \mu_i, E_i, \mu_j, E_j) \\ t_{ij}^+(x) &\equiv t^+(x, \mu_i, E_i, \mu_j, E_j) \end{aligned} \tag{2-5}$$

Then Eqs. (2-3) and (2-4) may be written in the discrete approximation as

$$\phi_i^-(0) = \sum_{j=1}^{N} \Delta\mu_j \Delta E_j r_{ij}^+(x) \phi_j^+(0) \tag{2-6}$$

$$\phi_i^+(x) = \sum_{j=1}^{N} \Delta\mu_j \Delta E_j t_{ij}^+(x) \phi_j^+(0) \tag{2-7}$$

If we further define

$$\rho_{ij}^+(x) \equiv \Delta\mu_j \Delta E_j r_{ij}^+(x) \tag{2-8}$$

$$\tau_{ij}^{+}(x) \equiv \Delta\mu_j \Delta E_j t_{ij}^{+}(x) \tag{2-9}$$

then Eqs. (2-6) and (2-7) can be written as

$$\phi^{-}(0) = \rho^{+}(x)\phi^{+}(0) \tag{2-10}$$

$$\phi^{+}(x) = \tau^{+}(x)\phi^{+}(0) \tag{2-11}$$

where the ϕ's are N-vectors and ρ^{+} and τ^{+} are $N \times N$ matrices, which we will call the reflection and transmission matrices (or collectively the response matrices).

In a similar fashion the reflected and transmitted angular fluxes due to an incident angular flux $\phi^{-}(x)$ from the right are

$$\phi^{+}(x) = \rho^{-}(x)\phi^{-}(x)$$
$$\phi^{-}(0) = \tau^{-}(x)\phi^{-}(x) \quad .$$

For a homogeneous slab no distinction between left and right response matrices is necessary as $\rho^{+}(x) = \rho^{-}(x)$ and $\tau^{+}(x) = \tau^{-}(x)$.

2. Macroscopic Relations

The adding relations giving the response matrices of a composite slab in terms of the response matrices of its constituent slabs form the basis of the macroscopic response function approach.

Consider a slab of thickness $x + y$ with an angular flux $\phi^{+}(0)$ incident from the left (Fig. 2). Then the following relations hold:

$$\phi^{-}(0) = \rho^{+}(x)\phi^{+}(0) + \tau^{-}(x)\phi^{-}(x) \tag{2-12}$$

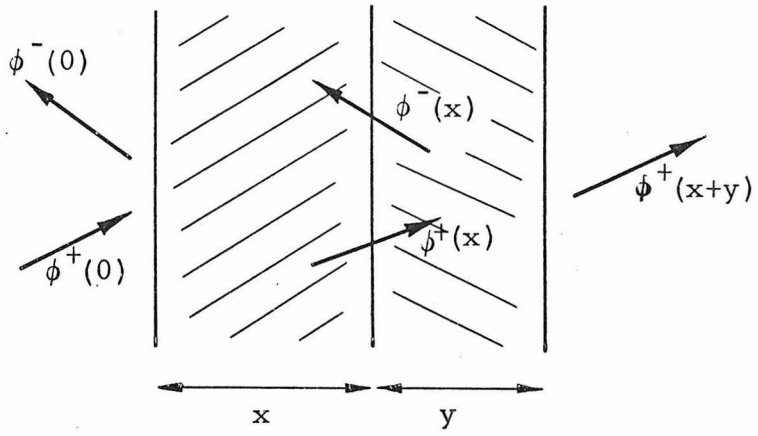

Fig. 2

$$\phi^+(x) = \tau^+(x)\phi^+(0) + \rho^-(x)\phi^-(x) \tag{2-13}$$

$$\phi^-(x) = \rho^+(y)\phi^+(x) \tag{2-14}$$

$$\phi^+(x+y) = \tau^+(y)\phi^+(x) \quad . \tag{2-15}$$

Eliminating $\phi^+(x)$ and $\phi^-(x)$ from these equations and using Eqs. (2-10) and (2-11), we have

$$\begin{aligned}\phi^-(0) &= \rho^+(x)\phi^+(0) + \tau^-(x)\rho^+(y)[\,I-\rho^-(x)\rho^+(y)]^{-1}\tau^+(x)\phi^+(0) \\ &= \rho^+(x+y)\phi^+(0)\end{aligned}$$

$$\begin{aligned}\phi^+(x) &= \tau^+(y)[\,I-\rho^-(x)\rho^+(y)]^{-1}\tau^+(x)\phi^+(0) \\ &= \tau^+(x+y)\phi^+(0) \quad .\end{aligned}$$

Since these equations hold for all incident distributions $\phi^+(0)$, we have

$$\rho^+(x+y) = \rho^+(x) + \tau^-(x)\rho^+(y)[\,I-\rho^-(x)\rho^+(y)]^{-1}\tau^+(x) \tag{2-16}$$

$$\tau^+(x+y) = \tau^+(y)[\,I-\rho^-(x)\rho^+(y)]^{-1}\tau^+(x) \quad . \tag{2-17}$$

These functional equations we will call the <u>adding relations</u>. They

were first derived in the context of neutron transport by Bellman et al[11]. Similar relations hold for $\rho^-(x+y)$ and $\tau^-(x+y)$. To simplify notation we will drop the + and - superscripts from now on. When working with heterogeneous slabs, however, one must remember to take them into account. Without superscripts, Eqs. (2-16) and (2-17) are

$$\rho(x+y) = \rho(x) + \tau(x)\rho(y)[I-\rho(x)\rho(y)]^{-1}\tau(x) \qquad (2-18)$$

$$\tau(x+y) = \tau(y)[I-\rho(x)\rho(y)]^{-1}\tau(x) \quad . \qquad (2-19)$$

To obtain the adding relations we eliminated $\phi^+(x)$ and $\phi^-(x)$ from Eqs. (2-12) - (2-15). This is not possible if $[I-\rho(x)\rho(y)]$ is singular, that is if

$$\det[I - \rho(x)\rho(y)] = 0 \quad . \qquad (2-20)$$

This is the criticality condition about which we will have more to say later.

Doubling relations are obtained immediately from the adding relations by simply letting $y = x$. Then

$$\rho(2x) = \rho(x) + \tau(x)\rho(x)[I-\rho^2(x)]^{-1}\tau(x) \qquad (2-21)$$

$$\tau(2x) = \tau(x)[I - \rho^2(x)]^{-1}\tau(x) \quad . \qquad (2-22)$$

The doubling relations are explicit expressions for $\rho(2x)$ and $\tau(2x)$ in terms of $\rho(x)$ and $\tau(x)$. This leads one to ask whether it is possible to invert these relations to get expressions for $\rho(x)$ and $\tau(x)$ in terms of $\rho(2x)$ and $\tau(2x)$, i.e. halving relations. So far we

have not been able to obtain such expressions. An iterative scheme for halving has been devised, however, which we will now describe.

First let us write the doubling relations (2-21) and (2-22) as

$$\rho(x) = \rho(x/2) + \tau(x/2)\rho(x/2)[I-\rho^2(x/2)]^{-1}\tau(x/2) \qquad (2-23)$$

$$\tau(x) = \tau(x/2)[I-\rho^2(x/2)]^{-1}\tau(x/2) \quad . \qquad (2-24)$$

Using (2-24) in (2-23) we have

$$\rho(x) = \rho(x/2) + \tau(x/2)\rho(x/2)\tau^{-1}(x/2)\tau(x) \quad . \qquad (2-25)$$

Equations (2-25) and (2-24) then suggest the following iteration scheme for finding $\rho(x/2)$ and $\tau(x/2)$.

$$\rho_{k+1}(x/2) = \frac{1}{2}\{\rho_k(x/2) + \rho(x) - \tau_k(x/2)\rho_k(x/2)\tau_k^{-1}(x/2)\tau(x)\} \qquad (2-26)$$

$$\tau_{k+1}(x/2) = \frac{1}{2}\{\tau_k(x/2) + [I - \rho_{k+1}^2(x/2)]\tau_k^{-1}(x/2)\tau(x)\} \qquad (2-27)$$

with

$$\rho_o(x/2) = \frac{1}{2}\rho(x) \qquad (2-28)$$

$$\tau_o(x/2) = \frac{1}{2}[I + \tau(x)] \quad . \qquad (2-29)$$

This scheme is more efficient than the one we described in Ref. 48, requiring only one matrix inversion and five matrix multiplications per iteration. A convergence problem still arises, however, when the thickness x approaches the order of the mean free path of the lowest energy group. Modification of the above scheme is then necessary.

This will be discussed in detail in Chapter IV.

For an arbitrary thickness z we can use a combination of doubling, halving, and adding to get $\rho(z)$ and $\tau(z)$ from a given $\rho(x)$ and $\tau(x)$ provided the slab is homogeneous. It is this ability to get the response matrices at one thickness from those at another thickness that makes this approach so useful. For a heterogeneous slab we need the reflection and transmission matrices for a single thickness of each material.

3. Response Functions and Cross-sections

The macroscopic relations derived above do not explicitly contain any cross-sections. For a slab of small thickness, however, the response functions are simply related to the cross-sections as we now show.

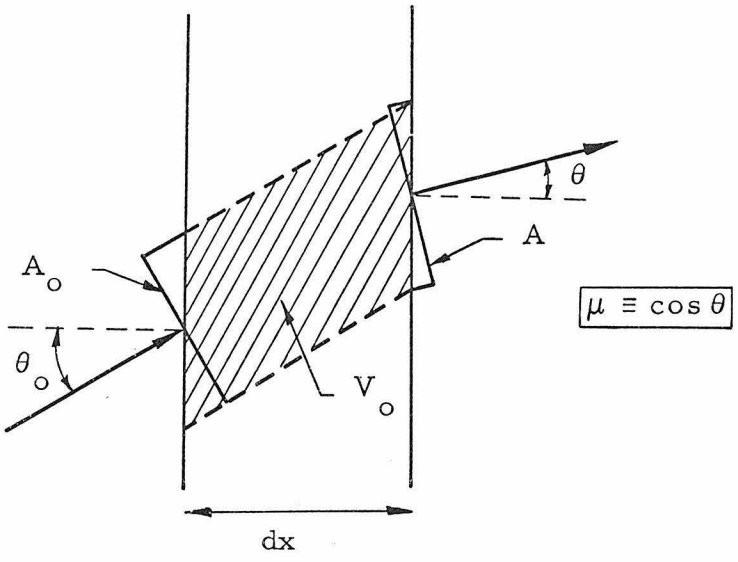

Fig. 3

Consider the slab of thickness dx shown in Fig. 3. Then the relevant quantities and their corresponding physical interpretations are listed below.

$\phi_o \equiv \phi(0, \mu_o, E_o)$: angular flux (neutrons per unit time per unit area) incident on slab

$\Sigma_t(E_o)\phi_o$: collisions per unit time per unit volume due to incident flux ϕ_o

$\Sigma_t(E_o)\phi_o A_o \frac{dx}{\mu_o}$: collisions per unit time in $V_o = A_o \frac{dx}{\mu_o}$ due to incident flux ϕ_o

$f(dx, \phi_o, \mu, E, \mu_o, E_o)d\mu dE \equiv \Sigma_t(E_o)\phi_o A_o \frac{dx}{\mu_o} k(\mu, E, \mu_o, E_o)d\mu dE$:
neutrons per unit time emitted from V_o into $d\mu$ about μ with energy dE about E due to an incident flux ϕ_o (2-30)

where the frequency function

$k(\mu, E, \mu_o, E_o)\, d\mu dE \equiv$ the number of neutrons emitted per collision in $d\mu$ about μ and dE about E due to an incident neutron moving in direction μ_o with energy E_o. (Fission as well as scattered neutrons are included.) (2-31)

Next define the <u>transfer cross-section</u> as

$$\Sigma(\mu, E, \mu_o, E_o) \equiv \Sigma_t(E_o)k(\mu, E, \mu_o, E_o) \quad . \tag{2-32}$$

In terms of the scattering and fission processes

$$\Sigma(\mu, E, \mu_o, E_o) = \int_o^{2\pi} d\varphi\ \Sigma^s(\vec{\Omega}\cdot\vec{\Omega}_o, E, E_o) + \frac{1}{2}\chi(E)[\nu\Sigma_f](E_o) \tag{2-33}$$

$$\text{where } \vec{\Omega}\cdot\vec{\Omega}_o = \mu\mu_o + \sqrt{1-\mu^2}\sqrt{1-\mu_o^2}\cos\varphi \quad .$$

From Fig. 3 we see that

$$\frac{A_o}{\mu_o} = \frac{A}{\mu} \quad . \tag{2-34}$$

Equations (2-32) and (2-34) in (2-30) yield

$$f(dx, \phi_o, \mu, E, \mu_o, E_o)d\mu dE = \Sigma(\mu, E, \mu_o, E_o)\phi_o A \frac{dx}{\mu} \, d\mu dE \, . \tag{2-35}$$

Finally comparing Eqs. (2-1) and (2-2) with (2-30) and (2-35) we have

$$\begin{aligned} & r(dx, \mu, E, \mu_o, dE_o)d\mu dE \\ & \quad = \frac{1}{A} \, f(dx, 1, -\mu, E, \mu_o, E_o) \, d\mu dE \\ & \quad = \Sigma(-\mu, E, \mu_o, E_o) \, \frac{dx}{\mu} \, d\mu dE \, \frac{\text{neutrons}}{\text{area} \cdot \text{time}} \, ^* \end{aligned} \tag{2-36}$$

and

$$\begin{aligned} & t(dx, \mu, E, \mu_o, E_o)d\mu dE \\ & \quad = \left(1 - \Sigma_t(E_o) \, \frac{dx}{\mu_o}\right) \delta(\mu - \mu_o)\delta(E - E_o)d\mu dE \, \frac{\text{neutrons}}{\text{area} \cdot \text{time}} \, ^* \\ & \qquad + \frac{1}{A} \, f(dx, 1, \mu, E, \mu_o, E_o)d\mu dE \\ & \quad = \left\{\left(1 - \Sigma_t(E_o) \, \frac{dx}{\mu_o}\right) \delta(\mu - \mu_o)\delta(E - E_o)d\mu dE \right. \\ & \qquad \left. + \Sigma(\mu, E, \mu_o, E_o) \, \frac{dx}{\mu} \, d\mu dE \right\} \frac{\text{neutrons}}{\text{area} \cdot \text{time}} \, ^* \quad . \end{aligned} \tag{2-37}$$

The first term in (2-37) is due to undeflected, transmitted neutrons.

Discretizing as in Eq. (2-5)

$$r_{ij}(dx) = \frac{\Sigma_{ij}^b}{\mu_i} \, dx \tag{2-38}$$

---

* This factor is necessary for the units to come out right. In the ensuing derivation, however, we will neglect it.

$$t_{ij}(dx) = \left(1 - \frac{\Sigma_i^t}{\mu_i} dx\right) \frac{\delta_{ij}}{\Delta\mu_j \Delta E_j} + \frac{\Sigma_{ij}^f}{\mu_i} dx \tag{2-39}$$

where

$$\begin{aligned} \Sigma_{ij}^b &\equiv \Sigma(-\mu_i, E_i, \mu_j, E_j) \\ \Sigma_{ij}^f &\equiv \Sigma(\mu_i, E_i, \mu_j, E_j) \\ \Sigma_i^t &\equiv \Sigma_t(E_i) \quad . \end{aligned} \tag{2-40}$$

Then

$$\rho_{ij}(dx) \equiv \Delta\mu_j \Delta E_j r_{ij}(dx) = \Delta\mu_j \Delta E_j \frac{\Sigma_{ij}^b}{\mu_i} dx$$

$$\tau_{ij}(dx) \equiv \Delta\mu_j \Delta E_j t_{ij}(dx) = \left(1 - \frac{\Sigma_i^t}{\mu_i} dx\right) \delta_{ij} + \Delta\mu_j \Delta E_j \frac{\Sigma_{ij}^f}{\mu_i} dx$$

or defining

$$\begin{aligned} S_{ij}^b &\equiv \Delta\mu_j \Delta E_j \frac{\Sigma_{ij}^b}{\mu_i} \\ S_{ij}^f &\equiv \Delta\mu_j \Delta E_j \frac{\Sigma_{ij}^f}{\mu_i} \\ M_{ij} &\equiv \frac{\Sigma_i^t}{\mu_i} \delta_{ij} \end{aligned} \tag{2-41}$$

we have

$$\rho(dx) = S^b dx \tag{2-42}$$

$$\tau(dx) = (I - M\,dx) + S^f dx = I + (S^f - M)dx \quad . \tag{2-43}$$

These are the equations relating the response matrices for a slab of small thickness dx to the cross-section matrices S^b, S^f and M.

4. Invariant Imbedding Equations

Using the adding relations (2-18) and (2-19) and the relations (2-42) and (2-43) just derived, we can easily obtain the invariant imbedding equations. Thus to first order

$$\rho(x+dx) = \rho(x) + \tau(x)S^b dx[I-\rho(x)S^b dx]^{-1}\tau(x)$$

$$= \rho(x) + \tau(x)S^b dx\,\tau(x)$$

$$\tau(x+dx) = [I + (S^f-M)dx][I-\rho(x)S^b dx]^{-1}\tau(x)$$

$$= [I + (S^f-M)dx + \rho(x)S^b dx]\tau(x)$$

so that

$$\frac{\partial}{\partial x}\rho(x) = \tau(x)S^b\tau(x) \qquad (2-44)$$

$$\frac{\partial}{\partial x}\tau(x) = [\rho(x)S^b + (S^f-M)]\tau(x) \quad . \qquad (2-45)$$

Alternatively

$$\rho(dx+x) = S^b dx + [I+(S^f-M)dx]\rho(x)[I-S^b dx\rho(x)]^{-1}[I+(S^f-M)dx]$$

$$= S^b dx+\rho(x)+(S^f-M)dx\,\rho(x)+\rho(x)S^b dx\,\rho(x)+\rho(x)(S^f-M)dx$$

$$\tau(dx+x) = \tau(x)[I-S^b dx\,\rho(x)]^{-1}[I+(S^f-M)dx]$$

$$= \tau(x)[I+S^b dx\,\rho(x) + (S^f-M)dx]$$

so that

$$\frac{\partial}{\partial x}\rho(x) = S^b+(S^f-M)\rho(x)+\rho(x)(S^f-M)+\rho(x)S^b\rho(x) \qquad (2-46)$$

$$\frac{\partial}{\partial x}\tau(x) = \tau(x)[S^b\rho(x) +(S^f - M)] \quad . \qquad (2-47)$$

These last two differential equations are the invariant imbedding equations in their usual form, although Eqs. (2-44) and (2-45) are equivalent. Our derivation is essentially the same as that given by Shimizu and Mizuta[18] and Mockel[23]. Ambarzumian[4] and Chandrasekhar[5] derived these same equations* from the transport equation using "invariance principles." Detailed particle counting has also been used[11,12], while more recently general mathematical procedures have been developed to go directly from the transport equation to the invariant imbedding equations[14,43]. This is useful when working in more complicated geometries.

For numerical purposes it is advantageous to separate the undeflected transmitted flux from that which is scattered[16]. Thus we define τ^o and τ^s by

$$\tau(x) \equiv \tau^o(x) + \tau^s(x) \tag{2-48}$$

$$\tau^o_{ij}(x) \equiv \exp(-\Sigma^t_i x/\mu_i)\delta_{ij} = \exp(-M_{ij}x) \quad . \tag{2-49}$$

Then the differential equation for the scattered transmission matrix is

$$\frac{\partial}{\partial x}\ \tau^s(x) = \tau^o(x)S^f + \tau^o(x)S^b\rho(x) + \tau^s(x)(S^f - M) + \tau^s(x)S^b\rho(x) \tag{2-50}$$

which bears some resemblance to the reflection equation (2-46).

From Eqs. (2-42) and (2-43) we see that the response functions satisfy the initial conditions

$$\rho(0) = 0 \tag{2-51}$$

*Although in considerably different notation.

$$\tau(0) = I \qquad (\tau^{o}(0) = I \quad , \quad \tau^{s}(0) = 0) \quad . \tag{2-52}$$

Before moving on to diffusion theory, we note that the so-called Stokes' relations[11] are obtained by comparing the right-hand sides of Eqs. (2-44) - (2-47). Thus

$$\tau(x)S^{b}\tau(x) = S^{b} + (S^{f}-M)\rho(x) + \rho(x)(S^{f}-M) + \rho(x)S^{b}\rho(x) \tag{2-53}$$

$$[\rho(x)S^{b} + (S^{f}-M)]\tau(x) = \tau(x)[S^{b}\rho(x) + (S^{f}-M)] \quad . \tag{2-54}$$

These equations will not be used in this thesis. We will return to the invariant imbedding equations, however, when we discuss calculational techniques in Chapter III.

B. Diffusion Theory

1. Definitions and Macroscopic Relations

For the diffusion theory treatment we will work with right and left partial currents instead of right and left angular fluxes. Then for a slab of thickness x with an incident current $j_j^{+}(0)$ in the j^{th} of n energy groups (see Fig. 4), the i^{th} group reflected current is

$$j_i^{-}(0) = \sum_{j=1}^{n} R_{ij}(x) j_j^{+}(0) \tag{2-55}$$

and the i^{th} group transmitted current

$$j_i^{+}(x) = \sum_{j=1}^{n} T_{ij}(x) j_j^{+}(0) \tag{2-56}$$

or in matrix form

$$j^{-}(0) = R\ (x)j^{+}(0) \tag{2-57}$$

$$j^{+}(x) = T\ (x)j^{+}(0) \quad . \tag{2-58}$$

R (x) and T (x) are the reflection and transmission matrices or collectively the response matrices for the diffusion theory approximation. The energy interval ΔE_i does not appear in Eqs. (2-55) and (2-56)

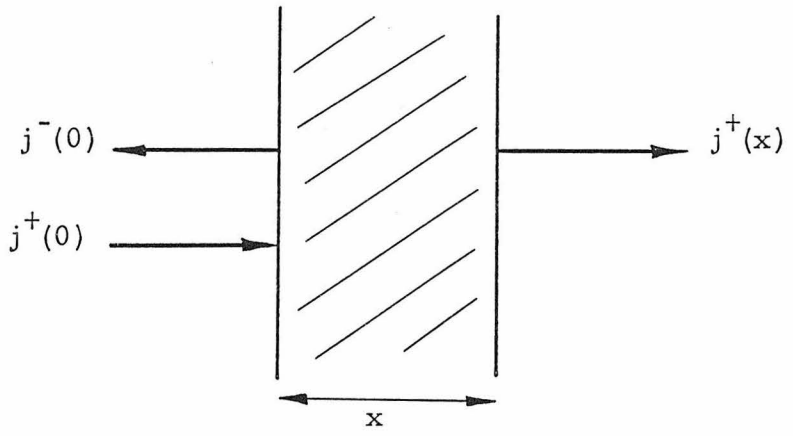

Fig. 4

as it did in Eqs. (2-6) and (2-7) since ΔE_i is lumped within $j_i^{\pm}(x)$ as is customary in diffusion theory. Thus $R_{ij}(x)$ gives the current in group i reflected from a slab of sickness x due to a unit incident current in group j, and similarly for $T_{ij}(x)$. In order to obtain well-defined response matrices, we assume that the angular distribution of the incident and exit currents is the same. Equations (2-57) and (2-58)

are precisely analogous to Eqs. (2-10) and (2-11) in the transport theory development. Identical arguments then lead to the diffusion theory adding relations

$$R(x+y) = R(x) + T(x)R(y)[\,I-R(x)R(y)]^{-1}T(x) \tag{2-59}$$

$$T(x+y) = T(y)[\,I-R(x)R(y)]^{-1}T(x) \tag{2-60}$$

and likewise to the doubling relations and halving scheme.

2. Invariant Imbedding Equations

The diffusion theory invariant imbedding equations can be obtained directly from the adding relations and the relations

$$R(dx) = P\,dx \tag{2-61}$$

$$T(dx) = I + Q\,dx \tag{2-62}$$

which are the analogues of Eqs. (2-42) and (2-43) in the transport theory case. The matrices P and Q are related to the cross-sections in a manner similar to their transport theory analogues and presumably can be determined from detailed microscopic considerations as in Section II. A. 3, although this has not been done.

Instead we derive the invariant imbedding equations directly from the multi-group diffusion equations using the mathematical procedure given by Bailey and Wing[14]. The multi-group diffusion equations may be written in slab geometry as[49]

$$D_j \frac{d^2}{dz^2}\phi_j - \Sigma_{r_j}\phi_j + \sum_{k\neq j}\Sigma_{k\to j}\phi_k + \chi_j\sum_k(\nu\Sigma_f)_k\phi_k = 0 \tag{2-63}$$

$$J_j = - D_j \frac{d}{dz} \phi_j \tag{2-64}$$

or in matrix form

$$\frac{d}{dz} J + S\phi = 0 \tag{2-65}$$

$$\frac{d}{dz} \phi + 3\Sigma J = 0 \tag{2-66}$$

where

$$\Sigma \equiv \begin{bmatrix} 1/3D_1 & 0 & \cdots & 0 \\ 0 & 1/3D_2 & \cdots & 0 \\ \cdot & \cdot & & \cdot \\ \cdot & \cdot & & \cdot \\ \cdot & \cdot & & \cdot \\ 0 & 0 & \cdots & 1/3D_n \end{bmatrix} \tag{2-67}$$

$$S \equiv \begin{bmatrix} -\Sigma_{r_1} + \chi_1 (\nu\Sigma_f)_1 & \Sigma_{2\to 1} + \chi_1 (\nu\Sigma_f)_2 & \cdots & \Sigma_{n\to 1} + \chi_1 (\nu\Sigma_f)_n \\ \Sigma_{1\to 2} + \chi_2 (\nu\Sigma_f)_1 & -\Sigma_{r_2} + \chi_2 (\nu\Sigma_f)_2 & \cdots & \Sigma_{n\to 2} + \chi_2 (\nu\Sigma_f)_n \\ \cdot & \cdot & & \cdot \\ \cdot & \cdot & & \cdot \\ \cdot & \cdot & & \cdot \\ \Sigma_{1\to n} + \chi_n (\nu\Sigma_f)_1 & \Sigma_{2\to n} + \chi_n (\nu\Sigma_f)_2 & \cdots & -\Sigma_{r_n} + \chi_n (\nu\Sigma_f)_n \end{bmatrix} \tag{2-68}$$

Define

$$u \equiv j^+ = \frac{1}{4} \phi + \frac{1}{2} J \tag{2-69}$$

$$v \equiv j^- = \frac{1}{4} \phi - \frac{1}{2} J \quad . \tag{2-70}$$

Then

$$\phi = 2(u+v) \tag{2-71}$$

$$J = u - v \quad . \tag{2-72}$$

Using these expressions in (2-63) and (2-64) we obtain

$$\frac{d}{dz} u - Qu - Pv = 0 \tag{2-73}$$

$$\frac{d}{dz} v + Pu + Qv = 0 \tag{2-74}$$

with

$$P \equiv S + \frac{3}{4} \Sigma \tag{2-75}$$

$$Q \equiv S - \frac{3}{4} \Sigma \quad . \tag{2-76}$$

Now define $u^i(z)$ and $v^i(z)$ to be those solutions of (2-73) and (2-74) such that

$$u^i(0) = \begin{bmatrix} 0 \\ \cdot \\ \cdot \\ \cdot \\ 0 \\ \cdot \\ \cdot \\ \cdot \\ 0 \end{bmatrix}, \quad v^i(x) = \begin{bmatrix} 0 \\ \cdot \\ \cdot \\ \cdot \\ 1 \\ \cdot \\ \cdot \\ \cdot \\ 0 \end{bmatrix} \begin{matrix} 1 \\ \cdot \\ \cdot \\ \cdot \\ i \\ \cdot \\ \cdot \\ \cdot \\ n \end{matrix} \tag{2-77}$$

that is, $u^i(z)$ and $v^i(z)$ are the partial currents due to a unit partial current in group i incident from the right on a slab of thickness x. If we further define

$$\begin{aligned} U &\equiv [u^1 u^2 \ . \ . \ . \ u^n] \\ V &\equiv [v^1 v^2 \ . \ . \ . \ v^n] \end{aligned} \tag{2-78}$$

then U and V must satisfy Eqs. (2-73) and (2-74)

$$\frac{\partial}{\partial z} U(z,x) = QU(z,x) + PV(z,x) \tag{2-79}$$

$$\frac{\partial}{\partial z} V(z,x) = - PU(z,x) - QV(z,x) \tag{2-80}$$

with the boundary conditions

$$U(0,x) = 0 \tag{2-81}$$

$$V(x,x) = I \tag{2-82}$$

where we have explicitly included the slab thickness x as an argument in U and V. Comparison with Eqs. (2-57) and (2-58) shows that

$$R(x) = U(x,x) \tag{2-83}$$

$$T(x) = V(0,x) \tag{2-84}$$

The invariant imbedding equation for R is obtained by considering

$$\frac{\partial}{\partial x} R(x) = U_1(x,x) + U_2(x,x) \tag{2-85}$$

where the subscripts denote partial differentiation. $U_1(x,x)$ is obtained directly from (2-79) as

$$\begin{aligned} U_1(x,x) &= QU(x,x) + PV(x,x) \\ &= QR(x) + P \quad . \end{aligned} \tag{2-86}$$

To get $U_2(x,x)$ we note that $U_2(z,x)$ and $V_2(z,x)$ satisfy the differential equations (2-79) and (2-80) with boundary conditions slightly different from (2-81) and (2-82). Specifically

$$\frac{\partial}{\partial z} U_2(z,x) = Q U_2(z,x) + P V_2(z,x) \tag{2-87}$$

$$\frac{\partial}{\partial z} V_2(z,x) = - P U_2(z,x) - Q V_2(z,x) \tag{2-88}$$

$$U_2(0,x) = 0 \tag{2-89}$$

$$V_2(x,x) = - V_1(x,x) \quad . \tag{2-90}$$

Because the systems of equations are linear, U_2 and V_2 are related to U and V by

$$U_2(z,x) = - U(z,x)V_1(x,x) \tag{2-91}$$

$$V_2(z,x) = - V(z,x)V_1(x,x) \quad . \tag{2-92}$$

In particular

$$\begin{aligned} U_2(x,x) &= - U(x,x)V_1(x,x) \\ &= U(x,x)[\, PU(x,x) + QV(x,x)] \\ &= R(x)[\, PR(x)+Q] \quad . \end{aligned} \tag{2-93}$$

Substituting (2-86) and (2-93) into (2-85) we finally have

$$\frac{\partial}{\partial x} R(x) = P + QR(x) + R(x)Q + R(x)PR(x) \quad . \tag{2-94}$$

Similarly for T we have

$$\begin{aligned} \frac{\partial}{\partial x} T(x) &= V_2(0,x) \\ &= - V(0,x)V_1(x,x) \\ &= V(0,x)[\, PU(x,x) + QV(x,x)] \\ &= T(x)[\, PR(x) + Q] \quad . \end{aligned} \tag{2-95}$$

Equations (2-94) and (2-95) are the diffusion theory invariant imbedding equations analogous to their transport theory counterparts, Eqs. (2-46) and (2-47). For numerical solution in the diffusion theory case, it is not necessary to separate the transmission function into its deflected and undeflected parts as we did in transport theory (cf. Eqs. (2-48) and (2-49)).

3. One-group Response Functions

In the case of one energy group we can obtain analytic expressions for the response functions. Although the quantitative results are only of academic interest, the qualitative behavior is similar to that in the general multi-group problem.

The one-group diffusion equation in slab geometry is

$$\frac{d^2}{dz^2}\,\phi(z) + B^2\phi(z) = 0 \quad ; \qquad B^2 \equiv \frac{\nu\Sigma_f - \Sigma_a}{D} \tag{2-96}$$

which has the general solution

$$\phi(z) = \alpha \sin Bx + \beta \cos Bx \quad . \tag{2-97}$$

If the slab extends from 0 to x with an incident unit current from the left, then the boundary conditions are

$$j^-(x) = \frac{1}{4}\,\phi(x) + \frac{D}{2}\,\phi'(x) = 0 \tag{2-98}$$

$$j^+(0) = \frac{1}{4}\,\phi(0) - \frac{D}{2}\,\phi'(0) = 1 \quad . \tag{2-99}$$

Substituting (2-97) into (2-98) and (2-99) we can solve for the constants α and β to obtain

$$\phi(z) = \frac{\sin B(x-z)+2DB\cos B(x-z)}{[\frac{1}{4}-(DB)^2]\sin Bx+DB\cos Bx} \tag{2-100}$$

so that the response functions are

$$R(x)\equiv j^-(0) = \frac{1}{4}\phi(0) + \frac{D}{2}\phi'(0) = \frac{[\frac{1}{4}+(DB)^2]\sin Bx}{[\frac{1}{4}-(DB)^2]\sin Bx+DB\cos Bx} \tag{2-101}$$

$$T(x) \equiv j^+(x) = \frac{1}{4}\phi(x) - \frac{D}{2}\phi'(x) = \frac{DB}{[\frac{1}{4}-(DB)^2]\sin Bx+DB\cos Bx} \tag{2-102}$$

Finally defining

$$P \equiv \frac{1}{D}[\tfrac{1}{4}+(DB)^2] \tag{2-103}$$

$$Q \equiv -\frac{1}{D}[\tfrac{1}{4}-(DB)^2] \tag{2-104}$$

(which is consistent with Eqs. (2-75) and (2-76)) we have

$$R(x) = \frac{P\sin Bx}{-Q\sin Bx+B\cos Bx} \tag{2-105}$$

$$T(x) = \frac{B}{-Q\sin Bx+B\cos Bx} = \frac{B}{P\sin Bx}R(x) \quad . \tag{2-106}$$

In the case of a non-multiplying medium

$$\Sigma_f = 0 \quad \text{so} \quad B^2 = -\frac{\Sigma_a}{D} = -\kappa^2 \tag{2-107}$$

$$P = \frac{1}{D}[\tfrac{1}{4}-(D\kappa)^2] = \frac{1}{4D}-\Sigma_a \tag{2-108}$$

$$Q = -\frac{1}{D}[\tfrac{1}{4}+(D\kappa)^2] = -\frac{1}{4D}-\Sigma_a \tag{2-109}$$

and

$$R(x) = \frac{P\sinh\kappa x}{-Q\sinh\kappa x+\kappa\cosh\kappa x} \tag{2-110}$$

$$T(x) = \frac{\kappa}{-Q \sinh \kappa x + \kappa \cosh \kappa x} \quad . \tag{2-111}$$

Equations (2-105), (2-106), (2-110), and (2-111) were first derived for neutron diffusion by Selengut[28] and Mizuta (in Shimizu[29]), although Stokes[1] had obtained the analogous equations for light a hundred years earlier.

Representative response functions are plotted in Fig. 5 for both a multiplying and non-multiplying material. Note that in the multiplying case there is a critical thickness x_c for which R and T become infinite. This critical thickness is obtained by setting the denominator of Eqs. (2-105) and (2-106) equal to zero. Then

$$\tan Bx_c = \frac{-DB}{[\frac{1}{4} - (DB)^2]} \tag{2-112}$$

or

$$\tan \frac{Bx_c}{2} = \frac{1}{2DB} \tag{2-113}$$

which is the usual diffusion theory result for the boundary conditions $j^+(0) = 0$ and $j^-(x_c) = 0$.

Using Eq. (2-112) in (2-105) we also have

$$R(x_c/2) = 1 \quad . \tag{2-114}$$

More will be said about this relationship in Section C of the next Chapter. Note also that (2-114) can be obtained directly from the doubling relation

$$R(x) = R(x/2) + \frac{R(x/2)T^2(x/2)}{1 - R^2(x/2)} \quad .$$

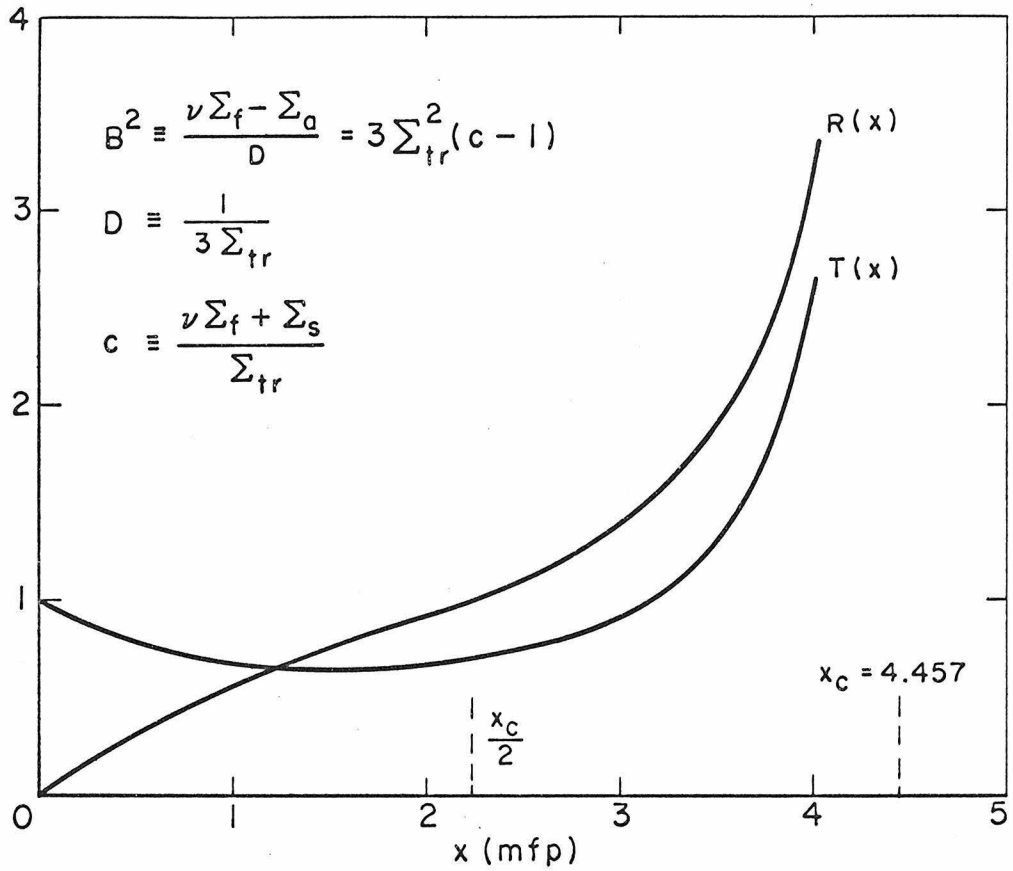

Fig. 5a Response functions for multiplying material with $\Sigma_{tr} = 1$, $c = 1.1$ ($D = 1/3$, $B^2 = .3$).

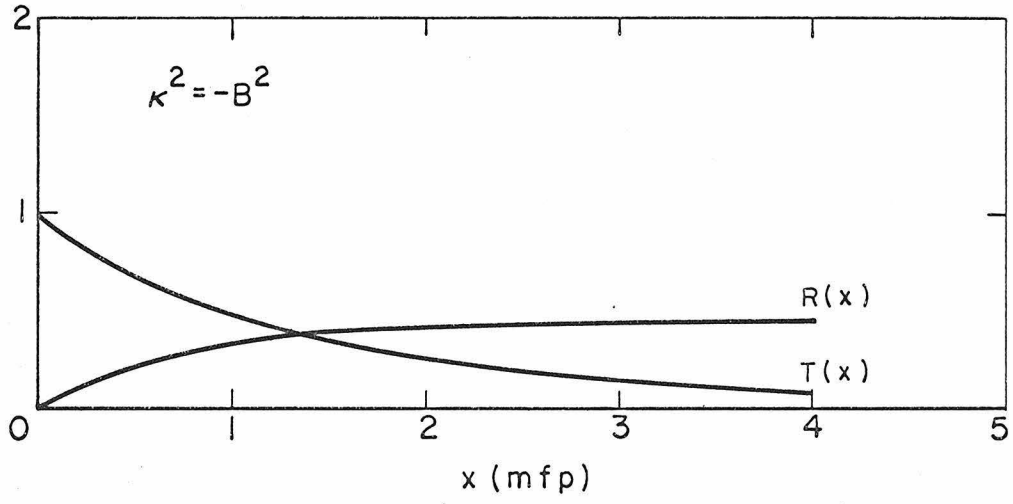

Fig. 5b Response functions for non-multiplying material with $\Sigma_{tr} = 1$, $c = .9$ ($D = 1/3$, $\kappa^2 = .3$).

III. USE OF RESPONSE FUNCTIONS IN CALCULATIONS

A. Albedo and Shielding Problems

All previous work with response functions has been concerned with utilizing them calculationally. It is apparent that the techniques we have developed are immediately applicable to certain problems, for example albedo and shielding problems, since here the quantities of interest are precisely the reflection and transmission functions, respectively.

Albedo (i.e. reflection)problems arise primarily in astrophysics, however, and are of only limited importance in reactor physics. Bellman et al[50] have done extensive one-speed calculations using straightforward step-by-step integration of the invariant imbedding reflection equation. As we pointed out in a recent article[49], a considerably faster procedure is to do one numerical integration of both invariant imbedding equations and then go to larger thicknesses using the doubling relations.

Shielding problems, on the other hand, are of considerable importance in reactor physics. Response functions have been used by Beissner[15,16] and Mathews et al[17] for neutron penetration and by Peebles and Plesset[26], Shimizu and Mizuta[18-20], and Aronson and Yarmush[34] for gamma ray penetration.

Mathews et al developed an exponential integration technique to solve the invariant imbedding equations. Although more efficient than the Runge-Kutta or finite difference methods, their exponential method is still a step-by-step procedure. If instead one doubles

TABLE I

Shielding Problems

Material	No. of Energy Groups	No. of Angle Groups	Initial Step Size (cm) II[b]	Initial Step Size (cm) D+II[c]	Time for Calculation(s)[a] II	Time for Calculation(s)[a] D+II	Numerical Agreement τ_{ij}	Numerical Agreement TOTFLX[d]
H_2O(210 cm)	6	2	0.00001	0.0128	237	5.0+(6.6)[e]	3%(15%)[f]	3%
Fe(10.16 cm)	5	2	0.00001	0.0198	13.0	2.0+(3.5)	4%(10%)	4%
Polythylene(30.48 cm)	5	2	0.00001	0.0149	31.7	2.6+(3.5)	4%(15%)	4%
Fe-Poly-Fe (2.99 cm) (15.24 cm) (10.16 cm)	5	2	0.00001	0.0117 0.0149 0.0198	36.9	6.5+(10.4)	7%(15%)	7%

[a] All times are for calculation only(i.e., exclusive of input and output) on an IBM-7094.

[b] Invariant imbedding.

[c] Doubling plus invariant imbedding.

[d] The total transmitted flux due to a unit, isotropic, fission source.

[e] The first time is that used in doubling. The time in parenthesis is that used by the invariant imbedding (Runge-Kutta integration) starting routine.

[f] The first percentage is the average difference in individual matrix elements at the final thickness obtained by the two methods. The percentage in parenthesis is the maximum difference.

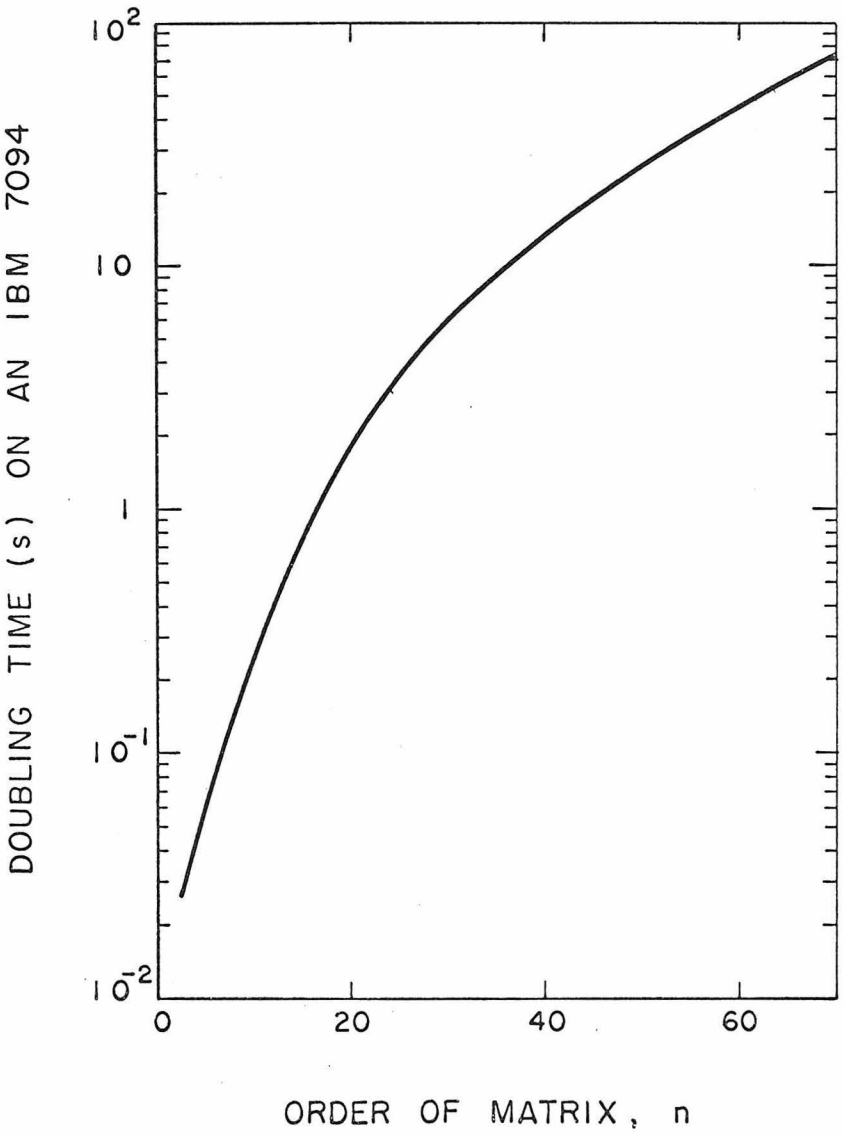

Fig. 6 Doubling time vs order of matrix.

after the first integration step, the computation time for large thicknesses is greatly reduced. Table I shows a time comparison between this latter technique (D + II) and that used by Mathews et al (II). As can be seen, the D + II method is significantly faster, especially for the thick water shield. Since Mathews et al indicated that their calculations were competitive with Monte Carlo for thick shields and with discrete ordinates for anisotropic scattering, it appears that the D + II method is the best available for these particular problems and probably for more general problems as well. As a guide for further calculations, an approximate graph of doubling time vs. matrix size is given in Fig. 6.

Note that more than half the computation time for the D + II calculations was spent generating the response matrices using the Runge-Kutta method. Perhaps a better starting technique would be to use Eqs. (2-42) and (2-43) to generate the response matrices for a very small thickness. Although more doubling would then be required, the initialization time would be less. Thus the total time should be comparable while the programming would be much simpler.

Shimizu and Mizuta[18-20] have introduced a modified transmission function which satisfies an even simpler doubling relation than Eqs. (2-21) and (2-22). An additional approximation must be made, however, to calculate the modified transmission function. Although their doubling technique should actually be slightly faster than ours, they have not redone Mathews' calculations (Table I) so no direct time comparison can be made.

B. Criticality Problems

Although it is less obvious, we can also use response functions to calculate criticality. Throughout the previous sections of this thesis we have assumed that the response functions were well-defined. For a slab of multiplying material, however, there exists a critical thickness above which the response functions are not defined. As the slab thickness approaches this critical thickness from below, the response functions approach infinity due to neutron multiplication.

Thus a straightforward technique for determining criticality is to calculate the response functions for increasing slab thicknesses until they become infinite. Using invariant imbedding one need only consider the reflection function. Mingle[25] has taken this approach, although for numerical reasons he makes the transformation,

$$\Lambda(x) = \frac{\rho(x)-1}{\rho(x)+1} \quad . \tag{3-1}$$

The reflection equation (2-46) can then be re-written as a differential equation for Λ with initial condition $\Lambda(0) = -1$ and critical condition $\Lambda(x_c) = 1$. The differential equation for Λ is then integrated step-by-step to obtain the critical thickness x_c. Numerical results are given[25] assuming mono-energetic transport and c (the number of secondaries per collision) = 2.

An alternative statement of the criticality condition was given in Chapter II as

$$\det[I - \rho(x)\rho(y)] = 0 \tag{2-20}$$

for a slab of thickness $x + y$. This is a special case of the more

general relation

$$\det[\lambda I - \rho(x)\rho(y)] = 0 \quad . \tag{3-2}$$

As shown physically by Shimizu[29] and mathematically by Ribarič[27], the largest eigenvalue λ_o (i.e. the spectral radius) is the multiplication constant. Thus the criticality condition (2-20) is simply that the spectral radius $\lambda_o = 1$.

Shimizu et al[30] used Eq. (3-2) with $x = y$ to determine the multiplication constant of a symmetrical slab reactor with various reflectors. The reflection matrices were calculated exactly using two-group diffusion theory for a fixed thickness and composition of the reactor.

It is also possible to use response matrices for a criticality search on the thickness. By generating the initial response matrices by invariant imbedding and then using adding and doubling* together with the criticality condition

$$\det[I - \rho^2(x)] = 0 \tag{3-3}$$

(i.e. Eq. (2-20) with $x = y$), we can develop an efficient procedure for the criticality search. A flow chart of this procedure for a two-region, symmetrical slab reactor is given in Fig. 7. The actual implementation of condition (3-3) is based upon the observation that for a subcritical reactor $\det[I - \rho^2(x)] > 0$, while for a supercritical one $\det[I - \rho^2(x)] < 0$.

---

*Halving is avoided as it is slower than adding and doubling.

Two-region, symmetrical slab reactor

Given: 1. Core composition
2. Reflector composition
3. Reflector thickness, x_r

Calculate: Critical thickness, $x_c \pm \delta$

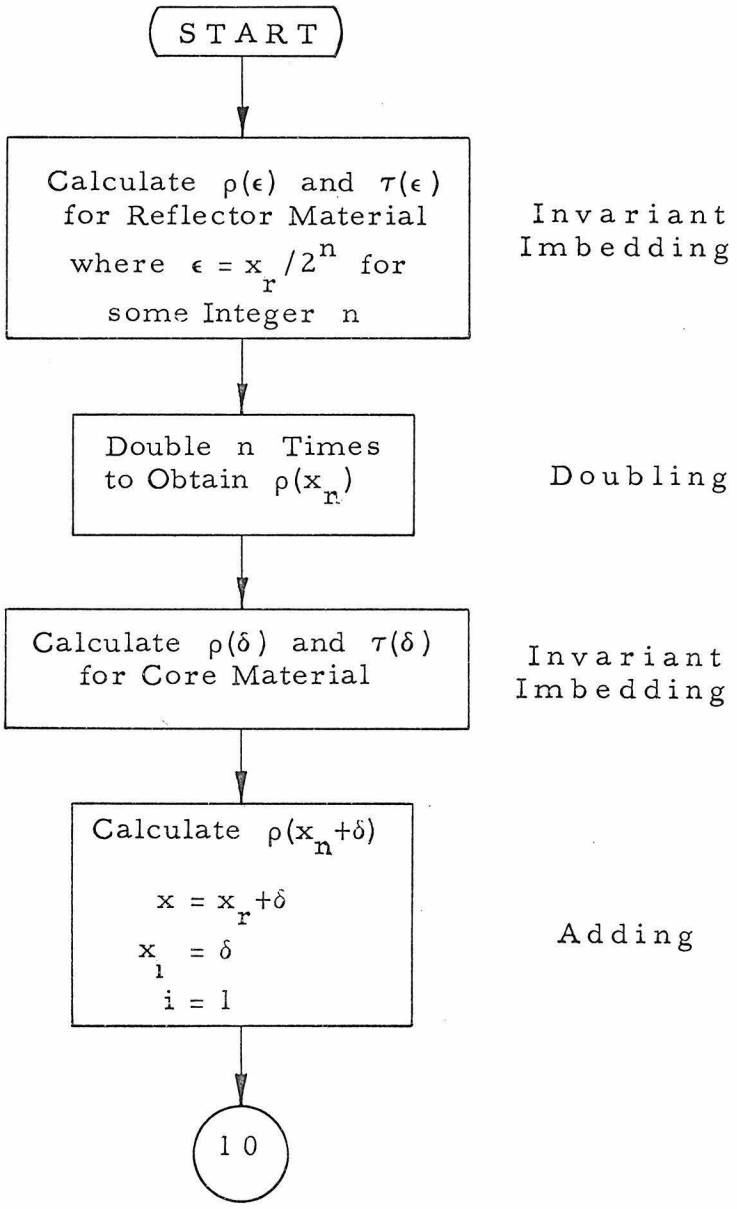

Fig. 7a

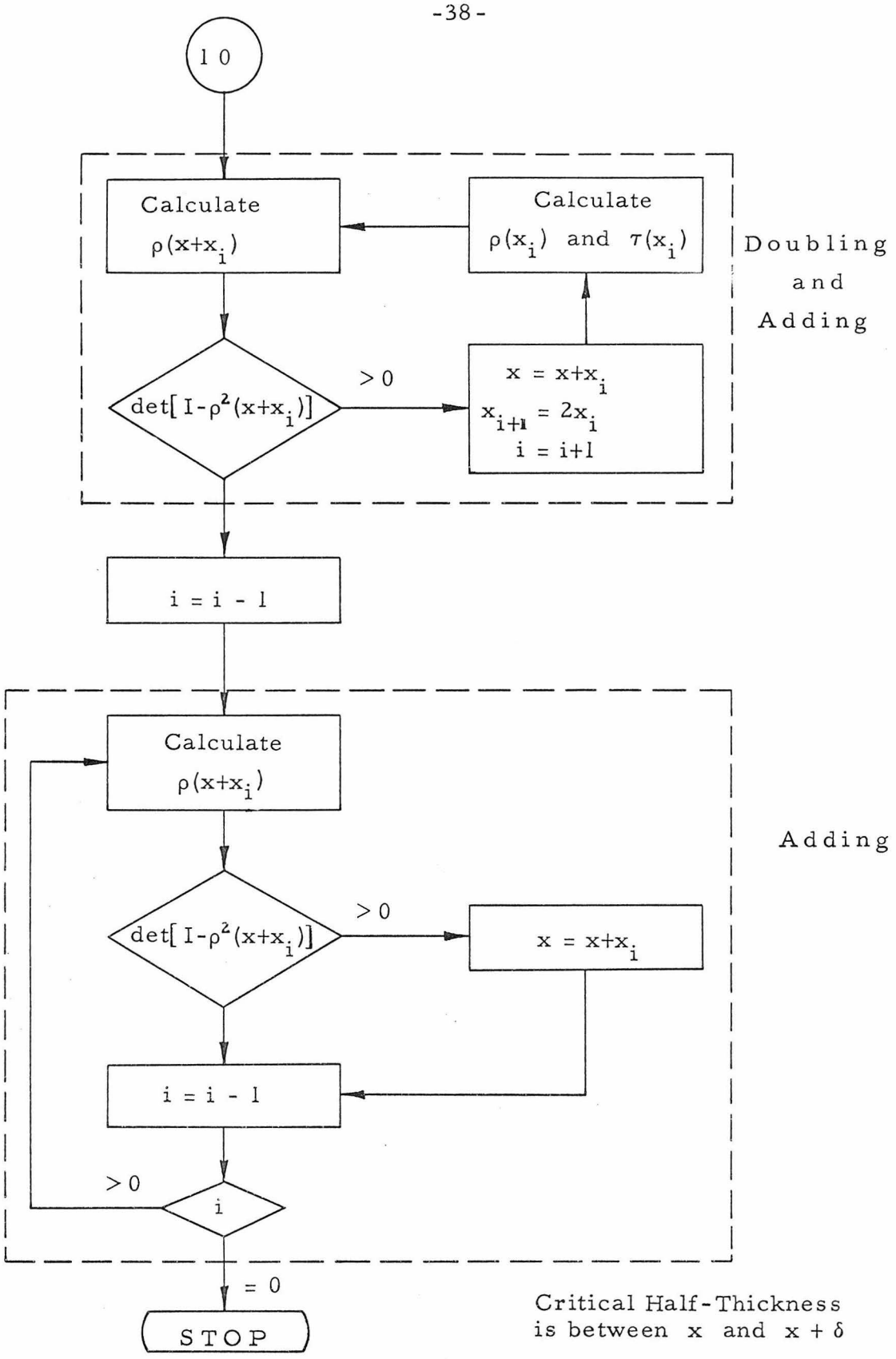
1 0
Calculate
$\rho(x+x_i)$
Calculate
$\rho(x_i)$ and $\tau(x_i)$
Doubling
and
Adding
$\det[I-\rho^2(x+x_i)]$
> 0
$x = x+x_i$
$x_{i+1} = 2x_i$
$i = i+1$
$i = i - 1$
Calculate
$\rho(x+x_i)$
Adding
$\det[I-\rho^2(x+x_i)]$
> 0
$x = x+x_i$
$i = i - 1$
> 0
i
= 0
STOP
Critical Half-Thickness
is between x and x + δ

Fig. 7b

TABLE II

Criticality Problems

Material	No. of Energy Groups	No. of Angle Groups	Initial Step Size(mfp)[a]		Time for Calculation(s)[b]		Critical Thickness(mfp)	
			II[c]	D+A+II[d]	II	D+A+II	II	D+A+II
Hypothetical	1	3	0.01	0.00005	2.2	0.78 +(0.05)[e]	0.6154	0.6155
isotropic	1	5	0.01	0.00005	7.0	1.6 +(0.2)	0.6220	0.6221
scattering	1	7	0.01	0.00005	16.3	3.4 +(0.3)	0.6220	0.6221
material	1	11	0.01	0.00005	53.0	10.0 +(1.1)	0.6217	0.6221
c = 2.0								

[a] Mean free paths.

[b] All times are for calculation only (i.e., exclusive of input and output) on an IBM-7094.

[c] Invariant imbedding.

[d] Doubling and adding plus invariant imbedding.

[e] The first time is that used in doubling and adding. The time in parenthesis is that used by the invariant imbedding (Runge-Kutta integration) starting routine.

As might be expected this procedure is considerably faster than the step-by-step integration performed by Mingle. The time comparison for the problem considered by Mingle[25] is given in Table II.

Generally one is interested in more than just the critical thickness. Response function techniques can also be used to get the internal neutron distribution. Thus at critical, no incident flux $\phi^+(0)$ is necessary to maintain an internal neutron flux. Equation (2-13) then becomes

$$\phi^+(x) = \rho(x)\phi^-(x) \tag{3-4}$$

which together with Eq. (2-14)

$$\phi^-(x) = \rho(y)\phi^+(x) \tag{2-14}$$

gives

$$[I - \rho(x)\rho(y)]\,\phi^+(x) = 0 \tag{3-5}$$

$$[I - \rho(y)\rho(x)]\,\phi^-(x) = 0 \quad . \tag{3-6}$$

Hence the angular fluxes $\phi^+(x)$ and $\phi^-(x)$ are just the eigenvectors corresponding to the $\lambda = 1$ eigenvalue for the matrices $\rho(x)\rho(y)$ and $\rho(y)\rho(x)$, respectively. For a symmetrical reactor we can set $y = x$, find the solution $\phi^+(x) = \phi^-(x)$ to

$$[I - \rho^2(x)]\,\phi^{\pm}(x) = 0 \tag{3-7}$$

and use the relations

$$\phi^-(x+h) = \tau^{-1}(h)[\phi^-(x) - \rho(h)\phi^+(x)] \tag{3-8}$$

$$\phi^{+}(x+h) = \tau(h)\phi^{+}(x) + \rho(h)\phi^{-}(x+h) \qquad (3-9)$$

(cf. Eqs. (2-12) and (2-13)) to get the angular flux at increments of thickness h within the reactor.

Shimizu et al[30] have carried out this procedure in the diffusion theory case and have shown it to be much faster than the conventional finite difference method of solution.

Unfortunately in the transport theory case, the stepping procedure given by Eqs. (3-8) and (3-9) is numerically unstable. One can still use Eqs. (3-5) and (3-6) to obtain accurate angular fluxes. The normalization, however, is arbitrary so that if one wants to relate the flux at one point to that at another in order to obtain a spatial flux shape, some sort of stepping procedure is required. As only Eqs. (3-8) and (3-9) have been tried, it may be possible to find a simple alternative which is stable.

C. Other Geometries

As reactors are never made in the form of infinite slabs, it is clearly desirable to have criticality techniques which are applicable to more general geometries. To this end Aoki and Shimizu[31] extended their response matrix method to two-dimensional reactors made up of rectangular rods. The response matrices of each rectangular rod were calculated exactly using two-group diffusion theory. An iterative procedure was then used to obtain the criticality constant and internal flux much faster than the conventional finite difference

method. This technique, however, is limited to two or at most three energy groups, since the response matrices are obtained analytically for each rod.

Another possibility for extension to other geometries is to generalize the invariant imbedding equations. For example, in spherical and infinite cylindrical geometry the invariant imbedding equations can be derived[44-46] and perhaps solved[47], but the doubling relations no longer hold. Without them it becomes necessary to integrate the invariant imbedding equations step-by-step which is prohibitively time-consuming for matrices of order larger than about 10.

For a finite cylinder, however, made up of disks as in a stack of coins, we can obtain doubling relations. Now, though, the incident beam is no longer introduced uniformly, but rather as a δ-function in the radial variable on the top of the cylinder as suggested by Mathews[51]. The resulting problem in the transport theory case is similar to the "searchlight problem" considered previously by Chandrasekhar[52]. Mathews' mathematical statement of the problem is incomplete, however, and no derivation was given. In Appendices A and B we derive both the transport and diffusion theory invariant imbedding equations, although we have been unable to solve them. The source of the difficulty is the presence of radial δ-function terms in the equations due to the incident beam. If these terms could be handled in some fashion so that the invariant imbedding equations could be solved for a thin disk, then the adding and doubling relations could be expected to provide an efficient means of calculating the critical height.

IV. FEASIBILITY OF USING RESPONSE FUNCTIONS IN EXPERIMENTS

Two kinds of experiments are presently being used in fast reactor physics, cross-section experiments done on small samples of materials and critical experiments done on full-size mock-ups of possible reactors. Both have notable shortcomings; cross-section experiments are time-consuming, while critical experiments are expensive. Much of the incentive for this thesis was provided by the possibility of doing response function experiments on moderate-sized samples as an alternative to the differential and integral experiments mentioned above. In this chapter we will show how one can use response function experiments both to obtain cross-sections quicker and critical information cheaper than at present. The required experimental set-up will be described followed by a study of how errors in the measured response functions propagate to the final quantities of interest.

A. Cross-section Determination - - Multiple Scattering Correction

1. Fast Cross-sections

A major stumbling block to accurate fast reactor calculations at present is the inaccuracy of many important cross-sections. Sensitivity studies[53-56] have shown that improvements in calculations can come only with improvements in cross-section measurements.*

*The situation is summed up by Greebler in (54) with "It is evident that the present status of fast reactor cross-section information is very confusing. Until this is resolved by a suitable program of energy point-wise and integral critical measurements, physics predictions of fast power reactor performance will remain highly unreliable." (p. 32)

Cross-section measurements, however, are difficult to carry out because they are differential in nature and because the various interaction processes must be separated. Moreover cross-sections are required for all constituent nuclides of a proposed reactor. Using this detailed microscopic information, an equivalent homogeneous core is calculated and average group cross-sections for the homogeneous material are obtained. They are then further combined into cross-section matrices which can be used in diffusion or transport calculations. A long, involved procedure[57] has been used to get from the detailed microscopic information to the cross-section matrices. It is the latter, however, that the reactor designer needs for his calculations. He is not much interested in the details of how they were obtained and in fact would prefer to avoid such tedious cross-section preparation procedures. Response function experiments provide a straightforward procedure for directly obtaining cross-section matrices for reactor design.

Response functions are first measured for some moderate thickness of the material of interest. The halving scheme developed in Chapter II then allows us to obtain response matrices for a differential thickness of the same material. Finally the cross-section matrices are simply related to the differential response matrices as shown previously (Eqs. (2-42) and (2-43)).

The advantages of this technique for cross-section determination are

(1) The experiment is integral rather than differential

with respect to the thickness of the slab, since the halving scheme essentially provides us with a sound technique for multiple scattering correction, and

(2) The separate interaction processes, such as fission, capture, inelastic scattering, and elastic scattering, need not be separately measured. Rather the cross-section matrices obtained are precisely in the form needed for input to a standard diffusion or transport theory code (see Appendix C). This point is most significant. It means that cross-section preparation problems are replaced by response matrix measurements. The measurements can be made on the same material to be considered for use in a reactor and may be slab-wise inhomogeneous. The halving technique will then produce homogenized cross-section matrices.

Description of experiment

Measurement of the transport theory response matrices requires knowledge of the incident neutron angle and energy as well as the exit neutron angle and energy.* This can be accomplished with the experimental set-up of Fig. 8, which is analogous to that described by Orphan, Carlson, and Hoot[58] for gamma-rays. An electron linear accelerator sends pulses of electrons into a heavy metal target (e.g. U or W). The electrons are decelerated producing bremsstrahlung which in turn produces neutrons by (γ,n) and

*The diffusion theory matrices are simply obtained from the transport theory matrices by angular integration.

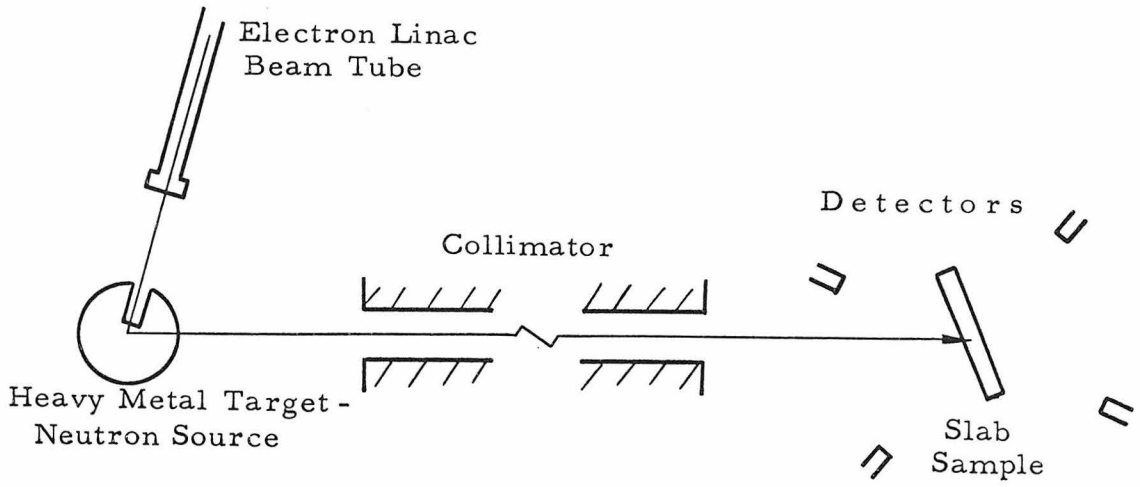

Fig. 8 Schematic of Experimental Set-up.

(γ, f) reactions. The resulting pulse of neutrons* travels down a flight path of ~ 15 m to the slab of material for which the response matrices are being measured. Energy sensitive neutron detectors (e.g. proton-recoil or Li^6 sandwich detectors[60,61]) are placed at various angles with respect to the slab. A time-of-flight measurement determines the energy of the incident neutron while pulse-height analysis determines the exit neutron energy. Thus both incident and exit energies are obtained in a single measurement.

*For a uranium target the". . . photoneutron-photofission spectrum is similar to the neutron-induced fission spectrum." (p. 525 of Ref. 59) It would probably be desirable to add a small amount of thermalizing material to the target in order to obtain a broader, lower energy spectrum.

Similarly measurements can be made for all exit angles simultaneously. Thus for each exit angle θ_i, detectors are placed at various azimuthal positions in order to carry out the azimuthal integration necessitated by our definition of the response functions (cf. Fig. 1). Clearly many detectors will be required. By doing the azimuthal integration with the detectors, however, we can take advantage of symmetry to introduce the incident neutrons as a parallel beam, rather than in the conical fashion indicated in Fig. 1. To obtain complete response functions the slab must be rotated and the measurements repeated for different incident angles, θ_j.

In order to use the halving scheme developed in Chapter II, we must convert the measured response functions to response matrices by introducing a group structure in both energy and angle. Although it is desirable to use as many groups as possible to avoid flux weighting problems, the order of the matrices involved is the product of the number of energies times the number of angles. In practice this will probably limit the fineness of the energy and angular meshes so that the resulting matrices are of order 100 or less.

Expected count rates

An order of magnitude estimate of the expected detector count rates can be made, based on the characteristics of the General Atomic LINAC. For a uranium target (see Fig. 8) the average neutron yield rate is 2×10^{14} neutrons/s[62]. For a 15.5 m flight path this produces a collimated, 15 cm diameter beam[58]. Thus the number

of neutrons per unit time incident on the slab sample is

$$\frac{\pi(7.5)^2}{4\pi(1550)^2} \times 2 \times 10^{14} = 1.2 \times 10^9 \text{ neutrons/s} \quad .$$

In the next sub-section we will show that the optimum slab thickness is about half a mean free path. Assuming an average value of $\mu = .5$ for the incident direction, then a fraction

$$1 - e^{-(\Sigma_t x/\mu)} = 1 - e^{-1} \approx .6$$

of the incident neutrons will interact with the sample (cf. Eq. (2-49)). The materials of interest in fast reactors are generally either slightly absorbing (Na, Fe) or slightly multiplying ($PuC-UC, PuO_2-UO_2$). In either case the fraction leaving the slab after experiencing an interaction will be roughly the same as the fraction interacting. Accordingly the number of neutrons per unit time arising from an interaction and leaving the slab will be about

$$.6 \times 1.2 \times 10^9 = 7 \times 10^8 \text{ neutrons/s} \quad .$$

If these neutrons were to leave isotropically, then a detector positioned 1.5 m* away would receive a flux of

$$\frac{\pi(1)^2}{4\pi(150)^2} \times 7 \times 10^8 = 8 \times 10^3 \text{ neutrons/(cm}^2\text{s)} \quad .$$

This compares with a flux level of 10^5 $cm^{-2}s^{-1}$ for Bennett's

*This distance is expected to give adequate angular resolution needed to account for the fact that the exit angular flux is not actually isotropic. Obviously a smaller distance would be desirable to increase the flux.

proton-recoil measurements[63] ,which gave a count rate of 2500 counts/s split roughly half and half between neutrons and background gammas.

Sensitivity of cross-sections to the experimental slab thickness

Given the material to be studied and the experimental set-up, the only remaining experimental variable is the slab thickness. Large thicknesses are desirable because of higher counting rates, hence less statistical error in a given time. As the slab thickness increases, however, the propagation of errors from the measured response matrices to the calculated cross-sections through the halving technique increases. The result is that there is an "optimum" experimental thickness which "minimizes" statistical errors in the cross-sections.

In order to make this quantitative, we have simulated experiments on various thicknesses of the PuC-UC core material considered by Moorhead in his sensitivity study[53]. Using 5 energies and 2 angles, response matrices were generated at several thicknesses of material from the assumed cross-sections. To simulate experimental statistical errors, we added normally distributed errors (with a 1% standard deviation) to each element of the response matrices.* Using these response matrices we then halved down to a small thickness (2^{-10} cm) to obtain the "experimental" cross-sections.

*With one exception - - for small thicknesses no errors were added to the main diagonal of the transmission matrix as these elements are due mainly to the undeflected beam and would be known more accurately than the others.

Finally these "experimental" cross-sections were compared to the assumed cross-sections. The resulting differences in the cross-sections were random (although correlated to the imposed response matrix errors) and the standard deviation of their differences gives a measure of the propagation of error through the halving procedure.

The actual results of this study are given in Table III. In the first row no errors were imposed on the response matrices (first two columns). The resulting errors in the calculated cross-sections (succeeding columns) are negligible and are due to the higher order terms in the relations (2-42) and (2-43). The succeeding rows in Table III simulate five experiments at each of four slab thicknesses. The standard deviations (σ_b and σ_f) of the cross-section errors are averaged at each thickness to give a quantitative measure of the propagation of error. These errors increase with increasing slab thickness as shown in Fig. 9. The count rate errors, however, decrease with increasing thickness as mentioned before. The "optimum" experimental thickness is that for which the rate of increase of the propagated errors with increasing thickness is equal to the rate of decrease of the count rate errors. A quantitative measure of these rates is the sensitivity, commonly used in control systems theory[64].

The sensitivity S_x^σ is defined as the percentage change in σ per percentage change in x. Mathematically

$$S_x^\sigma \equiv \frac{\partial\sigma/\sigma}{\partial x/x} \quad . \tag{4-1}$$

TABLE III

Propagation of Errors Study

Thickness	x		.5 cm[a]		1.0 cm[a]		2.0 cm		4.0 cm	
Standard Deviation (%)	$\sigma_{R(x)}$	$\sigma_{T(x)}$	σ_b	σ_f	σ_b	σ_f	σ_b	σ_f	σ_b	σ_f
"Control"	0	0	.04	.04	.04	.04	.04	.04	.07	.03
"Experiment"	- -	- -	- -	- -	- -	- -	- -	- -	- -	- -
1	1.02	1.06	1.38	1.32	1.85	1.76	3.04	3.14	9.01	14.0
2	1.03	1.00	1.39	1.33	1.85	1.86	3.06	3.39	7.22	12.2
3	1.03	1.09	1.25	1.52	1.61	2.04	2.48	3.46	6.74	12.4
4	.95	1.00	1.27	1.45	1.71	1.97	2.93	3.49	7.22	13.1
5	1.00	.98	1.27	1.24	1.67	1.64	2.86	3.13	7.46	14.7
	- -	- -	- -	- -	- -	- -	- -	- -	- -	- -
Average	1.01	1.03	1.31	1.37	1.74	1.85	2.87	3.32	7.53	13.3

[a]No errors were added to the main diagonal of the transmission matrix at these thicknesses.

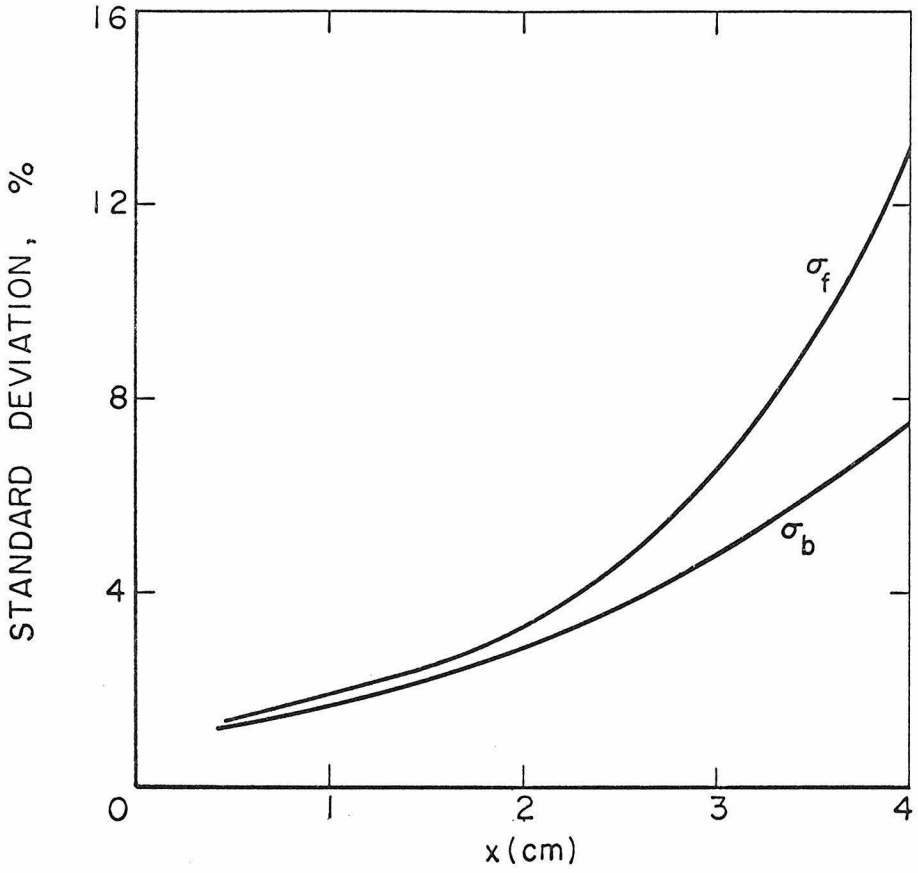

Fig. 9 Propagation of error as a function of experimental slab thickness.

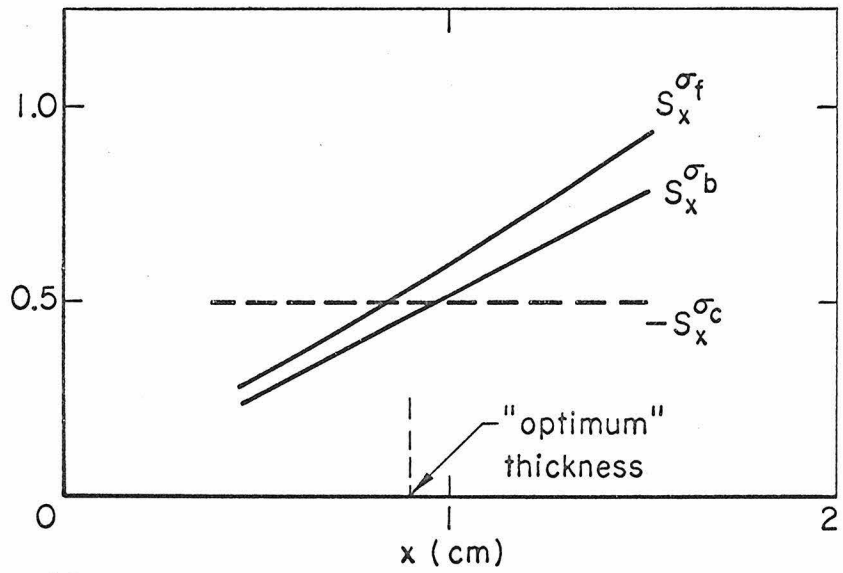

Fig. 10 Determination of "optimum" thickness.

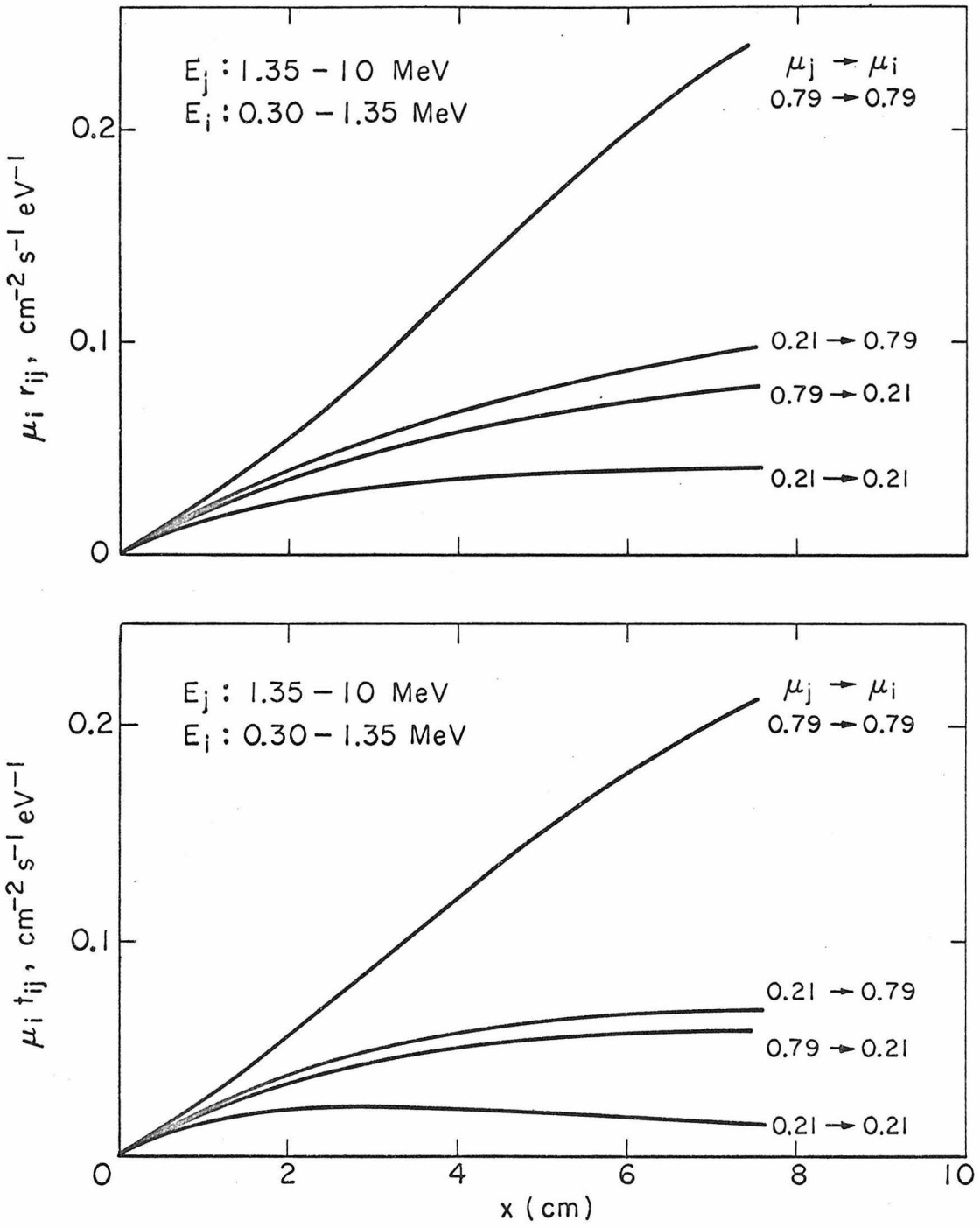

Fig. 11 Representative response matrix elements for PuC-UC mixture.

The sensitivities of σ_b and σ_f are obtained by graphically differentiating Fig. 9 and are shown in Fig. 10. To calculate the sensitivity of the count rate error, we note that if n neutrons are counted, the statistical error is $\sqrt{n}$.[65] Thus the relative count rate error is

$$\sigma_c = \frac{\sqrt{n}}{n} = \frac{1}{\sqrt{n}} \quad .$$

For thin slabs the count rate increases nearly linearly with thickness as shown in Fig. 11. Thus we can write

$$\sigma_c = \frac{1}{\sqrt{n_o x}}$$

for some constant n_o, and hence

$$S_x^{\sigma_c} = \frac{\partial \sigma_c / \sigma_c}{\partial x / x} = \frac{x}{\sigma_c} \frac{\partial \sigma_c}{\partial x} = -\frac{1}{2} \quad .$$

From our previous remarks, the "optimum" thickness is just that for which the magnitude of this sensitivity is equal to that of the propagated error sensitivities. For the PuC-UC core material this occurs at about .9 cm (see Fig. 10).

Nowhere in the above have we mentioned systematic errors due, for example, to fluctuations in the incident beam strength and uncertainties in the detector efficiencies. In practice they may well determine the actual accuracy attainable.

Halving difficulty

In Chapter II we mentioned a difficulty in halving when the slab thickness approaches the mean free path of the lowest energy group. For the material and group structure just studied this

thickness is about 2 cm. At this thickness some of the curves in Fig. 11 have begun to flatten out or even decrease. For "thin" slabs only 3 - 5 iterations are generally required for halving. However, for 1.0 cm of the PuC-UC core material, 12 iterations were required, while for 2.0 cm the scheme given by Eqs. (2-26) - (2-29) oscillated and eventually diverged.

In order to overcome this instability, various ad hoc strategems have been tried. First the halving scheme was "symmetrized" to

$$\rho_{k+1}(x/2) = 1/2\,\rho_k(x/2) + 1/4\{2\rho(x) - \tau_k(x/2)\rho_k(x/2)\tau_k^{-1}(x/2)\tau(x) + \tau(x)\tau_k^{-1}(x/2)\rho_k(x/2)\tau_k(x/2)\}$$

$$\tau_{k+1}(x/2) = 1/2\,\tau_k(x/2) + 1/4\{[I-\rho_{k+1}^2(x/2)]\,\tau_k^{-1}(x/2)\tau(x) + \tau(x)\tau_k^{-1}(x/2)[I-\rho_{k+1}^2(x/2)]\}$$

This produced convergence for $x = 2.0$ cm (after 20 iterations) but not for $x = 4.0$ cm. To achieve convergence for greater thicknesses a convergence parameter "a" was introduced to give the following iteration scheme

$$\rho_{k+1}(x/2) = (1-a)\rho_k(x/2) + a/2\{2\rho(x) - \tau_k(x/2)\rho_k(x/2)\tau_k^{-1}(x/2)\tau(x) + \tau(x)\tau_k^{-1}(x/2)\rho_k(x/2)\tau_k(x/2)\}$$

$$\tau_{k+1}(x/2) = (1-a)\tau_k(x/2) + a/2\{[I-\rho_{k+1}^2(x/2)]\,\tau_k^{-1}(x/2)\tau(x) + \tau(x)\tau_k^{-1}(x/2)[I-\rho_{k+1}^2(x/2)]\}$$

By making "a" smaller as the number of iterations increased, convergence was achieved for a thickness of x = 4.0 cm after 30 iterations. At 8.0 cm the procedure was apparently converging, albeit very slowly, and so was stopped after 100 iterations with "small" ($\sim 10^{-3}$) relative errors in the elements of the halved matrices.

Due to the complexity of the equations, no analytical treatment of when this procedure will converge has been given. However, in practice, the halving difficulty is not especially significant since the "optimum" experimental thickness is less than that for which the problem arises.

2. Thermal Double-differential Cross-sections

Currently considerable effort is being expended on the determination of double-differential cross-sections (ddc's) for various materials at thermal energies.* At present multiple scattering limits the thickness of the experimental slab that can be used. As in the fast neutron case of the previous section, the halving technique provides us with a reliable way of correcting for multiple scattering. Experiments can thus be done on thicker slabs.

The experimental set-up is somewhat different for thermal neutrons than for fast neutrons, however. Thermal neutrons can be produced either by a reactor or a LINAC with a thermalizer around the neutron source. Detectors are not available which can distinguish neutron energies of a fraction of an electron volt so that only time-of-

*A representative paper for scattering in water is Ref. 66.

flight can be used. Thus a velocity selector is used to produce a mono-energetic incident beam of neutrons from the reactor or LINAC and time-of-flight is used to determine the exit energy. As previously we can place detectors at several different angles and so do the angle measurements simultaneously. Now, however, we must do separate measurements for different input energies as well as angles.

Because of the time required to obtain good statistics with thin slabs, measurements are presently made for only one input angle (45°) and only several input energies. The resulting data do not give the ddc's directly because of multiple scattering within the slab. To correct for this, some theoretical model (e.g. McMurry-Russell or Haywood II) is required[67]. The resulting ddc's are found to be rather sensitive to the theoretical model used for the correction.

The halving technique, however, is entirely independent of any theoretical scattering model. By making measurements on thicker slabs, better statistics can be obtained in a given time allowing more input angles and energies to be used so that entire response matrices can be measured.

Outline of calculation

To demonstrate the feasibility of this correction procedure we have carried out a numerical study for thermal scattering in water. Water was chosen because detailed cross-sections are available as are the results of present correction techniques for comparison[67].

The Haywood II* kernel was used in the computer code FLANGE[70] to generate the double-differential scattering cross-sections. The total cross-sections were taken from BNL-325[71]. This cross-section information was used to generate fine-mesh cross-section matrices (70 × 70) and from them response matrices at a thickness of .125 cm which simulated the experimental measurements. These 70 × 70 matrices were "reduced" as described below to 24 × 24 response matrices which were then halved back to a small thickness (2^{-16} cm) to obtain the "corrected" ddc's. Finally a comparison was made between these "corrected" ddc's and the "actual" ddc's, i.e. those obtained by reducing the 70 × 70 cross-section matrices. A flowchart of this procedure is given in Fig. 12.

Group structure

The energy and angle groups used in the study are given in Tables IV and V. In both sets, there is a $\mu = 1$ angle. This is necessary in order to obtain the ddc's from the response matrices. This last point is important and is clarified in the sub-section below.

A major assumption in the choice of the energy group structure is that setting an upper limit of .10 eV will not seriously affect the accuracy of the calculations. The errors we make in ρ_{ij} and τ_{ij} by placing this upper limit are a result of neglecting upscattering from group j to k (where $E_k > .10$ eV) followed by downscattering to

*A model developed by Koppel[68] from Haywood's[69] experimental data.

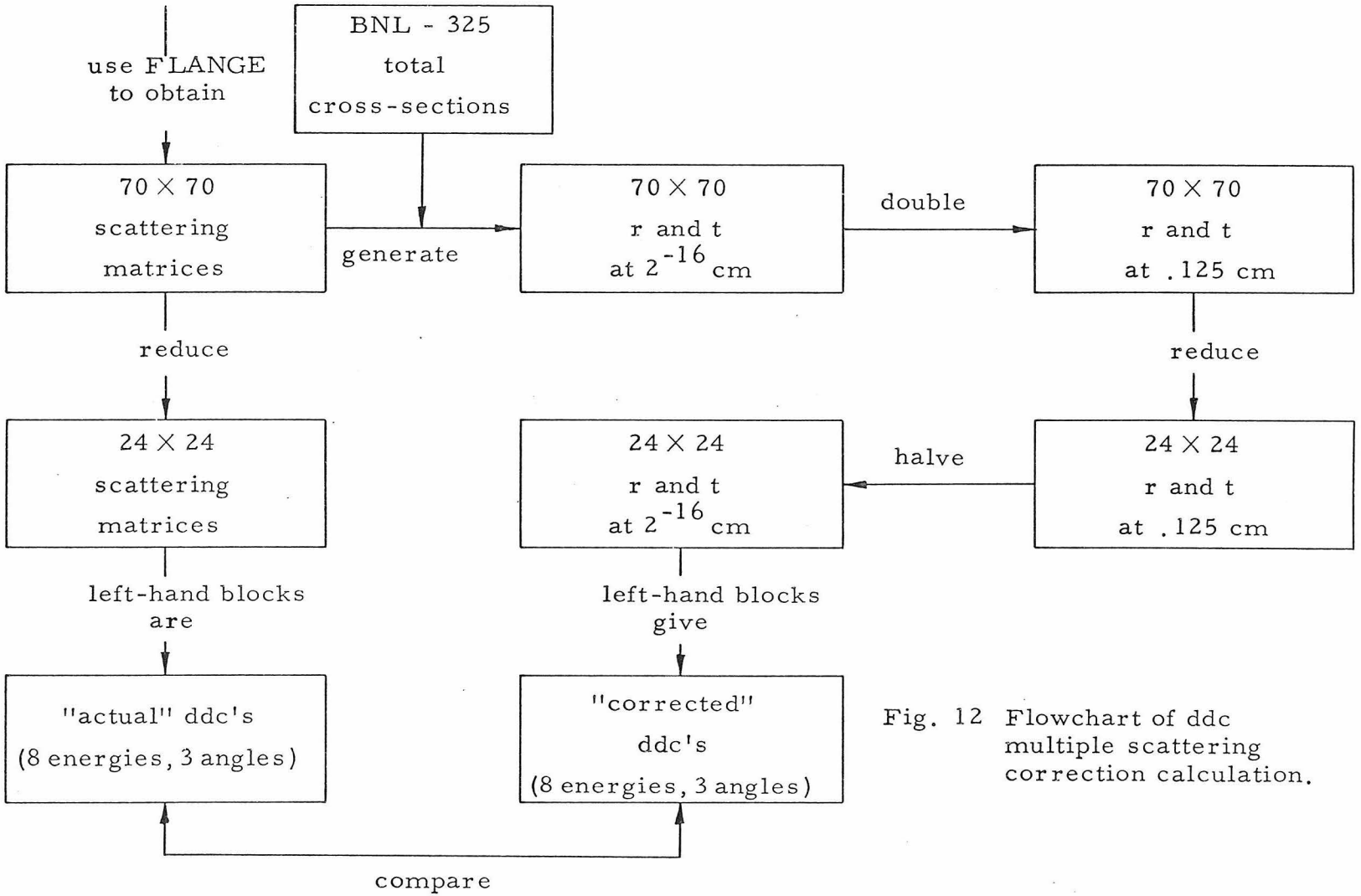

Fig. 12 Flowchart of ddc multiple scattering correction calculation.

TABLE IV

Energy and Angle Groups for 70 × 70 Matrices

	Energy Group (eV)	σ (b)[a]	μ	Δμ
1	0 - .005	192	1.0	.2
2	.005 - .010	151	.7	.2
3	.010 - .015	135	.5	.2
4	.015 - .020	123	.3	.2
5	.020 - .025	113	.1	.2
6	.025 - .030	103		
7	.030 - .035	96.7		
8	.035 - .040	91.8		
9	.040 - .050	86.3		
10	.050 - .060	81.4		
11	.060 - .070	77.8		
12	.070 - .080	74.9		
13	.080 - .090	72.5		
14	.090 - .100	70.6		

[a]Taken from BNL-325, Ref. 71

TABLE V

Energy and Angle Groups for 24 × 24 Matrices

	Energy Group (eV)	σ (b)[a]	μ	Δμ
1	0 - .010	164	1.0	.2
2	.010 - .020	128	.6	.4
3	.020 - .030	107	.2	.4
4	.030 - .040	94.0		
5	.040 - .050	86.3		
6	.050 - .060	81.4		
7	.060 - .080	76.1		
8	.080 - .100	71.3		

[a]Taken from BNL-325, Ref. 71

group i. This was expected to be small. A check calculation by adding a broad group from .10 - .25 eV to account for the upscattering gave matrix elements at .125 cm which differed from those previously obtained by less than 1% for the most part, the maximum difference being 5%. Thus energies above .10 eV are neglected in the following and the results we obtain are expected to be adequate to verify the feasibility of the halving technique for multiple scattering correction. It should be clearly understood that the restriction to 24×24 matrices was purely a matter of economics for check calculations and not a limitation of the size allowable for the halving technique to work. In practice one would no doubt include higher energy groups and a finer mesh at the lower energies. One or two more angles could also be used and the $\mu = 1$ angular interval could be made smaller in order to avoid the difficulties described later, which are associated with forward scattering.

To halve the 24×24 matrices from .125 to 2^{-16} cm required 4 min on an IBM 7094.* As a rule of thumb, doubling the order of the matrices increases the computer time by a factor of six. Thus although the computer times would be large for more detailed matrices, they would not be prohibitive because the multiple scattering correction need only be done once and would most likely represent only a small part of the total experimental expense.

---

*For "small" thicknesses the halving time per iteration is the same as the doubling time (see Fig. 6). For "large" thicknesses, i.e. those requiring that the halving scheme be "symmetrized," the halving time per iteration is approximately 1.4 times longer.

Cross-section matrices

The cross-section matrices S^b and S^f (Eq. (2-41)) are obtained from the ddc's according to Eq. (2-33)

$$\Sigma_{ij} = \int_o^{2\pi} d\varphi_{ij} \Sigma^s(\vec{\Omega}_i \cdot \vec{\Omega}_j, E_i, E_j)$$

with

$$\mu_{ij} \equiv \vec{\Omega}_i \cdot \vec{\Omega}_j = \mu_i\mu_j + \sqrt{1-\mu_i^2}\sqrt{1-\mu_j^2}\cos(\varphi_i - \varphi_j)$$
$$= \mu_i\mu_j + \sqrt{1-\mu_i^2}\sqrt{1-\mu_j^2}\cos\varphi_{ij} \quad .$$

Symmetry gives

$$\Sigma_{ij} = 2\int_o^{\pi} d\varphi_{ij} \Sigma^s(\mu_{ij}, E_i, E_j)$$

and approximating the integral by a sum, we have

$$\Sigma_{ij} = 2\sum_{\ell=1}^{M} \Delta\varphi_{ij}^{(\ell)} \Sigma^s(\mu_{ij}^{(\ell)}, E_i, E_j) \quad .$$

The integer M was taken to be 7 and the $\varphi_{ij}^{(\ell)}$ and $\Delta\varphi_{ij}^{(\ell)}$ used are given in Table VI. The ddc's $\Sigma^s(\mu_{ij}^{(\ell)}, E_i, E_j)$ were obtained from FLANGE.

In general, by integrating the ddc's over the azimuthal angle, we lose information and it is not possible to work backward from the cross-section matrices to the ddc's. If, however, we take one of our angle groups to be $\mu = 1$, then the azimuthal integral merely multiplies the ddc's by 2π for those matrix elements with $\mu_i = 1$ or $\mu_j = 1$. Thus by including a $\mu = 1$ angle group we can obtain the

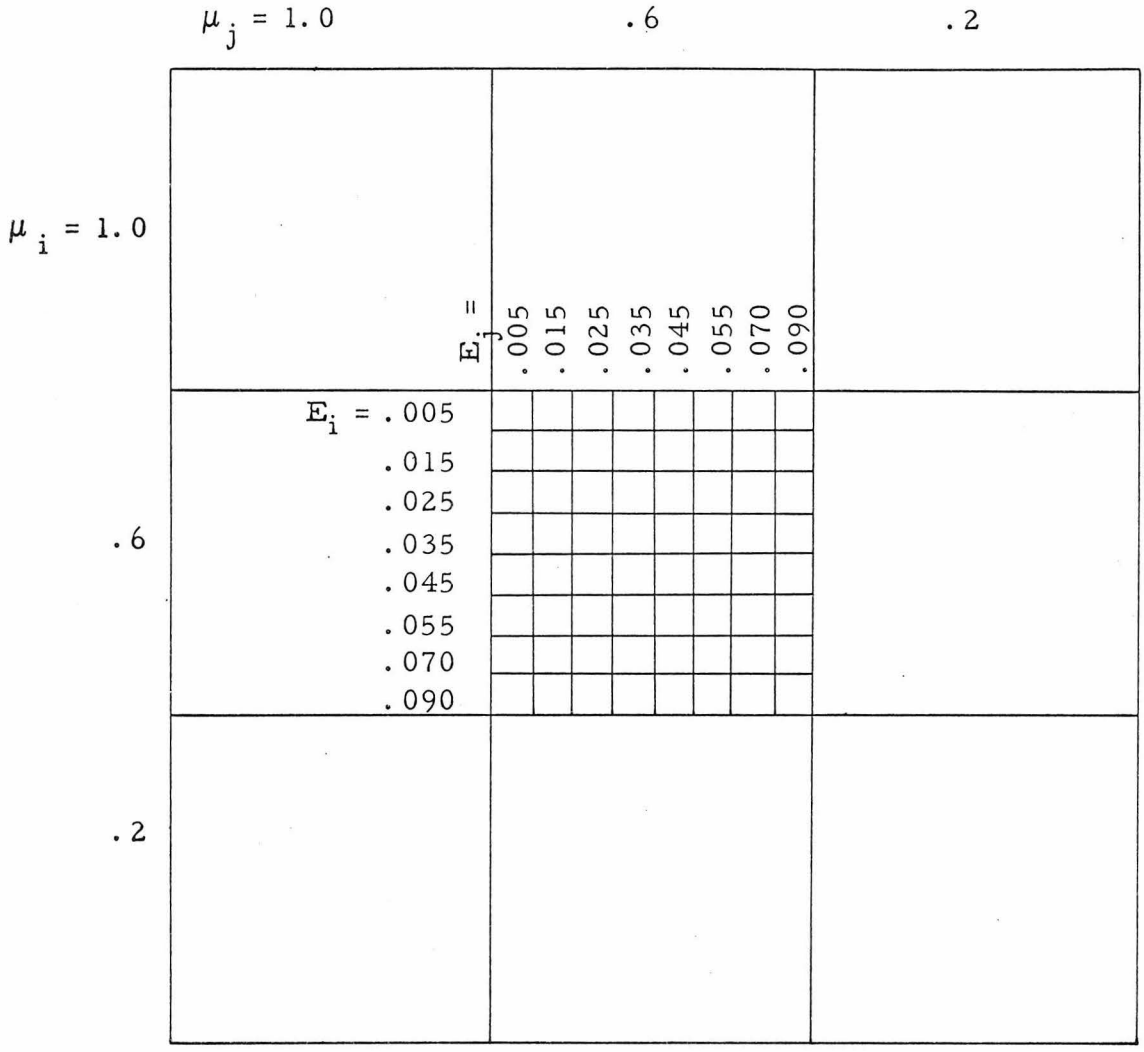

Fig. 13 Partitioning of the 24 × 24 matrices

TABLE VI
Azimuthal Angle Integration
Parameters

ℓ	$\varphi^{(\ell)}$	$\Delta\varphi^{(\ell)}$
1	0	$\pi/12$
2	$\pi/6$	$\pi/6$
3	$\pi/3$	$\pi/6$
4	$\pi/2$	$\pi/6$
5	$2\pi/3$	$\pi/6$
6	$5\pi/6$	$\pi/6$
7	π	$\pi/12$

ddc's from the cross section matrices. For the matrix partitioning shown in Fig. 13, the three left-hand blocks are just 2π times the ddc's. (By symmetry so are the three upper blocks.)

Reducing technique

The 24×24 "reduced" matrices were obtained from the 70×70 matrices by averaging $\mu_i r_{ij}$ and $\mu_i t^s_{ij}$ over the appropriate input and output energies and angles. These quantities were averaged because Σ_{ij} is smooth and Eqs. (2-38) and (2-39) show that for small thicknesses r_{ij} and t^s_{ij} vary like Σ_{ij}/μ_i. For larger thicknesses this behavior persists so that $\mu_i r_{ij}$ is smoother than r_{ij} (and similarly for t^s_{ij}). Physically,

$\mu_i r_{ij}(x)$ = the number of neutrons per unit time reflected from a unit area of slab of thickness x into state i due to an input of one neutron per unit time per unit area normal to the incident beam

in state j.

Experimental slab thickness

In Section A. 1 the "optimum" slab thickness was obtained by balancing the statistical counting errors with the propagated halving errors. For a non-multiplying medium, such as water, the transmission matrix elements do not increase monotonically with thickness as do the reflection matrix elements (Fig. 14), but rather peak at a thickness about equal to the mean free path (Fig. 15) and then die away. As a result, maximizing the count rate is the primary consideration in the choice of the slab thickness for a non-multiplying medium. For water this thickness is about .5 cm. In our study, the slab thickness was .125 cm, however, since the calculations were done before it was realized how to circumvent the halving difficulty mentioned in Section A. 1.

Results and conclusions

A tabular comparison between the "actual" and "corrected" ddc's is given in Table VII. Graphical comparisons of representative cross-sections are given in Fig. 16 and 17. Except for forward scattering($\mu = 1 \rightarrow \mu = 1$, which is not shown) the agreement is rather good. These results may be compared with Slaggie's* over the same energy range. There the average error between the "actual" and "corrected" ddc's appears to be about 25% while the maximum error is 50%. This

*See Fig. 2 in Ref. 72.

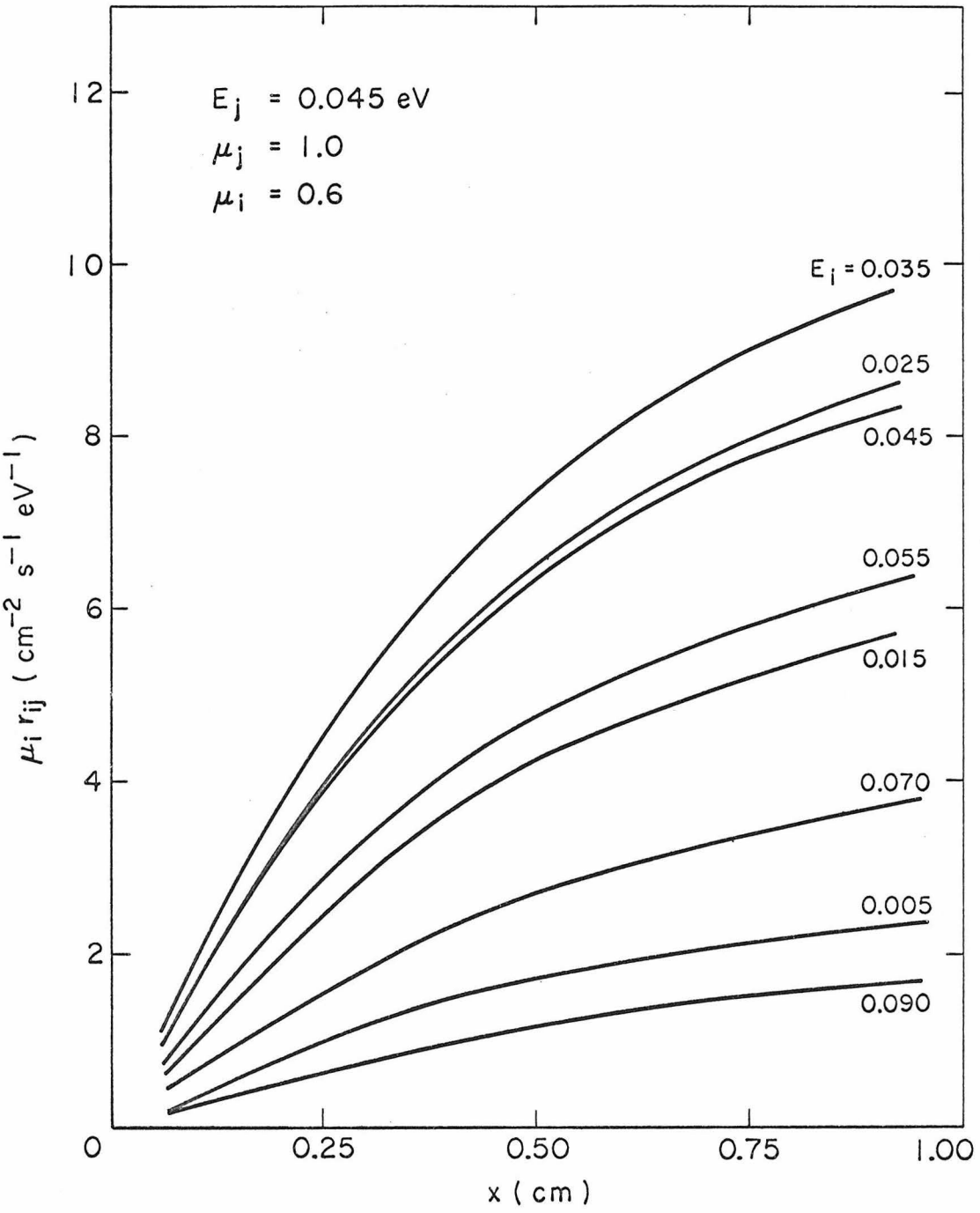

Fig. 14a Representative reflection matrix elements for water.

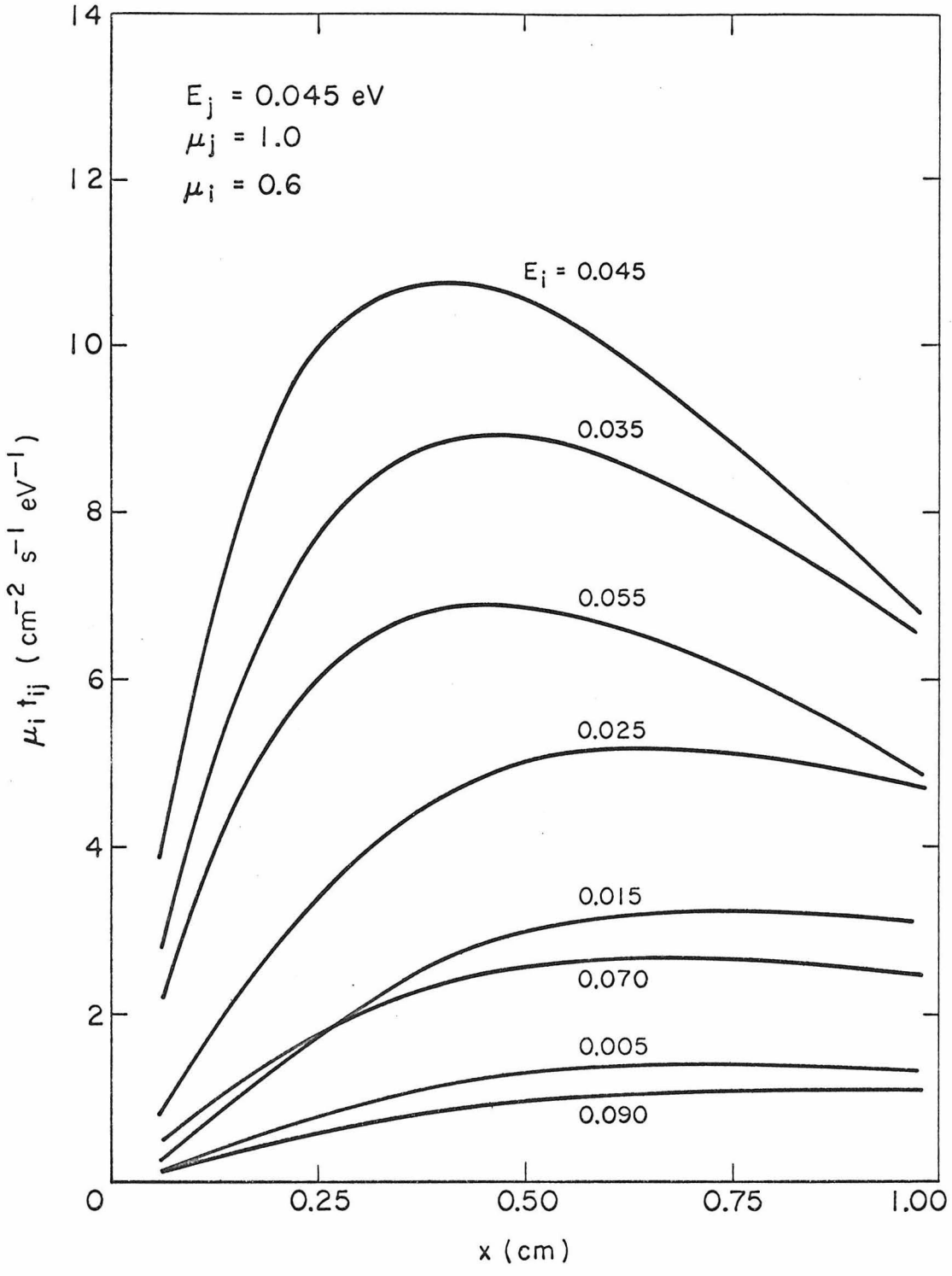

Fig. 14b Representative transmission matrix elements for water.

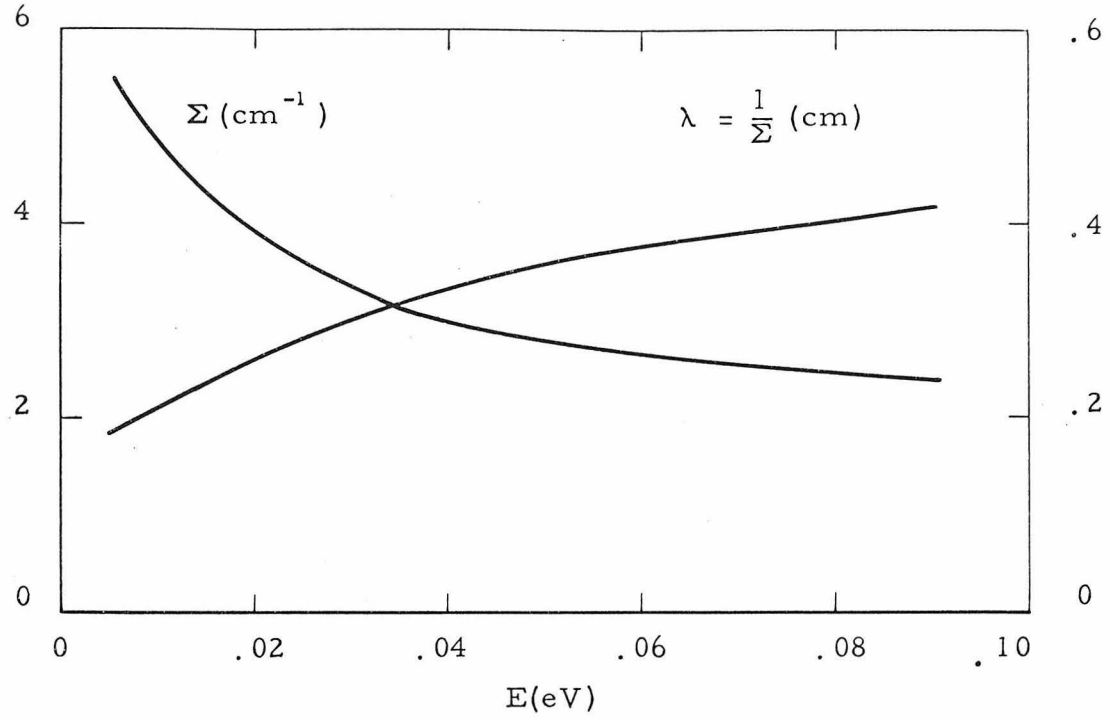

Fig. 15 Total cross-section and mean free path for water.

TABLE VII

Difference Between
"Actual" and "Corrected" DDC's

Block ($\mu_j \rightarrow \mu_i$)	Average Difference (%)	Maximum Difference (%)
1.0 → .6	8.0	22
1.0 → .2	3.4	20
1.0 → -.2	3.3	9
1.0 → -.6	6.9	9
1.0 → -1.0	8.6	11

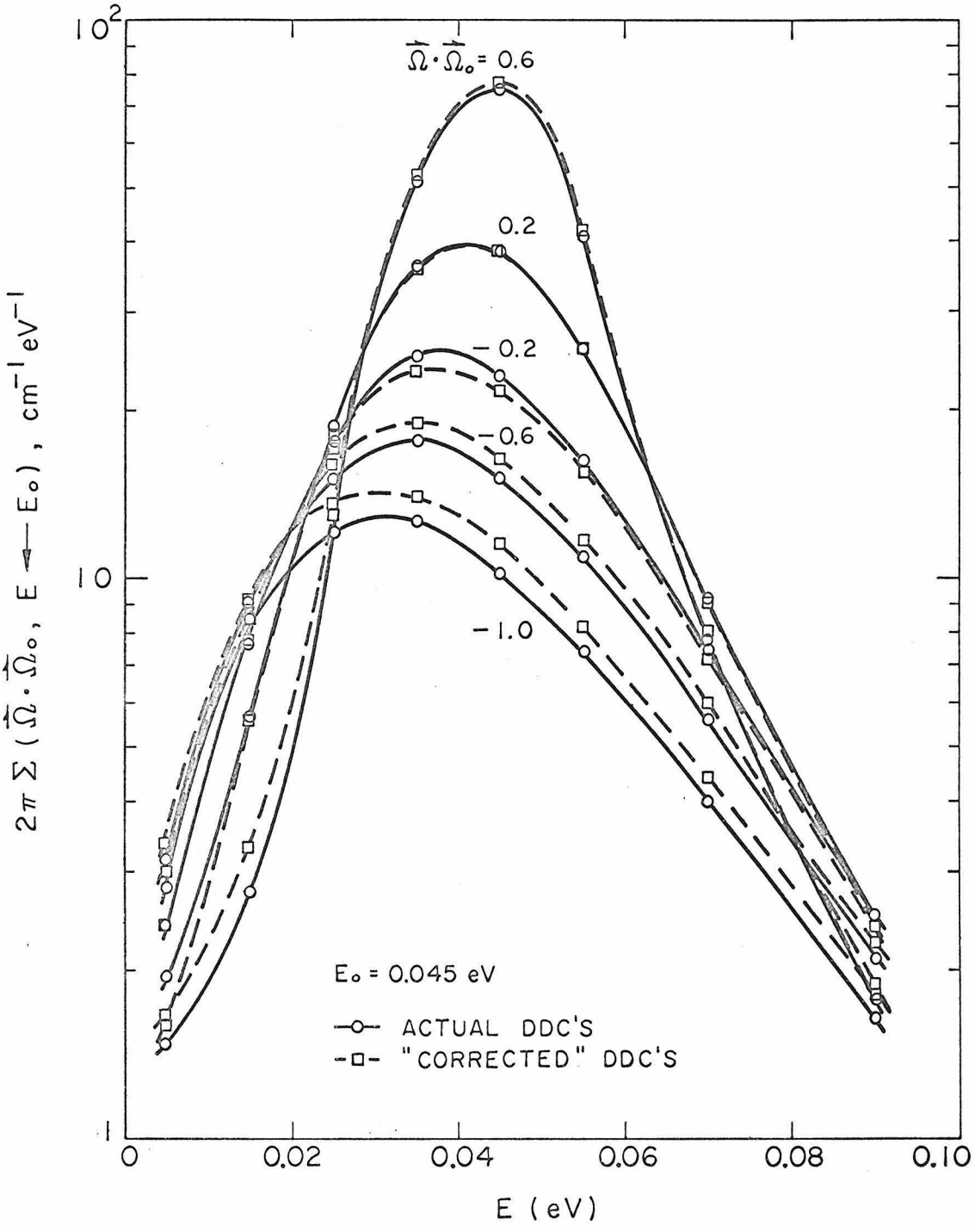

Fig. 16 Representative DDC's vs exit energy.

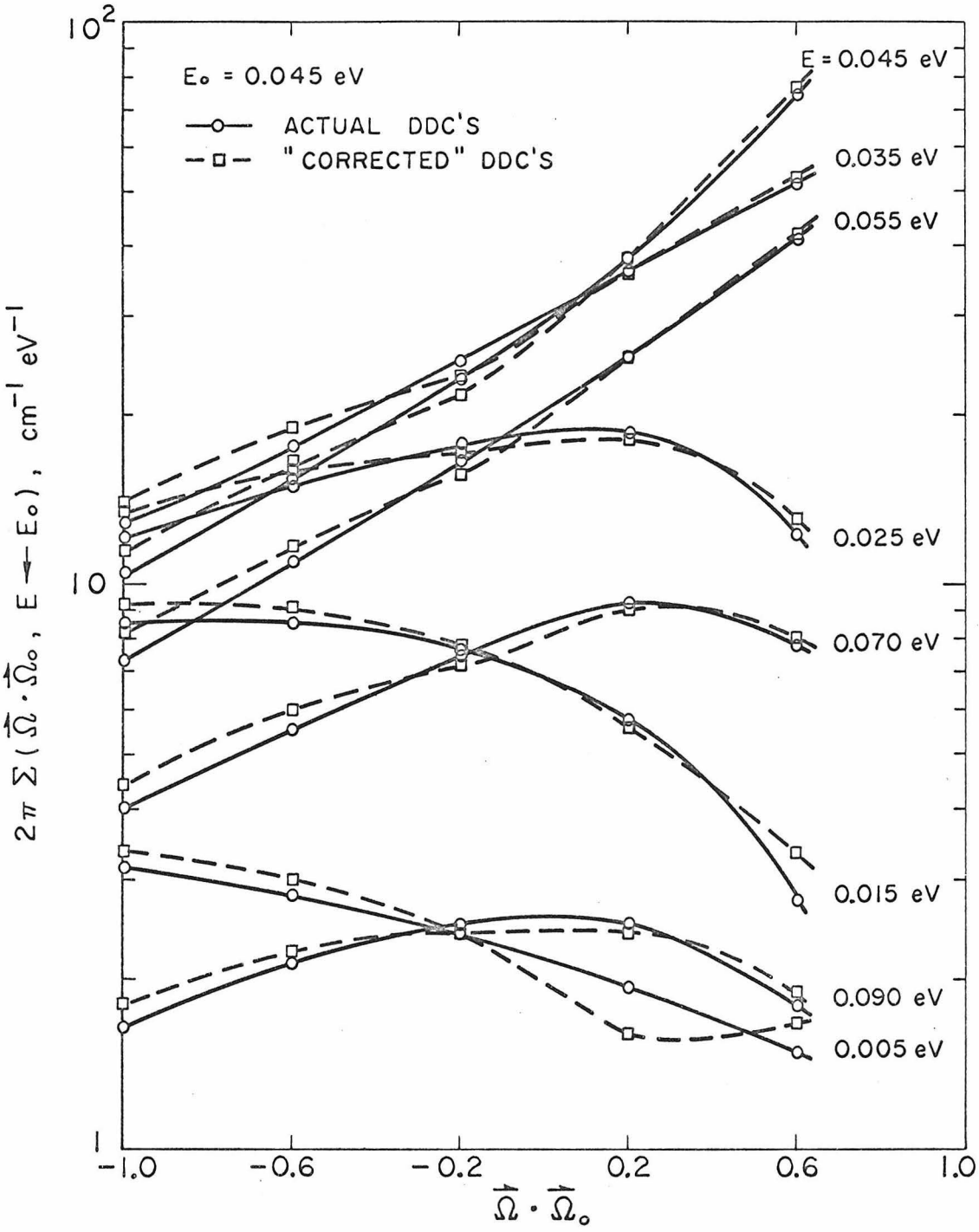

Fig. 17 Representative DDC's vs cosine of scattering angle.

is considerably poorer than our agreement.

Moreover, one should note that Slaggie's results are based upon a slab thickness of .025 cm. Ours, however, was .125 cm and with the improved halving scheme, could have been .5 cm (as mentioned above) to give high count rates. Hence the measurement of entire ρ and τ matrices could be performed in about the same time as present measurements. Use of the halving technique for multiple scattering correction would then result in better accuracy and more information than presently obtained.

The "corrected" ddc's are uniformly larger than the "actual" ddc's for forward scattering (not shown in Table VII) by roughly a factor of 4. This comes about as a result of the singular nature of the forward scattering. In our calculations, the "actual" ddc's for forward scattering were obtained directly from FLANGE. These ddc's were an order of magnitude smaller than those for small angle scattering. Actually a better procedure would have been to average the ddc's over the .8 - 1.0 μ-interval. The resulting ddc's would have been larger, presumably more like the "corrected" ddc's. Moreover in practice it is average values that one would measure.

B. Criticality Determination

As we mentioned at the beginning of this Chapter, experimentally measured response functions can also be used to directly determine criticality. Unfortunately the necessary calculational techniques developed in Section C of Chapter III are essentially restricted to

slab geometry so that the critical thickness which one determines will not be of much practical significance in itself. However, other quantities which we can obtain, such as the power distribution, neutron spectrum, and reactivity coefficients, may well be quite similar to those in a more realistic geometry.

The advantage of response function experiments over critical experiments is that much less material is used. This means that the experiment is considerably cheaper since (1) the fissile inventory is smaller, and(2)elaborate safety precautions are unnecessary because the slabs are always far subcritical. Some idea of the expense presently being considered can be obtained from the following.

> Fast reactor statics and transient physics characteristics must be obtained for large core loadings up to several thousand kilograms of plutonium. These tests will be extremely expensive. Up to $21,000,000 is estimated for fabricating a critical experiment loading for the ZPPR. (pp. 62 - 63 of Ref. 73).

The incentive to develop a more economical experimental technique should be clear.

Although the criticality information obtained from response functions would no doubt be less accurate than that obtainable from a critical experiment, it would probably be better than what one could calculate starting from existing cross-sections. This is because the response functions are macroscopic quantities which are "closer" to the final criticality parameters than are the cross-sections.

In order to check this hypothesis, we have studied the sensitivity of the critical thickness to errors in the measured response functions. The critical thickness was chosen for study because of its

ease of calculation. Moreover, the sensitivity of other quantities of interest is expected to vary similarly to that of the critical thickness (e.g. the sensitivity of reactivity coefficients is the same as that of the critical thickness).

1. Critical Thickness

A qualitative idea of the sensitivity of the critical thickness to the response functions can be quickly obtained from the one-group diffusion solution of Chapter II. If we define the sensitivities (cf. Eq. (4-1)) as

$$S^{x_c}_{R(x)} \equiv \frac{\partial x_c / x_c}{\partial R(x)/R(x)}$$

$$S^{x_c}_{T(x)} \equiv \frac{\partial x_c / x_c}{\partial T(x)/T(x)} \quad ,$$

then the curves for S as a function of x are as given in Fig. 18. As one might expect, the sensitivity is less the closer the experimental thickness x is to the critical thickness x_c.

The introduction of energy and angle dependence does not significantly change this picture. For example, representative elements of the 5-group diffusion matrices for the PuC-UC mixture of Ref. 53 are plotted in Fig. 19 and the corresponding sensitivities are given in Fig. 20.* Again the sensitivities decrease with increasing experimental

*It is interesting to note that the halving difficulty discussed in Section A. 1 was not encountered here until a thickness of 32 cm. Since the group structures were the same, the difficulty must be due in part to the angular variable in transport theory.

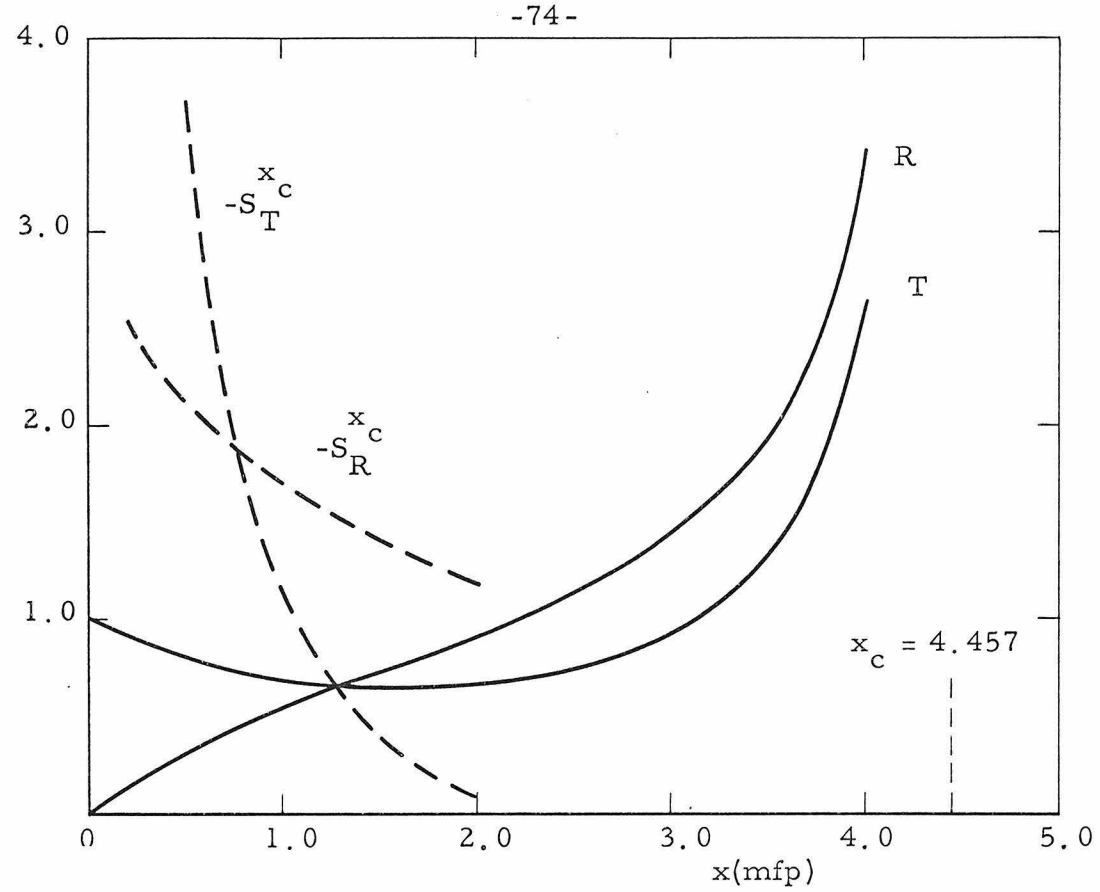

Fig. 18 Sensitivities for multiplying material with $\Sigma_{tr} = 1$, $c = 1.1$.

thickness.

It does not follow, though, that one should do the experiment on as large a thickness as possible since this would negate the advantages of the response function approach mentioned previously. Also the experiment becomes more difficult to analyze for large thicknesses. This is because all of the theory we have developed presumes uniform incident and exit beams, or in practice that the beam diameter is large compared to the slab thickness. If this is not the case, a considerable number of neutrons will be transported transversely within the slab. Thus the choice of the experimental thickness depends upon a combination of factors specific to the material under study and the particular

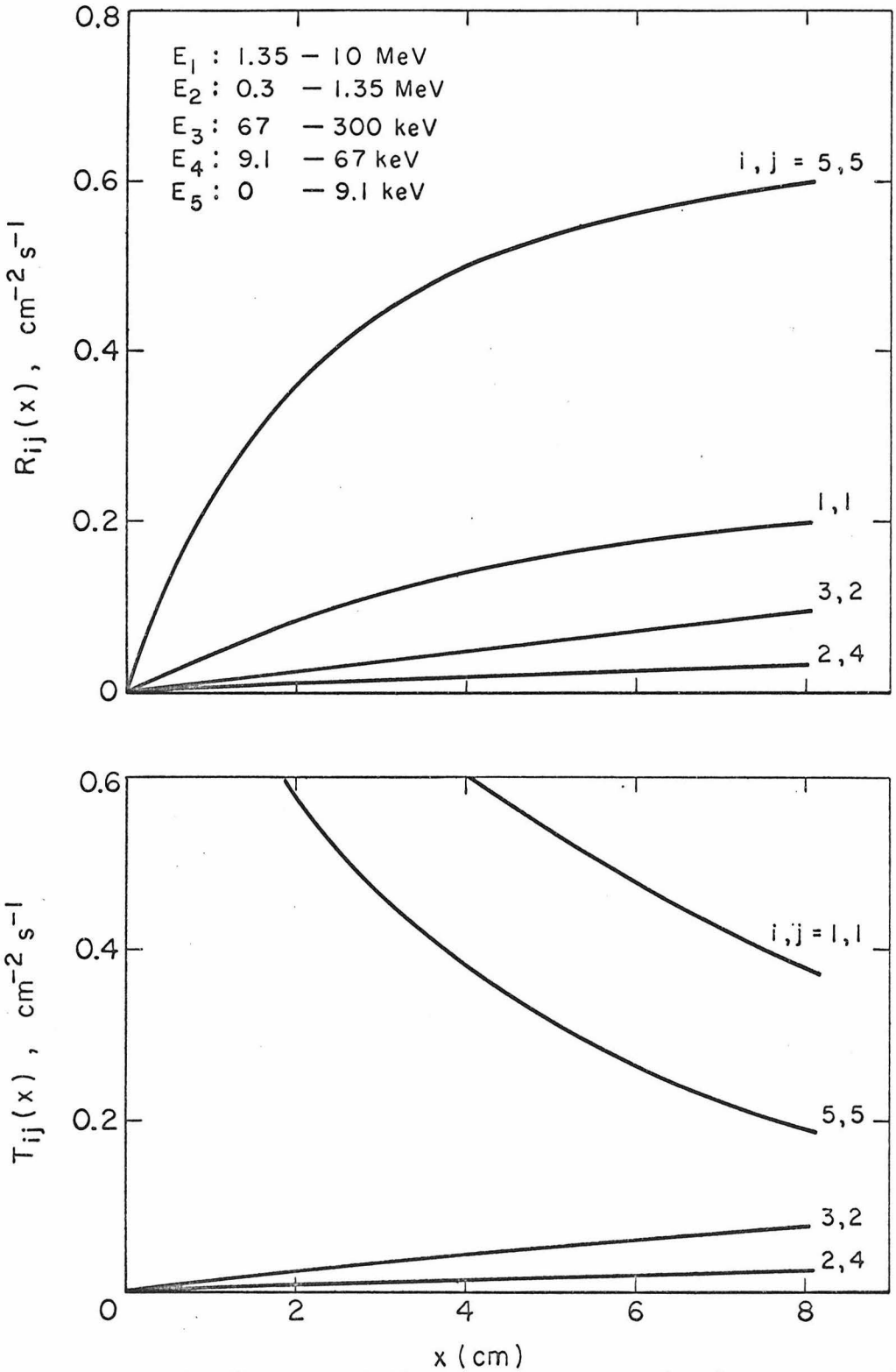

Fig. 19 Representative response matrix elements for PuC-UC mixture.

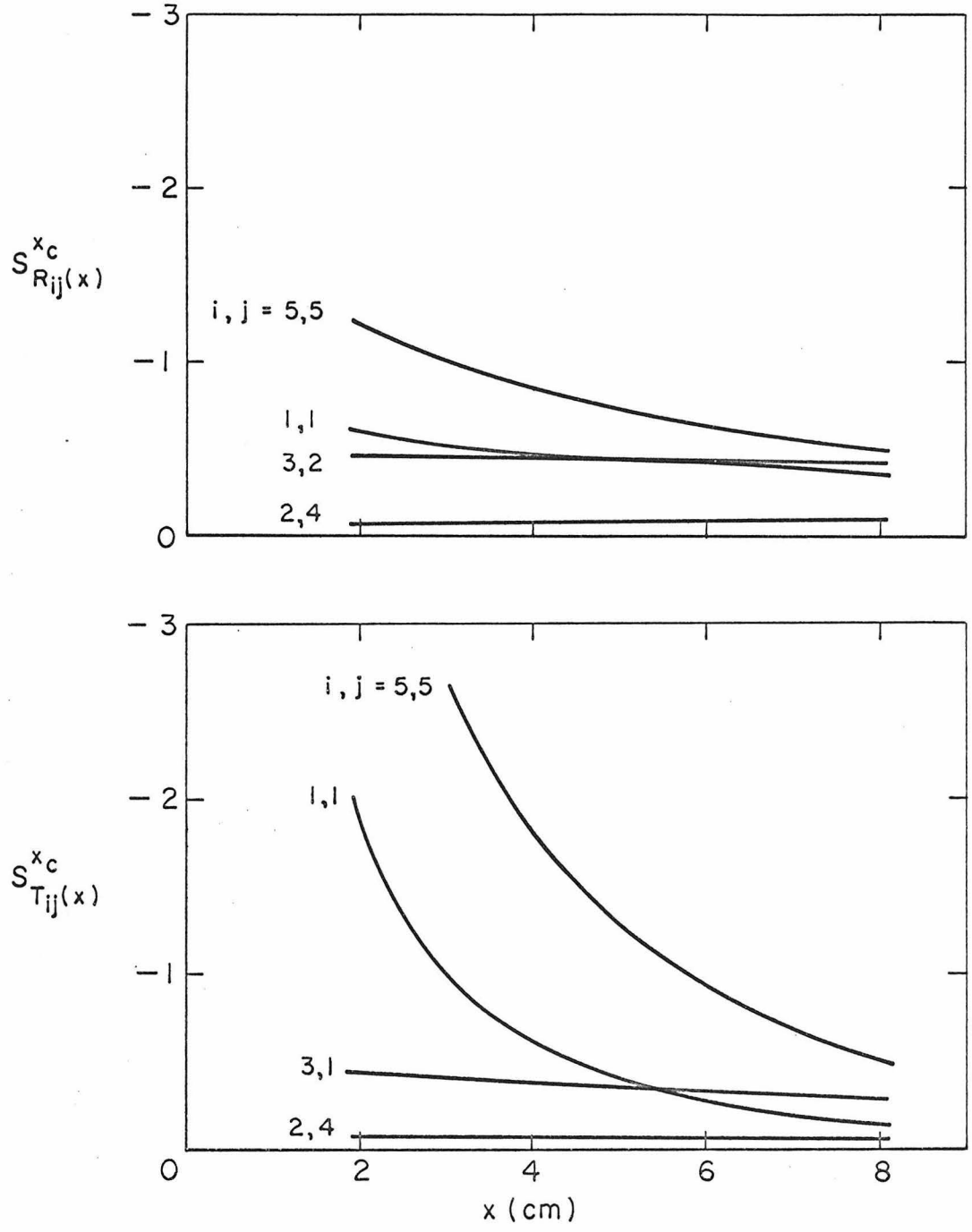

Fig. 20 Representative sensitivities for PuC-UC mixture.

experimental set-up. In any case, however, the thickness for this experiment will be larger than that for the cross-section experiment described in Section A. 1. This is the only difference between the two experiments.

If we assume that for the PuC-UC mixture the experiment would be done at a thickness of 8 cm, then a sensitivity comparison can be made with Moorhead[53].* Although the critical thickness is less sensitive to some of the cross-sections than to the response functions, it is more sensitive to ν and Σ_f. Presuming the response functions could be more accurately determined, the overall sensitivity should be less. Unfortunately this is still rather qualitative since it remains to be seen how accurately response function experiments can be done.

2. Reactivity Worth and Doppler Coefficient

The reactivity worth of a material X in a sample core could be simply obtained by response function measurements. The response functions would first be measured for a slab of core material. A small slab of material X would then be added and the measurements repeated. The difference in the calculated critical thickness is simply related to the reactivity worth of material X. Since in many cases the reactivity worth is a spectral rather than a spatial effect, the worth so obtained may be nearly the same as for other-than-slab geometries.

Similarly the Doppler coefficient may be obtainable by measuring the response functions on the same slab at two different temperatures

*See his Tables VII and VIII as well as Eq. (3).

and calculating the difference in critical thickness. Because the Doppler effect is rather small and difficult to measure using present techniques[74, 75], we have carried out a sample calculation to determine whether there would be measurable changes in the response functions. Diffusion theory response matrices were calculated at temperatures of 300° K and 900°K using the Russian 26-group cross-sections[76] for a slab of pure U^{238}. Of course to obtain criticality, some fissile isotope would be added, but for large power reactors U^{238} will predominate. The calculated response matrix elements in the resonance range were about 2% lower at 900° K than at 300° K for a slab thickness of 4 cm and about 5% lower for a slab thickness of 8 cm. It is anticipated that the errors in the measured response functions will be of this same order, 2 to 5%[59, 61]. However, the fact that all the calculated changes were in the same direction (lower), strongly suggests that the net effect will be to produce a noticeable change in reactivity due to the Doppler effect.

No thermal expansion was assumed in the above calculation. This effect can be treated as follows. At temperature T the invariant imbedding equation for ρ is

$$\frac{\partial}{\partial x}\rho(x) = S^b + (S^f - M)\rho(x) + \rho(x)(S^f - M) + \rho(x)S^b\rho(x) \quad . \qquad (2\text{-}46)$$

If there were no Doppler effect, but only expansion as a result of heating, then at temperature $T' = T + \Delta T$ we would have

$$\frac{\partial}{\partial x}\rho'(x) = S^{b'} + (S^{f'}-M')\rho'(x) + \rho'(x)(S^{f'}-M') + \rho'(x)S^{b'}\rho'(x)$$

$$= \frac{N'}{N}\left[S^{b} + (S^{f}-M)\rho'(x) + \rho'(x)(S^{f}-M) + \rho'(x)S^{b}\rho'(x)\right] \quad (4\text{-}2)$$

where N is the nuclear density, since (cf. Eq. (2-41))

$$S^{b'}_{ij} = \Delta\mu_j\Delta E_j \frac{\Sigma^{b'}_{ij}}{\mu_i} = N'\Delta\mu_j\Delta E_j \frac{\sigma^{b}_{ij}}{\mu_i} = \frac{N'}{N}\Delta\mu_j\Delta E_j \frac{N\sigma^{b}_{ij}}{\mu_i}$$

$$= \frac{N'}{N} S^{b}_{ij}$$

and similarly for S^{f} and M. Equation (4-2) can also be written as

$$\frac{\partial\rho'(x)}{\partial\left(\frac{N'}{N}x\right)} = S^{b} + (S^{f}-M)\rho'(x) + \rho'(x)(S^{f}-M) + \rho'(x)S^{b}\rho'(x)$$

or

$$\frac{\partial}{\partial x}\rho'\left(\frac{N}{N'}x\right) = S^{b} + (S^{f}-M)\rho'\left(\frac{N}{N'}x\right) + \rho'\left(\frac{N}{N'}x\right)(S^{f}-M)$$

$$+\rho'\left(\frac{N}{N'}x\right)S^{b}\rho'\left(\frac{N}{N'}x\right) \quad . \quad (4\text{-}3)$$

By comparing (2-46) and (4-3) we see that

$$\rho'\left(\frac{N}{N'}x\right) = \rho(x) \quad . \quad (4\text{-}4)$$

As a result of expansion the slab thickness becomes

$$x' = x + \Delta x = x + \alpha x\Delta T \quad (4\text{-}5)$$

while the nuclear density becomes

$$N' = N + \Delta N = N - 3\alpha N\Delta T \quad (4\text{-}6)$$

where α is the coefficient of linear expansion. Comparison of (4-5) and (4-6) gives

$$x' = x + \frac{1}{3}\frac{N-N'}{N}\,x \quad . \tag{4-7}$$

Thus the measured reflection function at temperature T' is related to that at T by

$$\begin{aligned}
\rho'(x') &= \rho'\left(x + \frac{1}{3}\frac{N-N'}{N}x\right) \\
&= \rho'\left(x + \frac{N-N'}{N}x - \frac{2}{3}\frac{N-N'}{N}x\right) \\
&= \rho'\left(x + \frac{N-N'}{N'}x - 2\alpha x\Delta T\right) \quad \text{(to first order)} \\
&= \rho'\left(\frac{N}{N'}x - 2\alpha x\Delta T\right) \\
&= \rho(x) - \frac{\partial\rho(x)}{\partial x}\,2\alpha x\Delta T
\end{aligned} \tag{4-8}$$

where we have used Eq. (4-4) and Taylor's theorem in the last step. Similarly for the transmission function

$$\tau'(x') = \tau(x) - \frac{\partial\tau(x)}{\partial x}\,2\alpha x\Delta T \quad . \tag{4-9}$$

The partial derivaties of ρ and τ in Eqs. (4-8) and (4-9) can be obtained from the invariant imbedding Equations (2-46) and (2-47).

3. Neutron Spectrum

Although carried out on a critical assembly, fast spectral measurements are not necessarily done at critical. For example, in Bennett et al[60], we find

> . . . It is not possible to operate a plutonium assembly near critical using proton-recoil detectors of fixed sensitivity . . . The spectrum measured was, consequently, the central spectrum for a subcritical assembly lacking about half its critical mass. (pp. 477 - 478).

To analyze this particular experiment the assumption was made that the subcritical spectrum was close to the critical spectrum.

In a response function experiment one would measure the reflected and transmitted spectra on a slab consisting of considerably less material than above. However, using the techniques of Chapter III one can calculate a critical spectrum which may be better than that obtained from the "critical" experiment.

V. SUMMARY AND CONCLUSIONS

The most fundamental quantity of interest in reactor physics is the neutron distribution (or flux) within the reactor. The neutron cross-sections are the basic physical parameters which determine the neutron distribution. Most reactor theories start from the cross-sections and end with the neutron distribution. This has given rise to two basic kinds of experiments, cross-section experiments and critical experiments which measure directly the initial and final quantities, respectively, of the theories. This preoccupation with cross-sections and fluxes, however, has allowed other approaches to be overlooked.

In this thesis we have investigated another approach to reactor analysis which is developed in terms of response functions. Although not of immediate interest in themselves, the response functions can be simply related to both the cross-sections and the neutron distribution and have the experimental advantage of being more easily measured than either of the other two quantities. Only limited theoretical and no experimental work using this approach has been done previously. We have reviewed and unified this work, as well as adding several new results, the most important of which we list below.

1) An iterative halving scheme was developed to obtain response matrices at half the thickness of the original matrices. No theoretical justification of the convergence properties of this scheme was given. Numerically, however, it was found that a convergence

problem arose only for slab thicknesses larger than the neutron mean free path and that this difficulty could apparently be solved by introducing a convergence factor.

2) An efficient calculational technique for deep-penetration shielding problems in slab geometry was developed by combining the doubling relations with invariant imbedding. As the time savings over existing Monte Carlo or discrete ordinates methods are significant, the response function approach should be seriously considered for future calculations.

3) Invariant imbedding equations have been derived, but not solved, for finite cylindrical geometry in both the transport and diffusion theory cases. Previously it was shown that response function techniques are very efficient for diffusion theory criticality calculations in one-dimensional slab and two-dimensional rectangular geometries. Consequently, it appears to be quite worthwhile to try to develop a similar diffusion theory technique in cylindrical geometry, starting from Eqs. (B-32) - (B-35).

4) We have shown how the halving scheme can be used to obtain cross-sections from response function experiments done on moderately thick samples. Of all the results of this thesis, this is the most significant due to the acknowledged, immediate need for better cross-sections, particularly for fast reactors. As a result of this work, it appears that these experiments should be carried out as soon as possible to determine whether they are as useful as our analysis indicates. The large gains possible at a relatively small expense

seem to warrant giving such experiments high priority in our fast reactor physics program.

APPENDIX A

TRANSPORT THEORY INVARIANT IMBEDDING IN CYLINDRICAL GEOMETRY

A. Preliminaries

For no internal source, the time independent Boltzmann equation is[77]

$$\vec{\Omega}\cdot\nabla\psi(\vec{r},E,\vec{\Omega}) + \Sigma_t(\vec{r},E)\psi(\vec{r},E,\vec{\Omega}) = \int_{E'} dE' \int_{\vec{\Omega}'} d\vec{\Omega}'\Sigma(\vec{r};E,\vec{\Omega}\leftarrow E',\vec{\Omega}')\psi(\vec{r},E',\vec{\Omega}') \quad . \qquad (A\text{-}1)$$

From the outset we assume that the reactor has azimuthal symmetry, i.e. the cross-sections are independent of ϕ where $\vec{r} = (\rho,\phi,z)$. In order not to obscure the arguments in the derivation, we will also take the cross-sections to be independent of ρ, z, and E as well. After we have obtained the invariant imbedding equations, it is an easy matter to re-incorporate the ρ, z, and E dependence.

In cylindrical geometry (see Fig. 21)

$$\vec{\Omega} = \sin\theta\cos\varphi\,\hat{\rho} + \sin\theta\sin\varphi\,\hat{\phi} + \cos\theta\,\hat{k}$$

$$= \sqrt{1-\mu^2}\cos\varphi\,\hat{\rho} + \sqrt{1-\mu^2}\sin\varphi\,\hat{\phi} + \mu\,\hat{k} \qquad (\mu \equiv \cos\theta)$$

and

$$\nabla\psi = \frac{\partial\psi}{\partial\rho}\hat{\rho} + \frac{1}{\rho}\frac{\partial\psi}{\partial\varphi}\hat{\phi} + \frac{\partial\psi}{\partial z}\hat{k}$$

so that the Boltzmann equation is

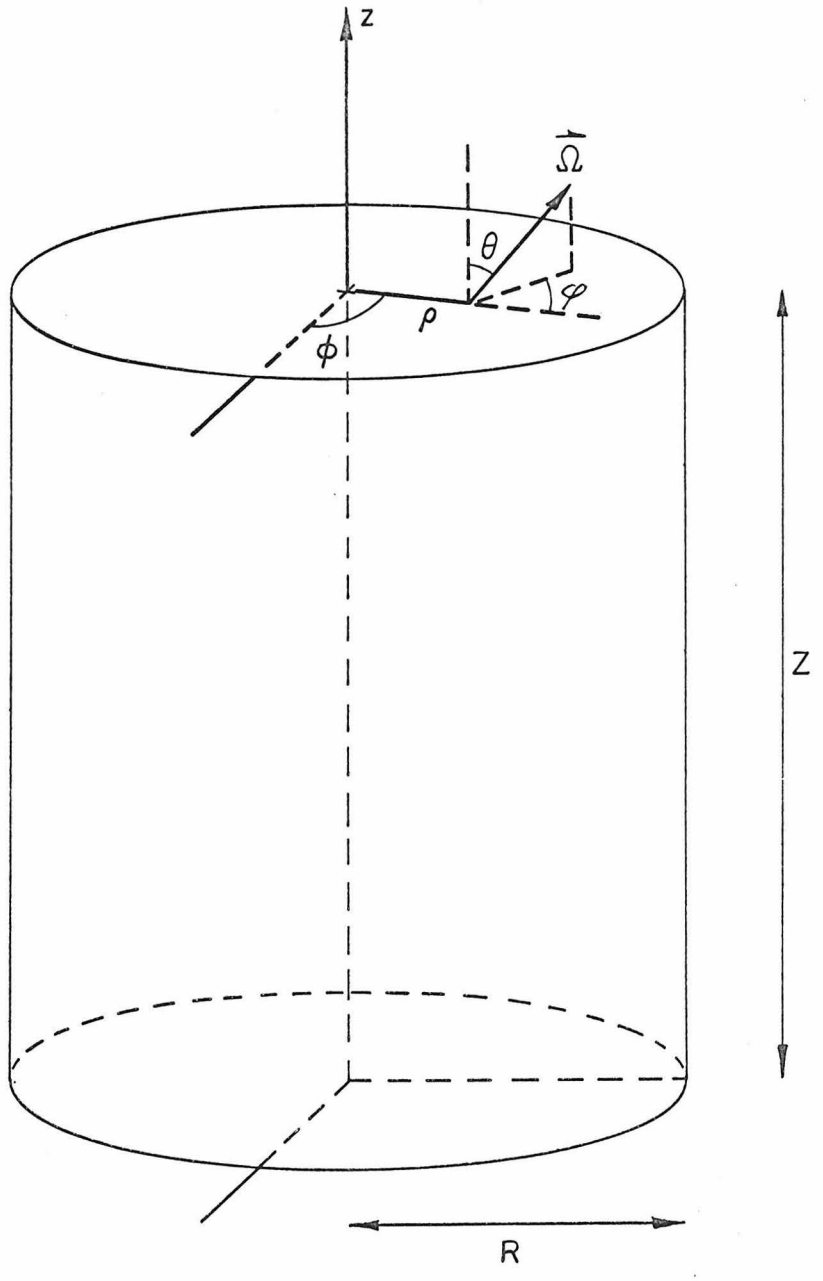

Fig. 21

$$\left[\sqrt{1-\mu^2}\cos\varphi\ \frac{\partial}{\partial\rho}+\sqrt{1-\mu^2}\ \frac{\sin\varphi}{\rho}\ \frac{\partial}{\partial\phi}+\mu\ \frac{\partial}{\partial z}+\Sigma_t\right]\psi(\vec{r},\vec{\Omega})$$
$$=\int_{-1}^{1}d\mu'\int_{o}^{2\pi}d\varphi'\,\Sigma(\mu,\mu',\varphi-\varphi')\psi(\vec{r},\vec{\Omega}') \qquad (A-2)$$

where we have noted that

$$\Sigma(\vec{\Omega}\leftarrow\vec{\Omega}') = \Sigma(\vec{\Omega}\cdot\vec{\Omega}') = \Sigma(\mu,\mu',\varphi-\varphi')$$

since

$$\vec{\Omega}\cdot\vec{\Omega}' = \mu\mu' + \sqrt{1-\mu^2}\ \sqrt{1-\mu'^2}\cos(\varphi-\varphi') \quad .$$

Note that

$$\psi(\vec{r},\vec{\Omega}) = \psi(\rho,\phi,z,\mu,\phi+\varphi) \quad .$$

It is also possible to consider

$$\psi(\vec{r},\vec{\Omega}) = \bar{\psi}(\rho,\phi,z,\mu,\varphi) \quad .$$

In this case we must include an extra derivative in the Boltzmann equation to take into account the fact that

$$\frac{\partial}{\partial\phi}\,\psi(\rho,\phi,z,\mu,\phi+\varphi)\Big|_{\phi+\varphi} = \left(\frac{\partial}{\partial\phi}\Big|_{\varphi} - \frac{\partial}{\partial\varphi}\Big|_{\phi}\right)\bar{\psi}(\rho,\phi,z,\mu,\varphi) \quad .$$

Then we have

$$\left[\sqrt{1-\mu^2}\cos\varphi\ \frac{\partial}{\partial\rho}+\sqrt{1-\mu^2}\ \frac{\sin\varphi}{\rho}\left(\frac{\partial}{\partial\phi}-\frac{\partial}{\partial\varphi}\right)\right.$$
$$\left.+\mu\ \frac{\partial}{\partial z}+\Sigma_t\right]\bar{\psi}(\rho,\phi,z,\mu,\varphi)$$
$$=\int_{-1}^{1}d\mu'\int_{o}^{2\pi}d\varphi'\Sigma(\mu,\mu',\varphi-\varphi')\bar{\psi}(\rho,\phi,z,\mu',\varphi') \quad . \qquad (A-3)$$

Now designate by

$$\bar{\psi}(\rho,\phi,z,\mu,\varphi;\rho_o,\phi_o,z_o,\mu_o,\varphi_o) \quad ; \qquad z_o = Z \quad , \quad -1 < \mu_o < 0$$

that solution of Eq. (A-3) with the boundary conditions

$$\bar{\psi}(\rho,\phi,Z,\mu,\varphi;\ \rho_o,\phi_o,Z,\mu_o,\varphi_o) = \frac{\delta(\rho-\rho_o)}{\rho}\ \delta(\mu-\mu_o)\ \frac{\delta(\varphi-\varphi_o)}{2\pi}$$

$$\text{for} \quad -1 < \mu < 0$$

$$\bar{\psi}(\rho,\phi,0,\mu,\varphi;\ \rho_o,\phi_o,Z,\mu_o,\varphi_o) = 0 \qquad \text{for} \quad 0 < \mu < 1 \qquad \text{(A-4)}$$

$$\bar{\psi}(R,\phi,z,\mu,\varphi;\rho_o,\phi_o,Z,\mu_o,\varphi_o) = 0 \qquad \text{for} \quad \pi/2 < \varphi < 3\pi/2 \quad .$$

Thus $\bar{\psi}$ is the Green's function for an arbitrary input (with azimuthal ϕ-symmetry) on the top of the cylinder. Because of the assumed symmetry, $\bar{\psi}$ is independent of ϕ and ϕ_o. Accordingly let us define

$$\psi(Z,z,\rho,\mu,\varphi,\rho_o,\mu_o,\varphi_o)$$

$$\equiv \frac{1}{2\pi}\int_o^{2\pi} d\phi \int_o^{2\pi} d\phi_o \bar{\psi}(\rho,\phi,z,\mu,\varphi;\ \rho_o,\phi_o,Z,\mu_o,\varphi_o)$$

which satisfies[77]

$$\left[\sqrt{1-\mu^2}\cos\varphi\ \frac{\partial}{\partial\varphi} - \sqrt{1-\mu^2}\ \frac{\sin\varphi}{\rho}\ \frac{\partial}{\partial\varphi} + \mu\ \frac{\partial}{\partial z} + \Sigma_t\right]\psi(Z,z,\rho,\mu,\varphi,\rho_o,\mu_o,\varphi_o)$$

$$= \int_{-1}^{1} d\mu' \int_o^{2\pi} d\varphi'\, \Sigma(\mu,\mu',\varphi-\varphi')\,\psi(Z,z,\rho,\mu',\varphi',\rho_o,\mu_o,\varphi_o) \qquad \text{(A-5)}$$

with the boundary conditions

$$\psi(Z, Z, \rho, \mu, \varphi, \rho_o, \mu_o, \varphi_o) = \frac{\delta(\rho-\rho_o)}{\rho}\ \delta(\mu-\mu_o)\delta(\varphi-\varphi_o)$$

$$\text{for} \quad -1 < \mu < 0$$

$$\psi(Z, 0, \rho, \mu, \varphi, \rho_o, \mu_o, \varphi_o) = 0 \qquad \text{for} \quad 0 < \mu < 1 \qquad \text{(A-6)}$$

$$\psi(Z, z, R, \mu, \varphi, \rho_o, \mu_o, \varphi_o) = 0 \qquad \text{for} \quad \pi/2 < \varphi < 3\pi/2 \quad .$$

Equations (A-5) and (A-6) comprise the problem we will consider in the next section. Physically

$$\psi(Z, z, \rho, \mu, \varphi, \rho_o, \mu_o, \varphi_o)$$

= the number of neutrons per unit time per unit area at z and ρ moving in unit solid angle about (μ, φ), due to an incident beam on the top of the cylinder of one neutron per unit time per unit area at ρ_o in direction (μ_o, φ_o). Both areas are measured normal to the neutron motion.

The height Z is included explicitly as an independent variable since it will be varied in the invariant imbedding equations.

B. Derivation of the Invariant Imbedding Equations

Using the procedure suggested by Bailey and Wing[14], the invariant imbedding equations can now be derived in a straightforward fashion. First we define the reflection and transmission functions

$$r(Z, \rho, \mu, \varphi, \rho_o, \mu_o, \varphi_o) \equiv \psi(Z, Z, \rho, \mu, \varphi, \rho_o, \mu_o, \varphi_o) \quad \text{for} \quad 0 < \mu < 1 \qquad \text{(A-7)}$$

and

$$t(Z,\rho,\mu,\varphi,\rho_o,\mu_o,\varphi_o) \equiv \psi(Z,0,\rho,\mu,\varphi,\rho_o,\mu_o,\varphi_o) \quad \text{for} \quad -1 < \mu < 0 \quad . \tag{A-8}$$

From Eq. (A-7) we have for r that

$$\frac{\partial}{\partial Z} r(Z,\rho,\mu,\varphi,\rho_o,\mu_o,\varphi_o) = \psi_1(Z,Z,\rho,\mu,\varphi,\rho_o,\mu_o,\varphi_o) + \psi_2(Z,Z,\rho,\mu,\varphi,\rho_o,\mu_o,\varphi_o) \quad \text{for} \quad 0 < \mu < 1 \tag{A-9}$$

where the subscripts denote partial differentiation. ψ_2 is obtained directly from Eq. (A-5). To obtain ψ_1 we note that upon differentiation of Eq. (A-5) with respect to Z, ψ_1 is a solution with the boundary conditions

$$\psi_1(Z,Z,\rho,\mu,\varphi,\rho_o,\mu_o,\varphi_o) = -\psi_2(Z,Z,\rho,\mu,\varphi,\rho_o,\mu_o,\varphi_o) \quad \text{for} \quad -1 < \mu < 0$$

$$\psi_1(Z,0,\rho,\mu,\varphi,\rho_o,\mu_o,\varphi_o) = 0 \quad \text{for} \quad 0 < \mu < 1$$

$$\psi_1(Z,z,R,\mu,\varphi,\rho_o,\mu_o,\varphi_o) = 0 \quad \text{for} \quad \pi/2 < \varphi < 3\pi/2 \quad .$$

Since Eq. (A-5) is linear we can superpose solutions to get

$$\psi_1(Z,z,\rho,\mu,\varphi,\rho_o,\mu_o,\varphi_o) = -\int_o^R \rho' d\rho' \int_{-1}^{o} d\mu' \int_o^{2\pi} d\varphi' \times$$

$$\times \psi_2(Z,Z,\rho',\mu',\varphi',\rho_o,\mu_o,\varphi_o)\, \psi(Z,z,\rho,\mu,\varphi,\rho',\mu',\varphi') \quad . \tag{A-10}$$

This step is the key to the transformation from the Boltzmann equation to the invariant imbedding equations. It is possible because the Boltzmann equation is linear and ψ is the appropriate Green's

function.

From Eq. (A-5) we have

$$\psi_2(Z, z, \rho, \mu, \varphi, \rho_o, \mu_o, \varphi_o)$$
$$= -\left[\frac{\sqrt{1-\mu^2}}{\mu}\cos\varphi\,\frac{\partial}{\partial\rho} - \frac{\sqrt{1-\mu^2}}{\mu}\,\frac{\sin\varphi}{\rho}\,\frac{\partial}{\partial\varphi} + \frac{\Sigma_t}{\mu}\right]\psi(Z, z, \rho, \mu, \varphi, \rho_o, \mu_o, \varphi_o)$$
$$+ \frac{1}{\mu}\int_{-1}^{1} d\mu' \int_{o}^{2\pi} d\varphi' \Sigma(\mu, \mu', \varphi-\varphi')\psi(Z, z, \rho, \mu', \varphi', \rho_o, \mu_o, \varphi_o) \quad . \tag{A-11}$$

Then using Eqs. (A-11), (A-6), and (A-7) in (A-10) we have

$$
\begin{aligned}
&\psi_1(Z, z, \rho, \mu, \varphi, \rho_o, \mu_o, \varphi_o) \\
&= -\int_o^R \rho' d\rho' \int_{-1}^{o} d\mu' \int_o^{2\pi} d\varphi' \psi(Z, z, \rho, \mu, \varphi, \rho', \mu', \varphi') \times \\
&\times \Bigg\{ -\left[\frac{\sqrt{1-\mu'^2}}{\mu'} \cos\varphi' \frac{\partial}{\partial \rho'} - \frac{\sqrt{1-\mu'^2}}{\mu'} \frac{\sin\varphi'}{\rho'} \frac{\partial}{\partial \varphi'} + \frac{\Sigma_t}{\mu'} \right] \times \\
&\qquad \times \psi(Z, Z, \rho', \mu', \varphi', \rho_o, \mu_o, \varphi_o) \\
&\qquad + \frac{1}{\mu'} \int_{-1}^{1} d\mu'' \int_o^{2\pi} d\varphi'' \, \Sigma(\mu', \mu'', \varphi' - \varphi'') \times \\
&\qquad \times \psi(Z, Z, \rho', \mu'', \varphi'', \rho_o, \mu_o, \varphi_o) \Bigg\} \\
&= \frac{\sqrt{1-\mu_o^2}}{\mu_o} \cos\varphi_o \int_o^R \rho' d\rho' \psi(Z, z, \rho, \mu, \varphi, \rho', \mu_o, \varphi_o) \frac{\partial}{\partial \rho'} \left[\frac{\delta(\rho' - \rho_o)}{\rho'} \right] \\
&- \frac{\sqrt{1-\mu_o^2}}{\mu_o} \int_o^{2\pi} d\varphi' \psi(Z, z, \rho, \mu, \varphi, \rho_o, \mu_o, \varphi') \sin\varphi' \frac{\partial}{\partial \varphi'} [\delta(\varphi' - \varphi_o)] \qquad \text{(A-12)} \\
&\qquad + \frac{\Sigma_t}{\mu} \psi(Z, z, \rho, \mu, \varphi, \rho_o, \mu_o, \varphi_o) \\
&\qquad - \int_{-1}^{o} d\mu' \int_o^{2\pi} d\varphi' \psi(Z, z, \rho, \mu, \varphi, \rho_o, \mu', \varphi') \frac{1}{\mu'} \Sigma(\mu', \mu_o, \varphi' - \varphi_o) \\
&\qquad - \int_o^R \rho' d\rho' \int_{-1}^{o} d\mu' \int_o^{2\pi} d\varphi' \psi(Z, z, \rho, \mu, \varphi, \rho', \mu', \varphi') \times \\
&\qquad \times \frac{1}{\mu'} \int_o^1 d\mu'' \int_o^{2\pi} d\varphi'' \Sigma(\mu', \mu'', \varphi' - \varphi'') r(Z, \rho', \mu'', \varphi'', \rho_o, \mu_o, \varphi_o) .
\end{aligned}
$$

Integrating the first integral on the right-hand side of Eq. (A-12) by

parts, we have

$$\int_o^R \rho' d\rho' \psi(Z, z, \rho, \mu, \varphi, \rho', \mu_o, \varphi_o) \frac{\partial}{\partial \rho'} \left[\frac{\delta(\rho' - \rho_o)}{\rho'} \right]$$

$$= -\left(\frac{\partial}{\partial \rho_o} + \frac{1}{\rho_o} \right) \psi(Z, z, \rho, \mu, \varphi, \rho_o, \mu_o, \varphi_o) \qquad \text{(A-13)}$$

and similarly for the second integral on the right-hand side of (A-12),

$$\int_o^{2\pi} d\varphi' \psi(Z, z, \rho, \mu, \varphi, \rho_o, \mu_o, \varphi_o) \sin\varphi' \frac{\partial}{\partial \varphi'} [\delta(\varphi' - \varphi_o)]$$

$$= -\left(\sin\varphi_o + \frac{\partial}{\partial \rho_o} \cos\varphi_o \right) \psi(Z, z, \rho, \mu, \varphi, \rho_o, \mu_o, \varphi_o) \ . \qquad \text{(A-14)}$$

Putting (A-13) and (A-14) in (A-12) we obtain

$$\psi_1(Z, z, \rho, \mu, \varphi, \rho_o, \mu_o, \varphi_o)$$

$$= -\left[\frac{\sqrt{1-\mu_o^2}}{\mu_o} \cos\varphi_o \frac{\partial}{\partial \rho_o} - \frac{\sqrt{1-\mu_o^2}}{\mu_o} \frac{\sin\varphi_o}{\rho_o} \frac{\partial}{\partial \varphi_o} - \frac{\Sigma_t}{\mu_o} \right] \times$$

$$\times \psi(Z, z, \rho, \mu, \varphi, \rho_o, \mu_o, \varphi_o)$$

$$- \int_{-1}^{o} d\mu' \int_o^{2\pi} d\varphi' \psi(Z, z, \rho, \mu, \varphi, \rho_o, \mu', \varphi') \frac{1}{\mu'} \Sigma(\mu', \mu_o, \varphi' - \varphi_o)$$

$$- \int_o^R \rho' d\rho' \int_{-1}^{o} d\mu' \int_o^{2\pi} d\varphi' \psi(Z, z, \rho, \mu, \varphi, \rho', \mu', \varphi') \times \qquad \text{(A-15)}$$

$$\times \frac{1}{\mu'} \int_o^1 d\mu'' \int_o^{2\pi} d\varphi'' \Sigma(\mu', \mu'', \varphi' - \varphi'') r(Z, \rho', \mu'', \varphi'', \rho_o, \mu_o, \varphi_o) \ .$$

Finally putting Eqs. (A-11), (A-15), and (A-7) in (A-9), we have

$$\frac{\partial}{\partial Z}\, r(Z,\rho,\mu,\varphi,\rho_o,\mu_o,\varphi_o)$$

$$= \frac{1}{\mu}\,\Sigma(\mu,\mu_o,\varphi-\varphi_o)\,\frac{\delta(\rho-\rho_o)}{\rho}$$

$$-\left[\frac{\sqrt{1-\mu^2}}{\mu}\cos\varphi\,\frac{\partial}{\partial\rho} - \frac{\sqrt{1-\mu_o^2}}{|\mu_o|}\cos\varphi_o\,\frac{\partial}{\partial\rho_o} - \frac{\sqrt{1-\mu^2}}{\mu}\,\frac{\sin\varphi}{\rho}\,\frac{\partial}{\partial\varphi}\right.$$

$$\left. + \frac{\sqrt{1-\mu_o^2}}{|\mu_o|}\,\frac{\sin\varphi_o}{\rho_o}\,\frac{\partial}{\partial\varphi_o} + \frac{\Sigma_t}{\mu} + \frac{\Sigma_t}{|\mu_o|}\right] r(Z,\rho,\mu,\varphi,\rho_o,\mu_o,\varphi_o) \qquad \text{(A-16)}$$

$$+ \frac{1}{\mu}\int_o^1 d\mu' \int_o^{2\pi} d\varphi'\,\Sigma(\mu,\mu',\varphi-\varphi')\,r(Z,\rho,\mu',\varphi',\rho_o,\mu_o,\varphi_o)$$

$$+ \int_{-1}^{o} d\mu' \int_o^{2\pi} d\varphi'\, r(Z,\rho,\mu,\varphi,\rho_o,\mu',\varphi')\,\frac{1}{|\mu'|}\,\Sigma(\mu',\mu_o,\varphi'-\varphi_o)$$

$$+ \int_o^R \rho'\,d\rho' \int_{-1}^{o} d\mu' \int_o^{2\pi} d\varphi'\, r(Z,\rho,\mu,\varphi,\rho',\mu',\varphi') \times$$

$$\times \frac{1}{|\mu'|}\int_o^1 d\mu'' \int_o^{2\pi} d\varphi''\,\Sigma(\mu',\mu'',\varphi'-\varphi'')\,r(Z,\rho',\mu'',\varphi'',\rho_o,\mu_o,\varphi_o) \quad .$$

This is the invariant imbedding equation for r. The initial condition is

$$r(0,\rho,\mu,\varphi,\rho_o,\mu_o,\varphi_o) = 0 \quad . \qquad \text{(A-17)}$$

For t (from Eq. (A-8)),

$$\frac{\partial}{\partial Z}\, t(Z,\rho,\mu,\varphi,\rho_o,\mu_o,\varphi_o) = \psi(Z,0,\rho,\mu,\varphi,\rho_o,\mu_o,\varphi_o)$$

$$\text{for} \quad -1 < \mu < 0 \quad . \qquad \text{(A-18)}$$

Then putting Eqs. (A-15) and (A-8) in (A-18), we have

$$\frac{\partial}{\partial Z}\, t(Z,\rho,\mu,\varphi,\rho_o,\mu_o,\varphi_o)$$

$$= -\left[-\frac{\sqrt{1-\mu_o^2}}{|\mu_o|}\cos\varphi_o\,\frac{\partial}{\partial\rho_o} + \frac{\sqrt{1-\mu_o^2}}{|\mu_o|}\,\frac{\sin\varphi_o}{\rho_o}\,\frac{\partial}{\partial\varphi_o} + \frac{\Sigma_t}{|\mu_o|}\right]\times$$

$$\times\, t(Z,\rho,\mu,\varphi,\rho_o,\mu_o,\varphi_o)$$

$$+\int_{-1}^{o} d\mu' \int_o^{2\pi} d\varphi' t(Z,\rho,\mu,\varphi,\rho_o,\mu',\varphi')\,\frac{1}{|\mu'|}\,\Sigma(\mu',\mu_o,\varphi'-\varphi_o)$$

$$+\int_o^R \rho' d\rho' \int_{-1}^{o} d\mu' \int_o^{2\pi} d\varphi' t(Z,\rho,\mu,\varphi,\rho',\mu',\varphi')\times \tag{A-19}$$

$$\times\,\frac{1}{|\mu'|}\int_o^1 d\mu'' \int_o^{2\pi} d\varphi''\,\Sigma(\mu',\mu'',\varphi-\varphi'')r(Z,\rho',\mu'',\varphi'',\rho_o,\mu_o,\varphi_o)$$

which is the invariant imbedding equation for t with initial condition

$$t(0,\rho,\mu,\varphi,\rho_o,\mu_o,\varphi_o) = \frac{\delta(\rho-\rho_o)}{\rho}\,\delta(\mu-\mu_o)\delta(\varphi-\varphi_o) \quad . \tag{A-20}$$

As they stand, Eqs. (A-16) and (A-19) cannot be integrated numerically in the straightforward manner that the slab geometry equations (2-46) and (2-47) were. The difficulty arises from the presence of the δ-function term in the reflection equation, which would also appear in the transmission equation if we separated out the undeflected beam. So far we have been unable to find a way to integrate over or separate out the offending term.

C. X-and Y-Functions

If we restrict our attention to mono-energetic transport so that the principle of reciprocity holds, then we can reduce the dimensionality of the problem by introducing the cylindrical geometry analogues of Chandrasekhar's X-and Y-functions. In fact most of Chapter VII of R. T.* can be generalized to cylindrical geometry. Using the principles of invariance one can arrive at Eqs. (A-16) and (A-19) above as well as the cylindrical analogues of Eqs. (2-44) and (2-45). We will not carry this out here, but will merely state the results.

Let us define

$$S(Z,\rho,\mu,\varphi,\rho_o,\mu_o,\varphi_o) \equiv \mu r(Z,\rho,\mu,\varphi,\rho_o-\mu_o,\varphi_o) + \mu r(Z,\rho,\mu,-\varphi,\rho_o,-\mu_o,\varphi_o) \qquad (A-21)$$

and

$$U(Z,\rho,\mu,\varphi,\rho_o,\mu_o,\varphi_o) \equiv |\mu| t^s(Z,\rho,-\mu,\varphi,\rho_o,-\mu_o,\varphi_o) + |\mu| t^s(Z,\rho,-\mu,-\varphi,\rho_o,-\mu_o,\varphi_o) \qquad (A-22)$$

which are the analogues of Chandrasekhar's S and T. These definitions fully use azimuthal symmetry so that we need only consider values of φ and φ_o in the interval 0 to π. The quantity t^s is the scattered transmission function just as in the slab geometry case (cf. Eq. (2-48)).

*Chandrasekhar's Radiative Transfer, Ref. 6. Some familiarity with this work is necessary for an understanding of this section.

We then define

$$X(Z,\rho,\rho_o,\mu,\varphi) \equiv \frac{\delta(\rho-\rho_o)}{\rho} + \int_o^1 d\mu' \int_o^\pi d\varphi' \frac{1}{\mu'} S(Z,\rho,\mu,\varphi,\rho_o,\mu',\varphi') \tag{A-23}$$

and

$$Y(Z,\rho,\rho_o,\mu,\varphi) \equiv e^{-\frac{\Sigma_t}{\mu}Z} \frac{\delta(f-\rho_o)}{f} + \int_o^1 d\mu' \int_o^\pi d\varphi' \frac{1}{\mu'} U(Z,\rho,\mu,\varphi,\rho_o,\mu',\varphi') \tag{A-24}$$

where

$$f = \sqrt{\rho^2 + \frac{(1-\mu_o^2)}{\mu_o^2} Z^2 - 2\rho Z \frac{\sqrt{1-\mu_o^2}}{|\mu_o|} \cos\varphi} \tag{A-25}$$

is due to the undeflected beam. By the principle of reciprocity

$$\mu r(Z,\rho,\mu,\varphi,\rho_o,\mu_o,\varphi_o) = |\mu_o| r(Z,\rho_o,\mu_o,\pi-\varphi_o,\rho,\mu,\pi-\varphi) \tag{A-26}$$

and

$$|\mu| t(Z,\rho,\mu,\varphi,\rho_o,\mu_o,\varphi_o) = |\mu_o| t(Z,\rho_o,\mu_o,\pi-\varphi_o,\rho,\mu,\pi-\varphi) \tag{A-27}$$

so that $X(Z,\rho_o,\rho,\mu_o,\pi-\varphi_o)$ and $Y(Z,\rho_o,\rho,\mu_o,\pi-\varphi_o)$ are simply the total fluxes at the top and bottom of the cylinder, respectively, for an incident flux on the top of

$$\frac{\delta(\rho-\rho_o)}{\rho}\ \delta(\mu-\mu_o)[\delta(\varphi-\varphi_o) + \delta(\varphi+\varphi_o)]\ ,$$

the $\delta(\varphi+\varphi_o)$ arising from our definitions of S and U.

In the case of isotropic scattering, i.e.

$$\Sigma(\mu, \mu_o, \varphi-\varphi_o) = \frac{\Sigma}{4\pi}$$

the invariant imbedding equations can then be written as

$$\begin{aligned}
&\frac{\partial}{\partial Z} S(Z, \rho, \mu, \varphi, \rho_o, \mu_o, \varphi_o) \\
&= -\left[\frac{\sqrt{1-\mu^2}}{\mu} \cos\varphi \frac{\partial}{\partial \rho} - \frac{\sqrt{1-\mu_o^2}}{\mu_o} \cos\varphi_o \frac{\partial}{\partial \rho_o} - \frac{\sqrt{1-\mu^2}}{\mu} \frac{\sin\varphi}{\rho} \frac{\partial}{\partial \varphi}\right. \\
&\quad \left. + \frac{\sqrt{1-\mu_o^2}}{\mu_o} \frac{\sin\varphi_o}{\rho_o} \frac{\partial}{\partial \varphi_o} + \frac{\Sigma_t}{\mu} + \frac{\Sigma_t}{\mu_o}\right] S(Z, \rho, \mu, \varphi, \rho_o, \mu_o, \varphi_o) \\
&\quad + \frac{\Sigma}{2\pi} \int_o^R \rho' d\rho' X(Z, \rho, \rho', \mu, \varphi) X(Z, \rho_o, \rho', \mu_o, \pi-\varphi_o)
\end{aligned} \tag{A-28}$$

$$\begin{aligned}
&\frac{\partial}{\partial Z} U(Z, \rho, \mu, \varphi, \rho_o, \mu_o, \varphi_o) \\
&= -\left[\frac{\sqrt{1-\mu^2}}{\mu} \cos\varphi \frac{\partial}{\partial \rho} - \frac{\sqrt{1-\mu^2}}{\mu} \frac{\sin\varphi}{\rho} \frac{\partial}{\partial \varphi} + \frac{\Sigma_t}{\mu}\right] \times \\
&\qquad \times U(Z, \rho, \mu, \varphi, \rho_o, \mu_o, \varphi_o) \\
&\quad + \frac{\Sigma}{2\pi} \int_o^R \rho' d\rho' X(Z, \rho, \rho', \mu, \varphi) Y(Z, \rho_o, \rho', \mu_o, \pi-\varphi_o)
\end{aligned} \tag{A-29}$$

$$\begin{aligned}
&\frac{\partial}{\partial Z} S(Z, \rho, \mu, \varphi, \rho_o, \mu_o, \varphi_o) \\
&= \frac{\Sigma}{2\pi} \int_o^R \rho' d\rho' Y(Z, \rho, \rho', \mu, \varphi) Y(Z, \rho_o, \rho', \mu_o, \pi-\varphi_o)
\end{aligned} \tag{A-30}$$

$$\frac{\partial}{\partial Z} U(Z, \rho, \mu, \varphi, \rho_o, \mu_o, \varphi_o)$$

$$= -\left[-\frac{\sqrt{1-\mu_o^2}}{\mu_o} \cos\varphi_o \frac{\partial}{\partial \rho_o} + \frac{\sqrt{1-\mu_o^2}}{\mu_o} \frac{\sin\varphi_o}{\rho_o} \frac{\partial}{\partial \varphi_o} + \frac{\Sigma_t}{\mu_o} \right] \times$$

$$\times U(Z, \rho, \mu, \varphi, \rho_o, \mu_o, \varphi_o) \qquad \text{(A-31)}$$

$$+ \frac{\Sigma}{2\pi} \int_o^R \rho' d\rho' Y(Z, \rho, \rho', \mu, \varphi) X(Z, \rho_o, \rho', \mu_o, \pi - \varphi_o) \quad .$$

The following correspondences exist between our equations and those in §54 of R. T.

(A-23) → (78)

(A-24) → (79)

(A-28) - (A-30) → (80)

(A-31) - (A-29) → (81)

(A-30) → (82)

$(1/\mu_o)$(A-29) - $(1/\mu)$(A-31) → (83) .

The analogues to Chandrasekhar's integral Equations ((84) and (85)) do not seem to be easily obtainable in our case because of the partial derivatives with respect to ρ and φ.

Integro-differential equations for X and Y (see §54 and §62 of R. T.), however, can be obtained by integrating Eqs. (A-30) and (A-29) with respect to μ_o and φ_o and then using Eqs. (A-23) and (A-24). We have

$$\frac{\partial}{\partial Z} X(Z,\rho,\rho_o,\mu,\varphi) = \frac{\Sigma}{2\pi}\int_o^R \rho' d\rho' Y(Z,\rho,\rho',\mu,\varphi)\times$$

$$\times\int_o^1 d\mu' \int_o^\pi d\varphi' \frac{1}{\mu'} Y(Z,\rho_o,\rho',\mu',\varphi') \qquad \text{(A-32)}$$

and

$$\frac{\partial}{\partial Z} Y(Z,\rho,\rho_o,\mu,\varphi)$$

$$= -\left[\frac{\sqrt{1-\mu^2}}{\mu}\cos\varphi\ \frac{\partial}{\partial\rho} - \frac{\sqrt{1-\mu^2}}{\mu}\frac{\sin\varphi}{\rho}\frac{\partial}{\partial\varphi} + \frac{\Sigma_t}{\mu}\right] Y(Z,\rho,\rho_o,\mu,\varphi) \qquad \text{(A-33)}$$

$$+ \frac{\Sigma}{2\pi}\int_o^R \rho' d\rho' X(Z,\rho,\rho',\mu,\varphi)\int_o^1 d\mu' \int_o^\pi d\varphi' \frac{1}{\mu'} Y(Z,\rho_o,\rho',\mu',\varphi') \ .$$

Equations (A-32) and (A-33) compare with (13) and (14) in §56 of R. T. The initial conditions are

$$X(0,\rho,\rho_o,\mu,\varphi) = \frac{\delta(\rho-\rho_o)}{\rho} \qquad \text{(A-34)}$$

$$Y(Z,\rho,\rho_o,\mu,\varphi) \to e^{-\frac{\Sigma_t}{\mu}Z}\ \frac{\delta(\rho-\rho_o)}{\rho} \qquad \text{as} \qquad Z\to 0 \ . \qquad \text{(A-35)}$$

We still cannot solve these differential equations in a straightforward manner because of the initial conditions. Equations (A-32) and (A-33) have a considerably simpler form, however, than the invariant imbedding equations (A-16) and (A-19).

APPENDIX B
DIFFUSION THEORY INVARIANT IMBEDDING IN CYLINDRICAL GEOMETRY

The general multi-group diffusion equations are (cf. Eqs. (2-63) and (2-64))

$$D_j \nabla^2 \phi_j - \Sigma_{rj}\phi_j + \sum_{k \neq j} \Sigma_{k \to j}\phi_k + \chi_j \sum_k (\nu\Sigma_f)_k \phi_k = 0 \qquad \text{(B-1)}$$

$$\vec{J}_j = - D_j \nabla \phi_j \qquad \text{(B-2)}$$

or

$$-\nabla \cdot \vec{J} + S\phi = 0 \qquad \text{(B-3)}$$

$$\nabla\phi + 3\Sigma \vec{J} = 0 \qquad \text{(B-4)}$$

where Σ and S are given by Eqs. (2-67) and (2-68).

In r-z geometry (i.e. assuming azimuthal symmetry), we have

$$\nabla\phi = \frac{\partial\phi}{\partial r}\,\hat{r} + \frac{\partial\phi}{\partial z}\,\hat{k} \qquad \text{(B-5)}$$

$$\nabla \cdot \vec{J} = \frac{1}{r}\frac{\partial}{\partial r}(rJ_r) + \frac{\partial}{\partial z}(J_z) \quad . \qquad \text{(B-6)}$$

The derivation now parallels that given in Section B.2 of Chapter II for slab geometry.

Define

$$u \equiv j_+(\vec{r}) = \frac{1}{4}\,\phi(\vec{r}) + \frac{1}{2}\,J_z(\vec{r}) \qquad \text{(B-7)}$$

$$v \equiv j_-(\vec{r}) = \frac{1}{4}\,\phi(\vec{r}) - \frac{1}{2}\,J_z(\vec{r}) \quad . \qquad \text{(B-8)}$$

Then

$$\phi = 2(u + v) \tag{B-9}$$

$$J_z = u - v \tag{B-10}$$

$$\vec{J} = J_r \hat{r} + J_z \hat{k} = - D\left(\frac{\partial \phi}{\partial r} \hat{r} + \frac{\partial \phi}{\partial z} \hat{k}\right) \tag{B-11}$$

with

$$D_{ij} \equiv D_j \delta_{ij} \quad . \tag{B-12}$$

Using these expressions, we can write Eq. (B-3) as

$$\frac{1}{r} \frac{\partial}{\partial r}\left[2Dr \frac{\partial}{\partial r} (u+v)\right] - \frac{\partial}{\partial z} (u-v) + 2S(u+v) = 0 \tag{B-13}$$

and the z-component of Eq. (B-4) as

$$2 \frac{\partial}{\partial z} (u+v) + 3\Sigma(u-v) = 0 \tag{B-14}$$

which can be combined to give

$$\frac{\partial}{\partial z} u - \frac{D}{r} \frac{\partial}{\partial r}\left[r \frac{\partial}{\partial r} (u+v)\right] - Qu - Pv = 0 \tag{B-15}$$

$$\frac{\partial}{\partial z} v + \frac{D}{r} \frac{\partial}{\partial r}\left[r \frac{\partial}{\partial r} (u+v)\right] + Pu + Qv = 0 \tag{B-16}$$

where P and Q are given by Eqs. (2-75) and (2-76).

Just as in the slab geometry case (cf. Eqs. (2-77) and (2-78)), we introduce matrices U and V which satisfy

$$\frac{\partial}{\partial z} U(z,x,r,r_o) = \frac{D}{r} \frac{\partial}{\partial r}\left[r \frac{\partial}{\partial r} (U(z,x,r,r_o)+V(z,x,r,r_o))\right]$$

$$+ QU(z,x,r,r_o) + PV(z,x,r,r_o) \tag{B-17}$$

$$- \frac{\partial}{\partial z} V(z,x,r,r_o) = \frac{D}{r} \frac{\partial}{\partial r} \left[r \frac{\partial}{\partial r} (U(z,x,r,r_o) + V(z,x,r,r_o)) \right]$$

$$+ PU(z,x,r,r_o) + QV(z,x,r,r_o) \qquad \text{(B-18)}$$

with the boundary conditions

$$U(0,x,r,r_o) = 0 \qquad \text{(B-19)}$$

$$V(x,x,r,r_o) = \frac{\delta(r-r_o)}{r} I \quad . \qquad \text{(B-20)}$$

Then

$$R(x,r,r_o) \equiv U(x,x,r,r_o) \qquad \text{(B-21)}$$

$$T(x,r,r_o) \equiv V(0,x,r,r_o) \quad . \qquad \text{(B-22)}$$

The invariant imbedding equation for R is obtained by considering

$$\frac{\partial}{\partial x} R(x,r,r_o) = U_1(x,x,r,r_o) + U_2(x,x,r,r_o) \quad . \qquad \text{(B-23)}$$

For U_1 we have

$$U_1(x,x,r,r_o) = \frac{D}{r} \frac{\partial}{\partial r} \left[r \frac{\partial}{\partial r} \left(R(x,r,r_o) + \frac{\delta(r-r_o)}{r} I \right) \right]$$

$$+ QR(x,r,r_o) + P \frac{\delta(r-r_o)}{r} \qquad \text{(B-24)}$$

while U_2 and V_2 are solutions of the differential equations (B-17) and (B-18) with the boundary conditions

$$U_2(0,x,r,r_o) = 0 \qquad \text{(B-25)}$$

$$V_2(x,x,r,r_o) = -V_1(x,x,r,r_o) \quad . \tag{B-26}$$

Hence

$$U_2(z,x,r,r_o) = -\int_o^R r'dr'U(z,x,r,r')V_1(x,x,r',r_o) \tag{B-27}$$

$$V_2(z,x,r,r_o) = -\int_o^R r'dr'V(z,x,r,r')V_1(x,x,r',r_o) \quad . \tag{B-28}$$

In particular

$$\begin{aligned} U_2(x,x,r,r_o) = &\int_o^R r'dr'R(x,r,r') \times \\ &\times\left\{\frac{D}{r'}\frac{\partial}{\partial r'}\left[r'\frac{\partial}{\partial r'}\left(R(x,r',r_o) + \frac{\delta(r'-r_o)}{r'}\,I\right)\right]\right. \\ &\left. + PR(x,r',r_o) + Q\,\frac{\delta(r'-r_o)}{r'}\right\} \end{aligned} \tag{B-29}$$

so that

$$\begin{aligned} &\frac{\partial}{\partial x}R(x,r,r_o) \\ &= \frac{D}{r}\frac{\partial}{\partial r}\left[r\,\frac{\partial}{\partial r}\left(R(x,r,r_o) + \frac{\delta(r-r_o)}{r}\,I\right)\right] + QR(x,r,r_o) \\ &\quad + P\,\frac{\delta(r-r_o)}{r} + \int_o^R r'dr'R(x,r,r') \times \\ &\quad \times\left\{\frac{D}{r'}\frac{\partial}{\partial r'}\left[r'\,\frac{\partial}{\partial r'}\left(R(x,r',r_o) + \frac{\delta(r'-r_o)}{r'}\,I\right)\right]\right. \\ &\quad \left. + PR(x,r',r_o) + Q\,\frac{\delta(r'-r_o)}{r'}\right\} \quad . \end{aligned} \tag{B-30}$$

Integrating by parts

$$\int_o^R r'dr'R(x,r,r') \frac{D}{r'} \frac{\partial}{\partial r'}\left[r' \frac{\partial}{\partial r'}\left(\frac{\delta(r'-r_o)}{r'}\right)\right]$$

$$= \frac{D}{r_o} \frac{\partial}{\partial r_o}\left[r_o \frac{\partial}{\partial r_o} R(x,r,r_o)\right] \quad . \tag{B-31}$$

Finally

$$\frac{\partial}{\partial x} R(x,r,r_o) = P \frac{\delta(r-r_o)}{r} + \frac{D}{r} \frac{\partial}{\partial r}\left[r \frac{\partial}{\partial r}\left(\frac{\delta(r-r_o)}{r}\right)\right]$$

$$+\left[\frac{D}{r} \frac{\partial}{\partial r}\left(r \frac{\partial}{\partial r}\right) + \frac{D}{r_o} \frac{\partial}{\partial r_o}\left(r_o \frac{\partial}{\partial r_o}\right)\right]R(x,r,r_o)$$

$$+ QR(x,r,r_o) + R(x,r,r_o)Q$$

$$+ \int_o^R r'dr'R(x,r,r')\left\{\frac{D}{r'} \frac{\partial}{\partial r'}\left[r' \frac{\partial}{\partial r'} R(x,r',r_o)\right]\right.$$

$$\left. + PR(x,r',r_o)\right\} \tag{B-32}$$

with the initial condition

$$R(0,r,r_o) = 0 \quad . \tag{B-33}$$

Similarly for T we have

$$\frac{\partial}{\partial x} T(x, r, r_o) = V_2(0, x, r, r_o)$$

$$= - \int_o^R r'dr'V(0, x, r, r')V_1(x, x, r', r_o)$$

$$= \frac{D}{r_o} \frac{\partial}{\partial r_o}\left(r_o \frac{\partial}{\partial r_o}\right) T(x, r, r_o)$$

$$+ T(x, r, r_o)Q$$

$$+ \int_o^R r'dr'T(x, r, r')\left\{\frac{D}{r'} \frac{\partial}{\partial r'}\left[r' \frac{\partial}{\partial r'} R(x, r', r_o)\right]\right.$$

$$\left. + PR(x, r', r_o)\right\} \qquad \text{(B-34)}$$

with the initial condition

$$T(0, r, r_o) = \frac{\delta(r-r_o)}{r} I \quad . \qquad \text{(B-35)}$$

APPENDIX C

EXPERIMENTALLY DETERMINED CROSS-SECTION MATRICES

In Section A. 1 of Chapter IV we stated that the cross-section matrices obtained from response function experiments are in precisely the form needed for input to conventional computer codes. This we demonstrate now.

A. Transport Theory

For a differential thickness dx, we have

$$\rho(dx) = S^b dx \tag{2-42}$$

$$\tau(dx) = I + (S^f - M)dx \tag{2-43}$$

so that repeated halving of the measured response functions just gives us the matrices S^b and $S^f - M$.

In slab geometry the transport equation can be written as[77]

$$\mu \frac{\partial}{\partial z} \psi(z, \mu, E) + \Sigma_t(E)\psi(z, \mu, E)$$
$$= \int_o^\infty dE' \int_{-1}^{1} d\mu' \Sigma(\mu, E, \mu', E')\psi(z, \mu', E') \quad . \tag{C-1}$$

Discretizing just as we did in Section A of Chapter II, we have

$$\mu_i \frac{\partial}{\partial z} \psi_i^{\pm}(z) + \Sigma_i^t \psi_i^{\pm}(z)$$
$$= \sum_{j=1}^{N} \Delta\mu_j \Delta E_j (\Sigma_{ij}^f \psi_{ij}^{\pm}(z) + \Sigma_{ij}^b \psi_{ij}^{\mp}(z)) \tag{C-2}$$

or

$$\frac{\partial}{\partial z}\psi^{\pm}(z) = (S^f - M)\psi^{\pm}(z) + S^b\psi^{\mp}(z) \quad . \tag{C-3}$$

Thus S^b and $S^f - M$ are sufficient to determine the solution to the transport equation in slab geometry. S^b and $S^f - M$ are related to the double-differential cross-sections through an azimuthal itegration (Eq. (2-33)) which takes advantage of the symmetry in slab geometry. However, by letting one of the angle groups be $\mu = 1$ as discussed in Section A. 2 of Chapter IV, we can obtain the double-differential cross-sections and so prepare cross-sections for any geometry.

B. Diffusion Theory

For a small thickness dx, we have

$$R(dx) = P\,dx \tag{2-61}$$

$$T(dx) = I + Q\,dx \tag{2-62}$$

so that repeated halving of measured R and T will give P and Q. The general multi-group diffusion equations, however, can be written as

$$-\nabla\cdot\vec{J} + S\phi = 0 \tag{B-3}$$

$$\nabla\phi + 3\Sigma\vec{J} = 0 \tag{B-4}$$

with (cf. Eqs. (2-75) and (2-76))

$$S = \frac{1}{2}(P + Q) \tag{C-4}$$

$$\Sigma = \frac{2}{3}(P - Q) \quad . \tag{C-5}$$

C. Individual Interaction Cross-sections

In the previous two sections of this Appendix and in Section A of Chapter IV, we emphasized that ""combined"" cross-sections are obtained from response function experiments. However, if so desired, the individual interaction cross-sections can be separated to a certain extent.

Thus suppose we have obtained the diffusion theory matrices Σ and S as shown in the previous section. These matrices were defined in Chapter II as

$$\Sigma \equiv \begin{bmatrix} 1/3D_1 & 0 & \cdots & 0 \\ 0 & 1/3D_2 & \cdots & 0 \\ \vdots & \vdots & & \vdots \\ 0 & 0 & \cdots & 1/3D_n \end{bmatrix} \tag{2-67}$$

$$S \equiv \begin{bmatrix} -\Sigma_{r_1} + \chi_1(\nu\Sigma_f)_1 & \Sigma_{2\to1} + \chi_1(\nu\Sigma_f)_2 & \cdots & \Sigma_{n\to1} + \chi_1(\nu\Sigma_f)_n \\ \Sigma_{1\to2} + \chi_2(\nu\Sigma_f)_1 & -\Sigma_{r_2} + \chi_2(\nu\Sigma_f)_2 & \cdots & \Sigma_{n\to2} + \chi_2(\nu\Sigma_f)_n \\ \vdots & \vdots & & \vdots \\ \Sigma_{1\to n} + \chi_n(\nu\Sigma_f)_1 & \Sigma_{2\to n} + \chi_n(\nu\Sigma_f)_2 & \cdots & -\Sigma_{r_n} + \chi_n(\nu\Sigma_f)_n \end{bmatrix} . \tag{2-68}$$

The elements of Σ are just the transport cross-sections Σ_{tr_j}. For

a non-fissile material the elements of S are the transfer cross-sections $\Sigma_{j\to i}$ and removal cross-sections Σ_{rj}. Moreover, summation of the j^{th} column gives the capture cross-section. Thus

$$\sum_{i\neq j} \Sigma_{j\to i} - \Sigma_{rj} = - \Sigma_{cj} \quad .$$

For a fissile material the analysis of S is slightly more involved. Since there is no fast upscattering,

$$\Sigma_{j\to i} = 0 \qquad \text{for} \qquad j > i$$

so that the elements above the diagonal are just $\chi_i(\nu\Sigma_f)_j$. If we assume the fission spectrum χ_i is well-known, then we have $(\nu\Sigma_f)_j$ for $j \neq 1$. Moreover we can then obtain the transfer cross-sections $\Sigma_{j\to i}(j < i)$ and the removal cross-sections Σ_{r_j} except for $j = 1$. By summing the j^{th} column we obtain the absorption cross-section

$$\Sigma_{aj} = \Sigma_{cj} + \Sigma_{fj}$$

since

$$\sum_{i\neq j} \Sigma_{j\to i} - \Sigma_{rj} + (\nu\Sigma_f)_j = - \Sigma_{cj} - \Sigma_{fj} + (\nu\Sigma_f)_j \qquad \text{(C-6)}$$

and we know $(\nu\Sigma_f)_j$.

Finally suppose $j = 1$. For the fissile isotopes, $\Sigma_{c_1} \approx 0$ (see Ref. 49 and 76). If in addition we presume that ν_1 is known from some other experiment, then we can get Σ_{f_1} from (C-6) and

thence the transfer cross-sections $\Sigma_{l \to i}$ from (2-68).

Summarizing the above, Σ_{tr_j} can be obtained from Σ and provided χ_i is known, $(\nu\Sigma_f)_j$, $\Sigma_{j \to i}$, and Σ_{aj} can be obtained from S. In particular we can get

$$\eta_j = \frac{(\nu\Sigma_f)_j}{\Sigma_{aj}}$$

which is of foremost significance in determining the breeding ratio of a fast reactor[78].

REFERENCES

1. G. G. Stokes, "On the Intensity of the Light Reflected From or Transmitted Through a Pile of Plates," Proc. Roy. Soc., 11, 545 - 557 (1862); also in G. G. Stokes, Mathematical and Physical Papers, Vol. IV, pp. 145 - 156, University Press, Cambridge (1904).

2. H. W. Schmidt, "Uber Reflexion und Absorption von β-Strahlen," Annalen der Physik, 23, Series 4, 671 - 697 (1907).

3. V. A. Ambarzumian, "Diffusion of Light by Planetary Atmospheres," Astron. Zh., 19, 30 (1942).

4. V. A. Ambarzumian, "Diffuse Reflection of Light by a Foggy Medium," Compt. Rend. (Doklady) Acad. Sci. U.S.S.R., 38, 229 - 232 (1943).

5. S. Chandrasekhar, "On the Radiative Equilibrium of a Stellar Atmosphere. XVII," Ap. J., 105, 441 - 460 (1947).

6. S. Chandrasekhar, Radiative Transfer, Clarendon Press, Oxford (1950); also Dover, New York (1960).

7. C. G. Montgomery, R. H. Dicke, and E. M. Purcell, Principles of Microwave Circuits, Ch. 5, McGraw-Hill, New York (1948).

8. R. M. Redheffer, "Remarks on the Basis of Network Theory," J. Math. and Phys., 28, 237 - 258 (1949).

9. A. R. Bobrowsky, "Analytical Method of Determining Transmission of Particles and Radiation through Great Thicknesses of Matter," NACA-TN-1712, National Advisory Committee for Aeronautics (1948).

10. R. Bellman and R. Kalaba, "On the Principle of Invariant Imbedding and Propagation Through Inhomogeneous Media," Proc. Nat. Acad. Sci. U.S.A., 42, 629 - 632 (1956).

11. R. Bellman, R. Kalaba, and G. M. Wing, "Invariant Imbedding and Mathematical Physics. I. Particle Processes," J. Math. Phys., 1, 280 - 308 (1960).

12. G. M. Wing, An Introduction to Transport Theory, John Wiley and Sons, New York (1962).

13. G. M. Wing, "The Method of Invariant Imbedding with Applications to Transport Theory and Other Areas of Mathematical Physics," Socony Mobil Colloquium Lectures in Pure and Applied Science, No. 10, Dallas (1965).

14. P. B. Bailey and G. M. Wing, "Some Recent Developments in Invariant Imbedding with Applications," J. Math. Phys., 6, 453 - 462 (1965).

15. R. E. Beissner, "The Application of Invariant Imbedding to Shielding Problems," MR-N-287 (NARF-61-41T), General Dynamics, Fort Worth (1962).

16. R. E. Beissner, "An Analysis of Fast-Neutron Energy-Angle Distributions," FZK-9-186 (NARF-63-5T), General Dynamics, Fort Worth (1963).

17. D. R. Mathews, K. F. Hansen, and E. A. Mason, "Deep Penetration of Radiation by the Method of Invariant Imbedding," Nucl. Sci. Eng., 27, 263 - 270 (1967).

18. A. Shimizu and H. Mizuta, "Application of Invariant Imbedding to the Reflection and Transmission Problem of Gamma Rays, (I)," J. Nucl. Sci. Tech., 3, 57 - 66 (1966).

19. A. Shimizu and H. Mizuta, "Application of Invariant Imbedding to the Reflection and Transmission Problem of Gamma Rays, (II)," J. Nucl. Sci. Tech., 3, 441 - 447 (1966).

20. A. Shimizu, "Calculation of the Penetration of Gamma Rays Through Slabs by the Method of Invariant Imbedding," Nucl. Sci. Eng., 32, 184 - 194 (1968).

21. R. Bellman, R. Kalaba, and M. Prestrud, "On a New Computational Solution of Time-dependent Transport Processes - - I: One-Dimensional Case," Proc. Nat. Acad. Sci. U.S.A., 47, 1072 - 1074 (1961).

22. R. E. Bellman, H. H. Kagiwada, R. E. Kalaba, and M. C. Prestrud, Invariant Imbedding and Time-dependent Transport Processes, American Elsevier, New York (1964).

23. A. Mockel, "Invariant Imbedding and Polyenergetic Neutron Transport Theory - - Part I: Theory," Nucl. Sci. Eng., 29, 43 - 50 (1967).

24. A. Mockel, "Invariant Imbedding and Polyenergetic Neutron Transport Theory - - Part II: Numerical Results," Nucl. Sci. Eng., 29, 51 - 57 (1967).

25. J. O. Mingle, "Applications of the Invariant Imbedding Method to Monoenergetic Neutron Transport Theory in Slab Geometry," Nucl. Sci. Eng., 28, 177 - 189 (1967).

26. G. H. Peebles and M. S. Plesset, "Transmission of Gamma-Rays Through Large Thicknesses of Heavy Materials," Phys. Rev., 81, 430 - 439 (1951).

27. M. Ribarič, "The Relation between the Reflection Properties of the Body and the Reflection Properties of its Parts," Arch. Ratl. Mech. Anal., 8, 381 - 407 (1961).

28. D. S. Selengut, "Partial Current Representations in Reactor Physics," in Reactor Technology, KAPL-2000-20, Knolls Atomic Power Laboratory (1963).

29. A. Shimizu, "Response Matrix Method," J. At. Energy Soc. Japan, 5, 359 - 368 (1963).

30. A. Shimizu, K. Monta, and T. Miyamoto, "Application of the Response Matrix Method to Criticality Calculations of One-dimensional Reactors," J. At. Energy Soc.Japan, 5, 369 - 376 (1963).

31. K. Aoki and A. Shimizu, "Application of the Response Matrix Method to Criticality Calculations of Two-Dimensional Reactors," J. Nucl. Sci. Tech., 2, 149 - 159 (1965).

32. P. Vértes, "On the Generalized Albedo Method," Nukleonik, 10, 148 - 153 (1967).

33. E. Nuding, "Reaktorberechnungen mit Hilfe von Transmissions - und Reflexionsmatrizen," Nukleonik, 10, 303 - 315 (1968).

34. R. Aronson and D. L. Yarmush, "Transfer-Matrix Method for Gamma-Ray and Neutron Penetration," J. Math. Phys., 7, 221 - 237 (1966).

35. H. J. Carlin, "The Scattering Matrix in Network Theory," I.R.E. Trans. on Circuit Theory, CT-3, 88 - 97 (1956).

36. C. T. Molloy, "Four Pole Parameters in Vibration Analysis," in Colloquium on Mechanical Impedance Methods for Mechanical Vibrations, A.S.M.E. Applied Mechanics Division, (1958).

37. E. C. Pestel and F. A. Leckie, Matrix Methods in Elasto-mechanics, McGraw-Hill, New York (1963).

38. S. Rubin, "Transmission Matrices for Vibration and Their Relation to Admittance and Impedance," J. of Engineering for Industry, Trans. A.S.M.E., Series B, 86, 9 - 21 (1964).

39. R. Redheffer, "On the Relation of Transmission-Line Theory to Scattering and Transfer," J. Math. and Phys., 41, 1 - 41 (1962).

40. R. Redheffer, "On Solutions of Riccati's Equation as Functions of the Initial Values," J. Ratl. Mech. Anal., 5, 835 - 848 (1956).

41. W. T. Reid, "Solutions of a Riccati Matrix Differential Equation as Functions of Initial Values," J. Math. Mech., 8, 221 - 230 (1959).

42. P. B. Bailey, "A Rigorous Derivation of Some Invariant Imbedding Equations of Transport Theory," J. Math. Anal. Appl., 8, 149 - 169 (1964).

43. J. Devooght, "Generalized Invariant Imbedding of Transport Theory," J. Math. Anal. Appl., 13, 216 - 244 (1966).

44. R. Bellman and R. Kalaba, "On the Principle of Invariant Imbedding and Diffuse Reflection from Cylindrical Regions," Proc. Nat. Acad. Sci. U.S.A., 43, 514 - 517 (1957).

45. R. E. Bellman, R. E. Kalaba, and G. M. Wing, "Invariant Imbedding and Neutron Transport Theory IV - - Generalized Transport Theory," J. Math. Mech., 8, 575 - 584 (1959).

46. P. B. Bailey and G. M. Wing, "A Correction to Some Invariant Imbedding Equations of Transport Theory Obtained by 'Particle Counting'," J. Math. Anal. Appl., 8, 170 - 174 (1964).

47. R. Bellman, H. Kagiwada, and R. Kalaba, "Invariant Imbedding and Radiative Transfer in Spherical Shells," J. Comp. Phys., 1, 245 - 256 (1966).

48. W. Pfeiffer and J. L. Shapiro, "Applications of a Macroscopic Formulation of Transport Theory," Nucl. Sci. Eng., 34, 336 - 339 (1968).

49. Reactor Physics Constants, ANL-5800, 2nd ed., Section 7.1, Argonne National Laboratory (1963).

50. R. E. Bellman, R. E. Kalaba, and M. C. Prestrud, Invariant Imbedding and Radiative Transfer in Slabs of Finite Thickness, American Elsevier, New York (1963).

51. D. R. Mathews, "Calculation of the Deep Penetration of Radiation by the Method of Invariant Imbedding," pp. 82 - 84, Ph.D. Thesis, Massachusetts Institute of Technology (1966).

52. S. Chandrasekhar, "On the Diffuse Reflection of a Pencil of Radiation by a Plane-Parallel Atmosphere," Proc. Natl. Acad. Sci. U.S.A., 44, 933 - 940 (1958).

53. T. P. Moorhead, "The Effects of Errors in Cross-section Data on Calculations for a Large Dilute Fast Reactor," in Seminar on the Physics of Fast and Intermediate Reactors, Vol. II, I.A.E.A., Vienna (1961).

54. P. Greebler, et al, "Calculated Physics Parameters and Their Uncertainties in a 1000-MW(e) Fast Ceramic Reactor," in Conference on Safety, Fuels, and Core Design in Large Fast Power Reactors, ANL-7120, Argonne National Laboratory (1965).

55. P. Greebler and B. A. Hutchins, "User Requirements for Cross Sections in the Energy Range from 100 eV to 100 keV," in Conference on Neutron Cross Section Technology, CONF-660303, Vol. I, Washington, D.C. (1966).

56. P. Greebler, B. A. Hutchins, and B. Wolfe, "Significance of Neutron Data to Fast Reactor Power Plant Design," in Conference on Neutron Cross Sections and Technology, 2nd, NBS 299, Vol. I, Washington, D.C. (1968).

57. D. M. O'Shea, B. J. Toppel, and A. L. Rago, "The Automated Preparation of Multigroup Cross Sections for Fast Reactor Analysis Using the MC^2 Code," in International Conference on Fast Critical Experiments and Their Analysis, ANL-7320,

Argonne National Laboratory (1966).

58. V. J. Orphan, A. D. Carlson, and O. G. Hoot, "Measurement of Gamma-Ray Production Cross Sections Using a LINAC," in Conference on Neutron Cross Sections and Technology, 2nd, NBS 299, Vol. I, Washington, D.C. (1968).

59. A. E. Profio, et al, "Time-of-flight Measurements of Neutron Spectra in U^{235} and Tungsten," in International Conference on Fast Critical Experiments and Their Analysis, ANL-7320, Argonne National Laboratory (1966).

60. E. F. Bennett, R. Gold, and R. J. Huber, "Spectrum Measurements in a Large Dilute Plutonium-fueled Fast Reactor," in International Conference on Fast Critical Experiments and Their Analysis, ANL-7320, Argonne National Laboratory (1966).

61. E. F. Bennett, "Fast Neutron Spectroscopy by Proton-Recoil Proportional Counting," Nucl.Sci. Eng., 27, 16 - 27 (1967).

62. J. C. Young, et al, "Neutron-Spectrum Measurements in H_2O, CH_2, and C_6H_6," Nucl. Sci. Eng., 18, 376 - 399 (1964).

63. E. F. Bennett, "Neutron Spectrum Measurement in a Fast Critical Assembly," Nucl. Sci. Eng., 27, 28 - 33 (1967).

64. O. I. Elgerd, Control Systems Theory, p. 164, McGraw-Hill, New York, (1967).

65. W. J. Price, Nuclear Radiation Detection, 2nd ed., pp. 59 - 60, McGraw-Hill, New York (1964).

66. H. L. McMurry, G. J. Russell, and R. M. Brugger, "Slow Neutron Scattering by Water," Nucl. Sci. Eng., 25, 248 - 260 (1966).

67. E. L. Slaggie, "Multiple Scattering in Slow-Neutron Double-Differential Measurements," Nucl. Sci. Eng., 30, 199 - 212 (1967).

68. J. U. Koppel, "Neutron Scattering by Hydrogenous Moderators," GA-7055, General Atomic (1966).

69. B. C. Haywood, "The Spectral Density of Hydrogen in Water," J. Nucl. Energy, 21, 249 - 262 (1967).

70. FLANGE, Appendix E, "Integral Neutron Thermalization Annual Summary Report," GA-6824, General Atomic (1965).

71. D. J. Hughes and R. B. Schwartz, Neutron Cross Sections, BNL-325, 2nd ed., Brookhaven National Laboratory (1958).

72. E. L. Slaggie, "Multiple Scattering in Neutron Double Differential Cross Section Measurements," GA-8052, General Atomic (1967).

73. M. Shaw, "Fast Breeder Reactor Programme in the United States," in London Conference on Fast Breeder Reactors, Pergamon Press, Oxford (1967).

74. Session VI-B in Conference on Safety, Fuels, and Core Design in Large Fast Power Reactors, ANL-7120, Argonne National Laboratory (1965).

75. Session IV in International Conference on Fast Critical Experiments and Their Analysis, ANL-7320, Argonne National Laboratory (1966).

76. L. P. Abagyan, N. O. Bazazyants, I. I. Bondarenko, and M. N. Nikolaev, Group Constants for Nuclear Reactor Calculations, Consultants Bureau, New York (1964).

77. A. M. Weinberg and E. P. Wigner, The Physical Theory of Neutron Chain Reactors, pp. 221 - 223, 275 - 276, The University of Chicago Press, Chicago (1958).

78. S. Glasstone and A. Sesonske, Nuclear Reactor Engineering, pp. 702 - 707, Van Nostrand, Princeton (1967).